In Vivo Generation of 'Vaccination Nodes' Using Injectable Alginate Hydrogels for Cancer Immunotherapy

by

Yuki Hori

S.B. in Materials Science and Engineering
Massachusetts Institute of Technology, 2004

SUBMITTED TO THE DEPARTMENT OF MATERIALS SCIENCE AND ENGINEERING IN PARTIAL FULFILLMENT OF THE REQUIREMENTS FOR THE DEGREE OF

DOCTOR OF PHILOSOPHY IN MATERIALS SCIENCE AND ENGINEERING
AT THE
MASSACHUSETTS INSTITUTE OF TECHNOLOGY

June 2009

Signature of Author: _____
Program for Polymer Science and Technology
Department of Materials Science and Engineering
May 22nd, 2009

Certified by: _____
Darrell J. Irvine
Associate Professor
Thesis Supervisor

Accepted by: _____
Christine Ortiz
Chair, Departmental Committee on Graduate Students

In Vivo Generation of 'Vaccination Nodes' Using Injectable Alginate Hydrogels for Cancer Immunotherapy

by

Yuki Hori

Submitted to the Department of Materials Science and Engineering
on May 22nd, 2009, in Partial Fulfillment of the Requirements for the degree of
Doctor of Philosophy in Materials Science and Engineering.

ABSTRACT

Despite the amount of ongoing intensive research, tumor cells have continued to outwit us in the effort to combat and prevent cancer by exerting a number of mechanisms to evade and suppress anti-tumor immune responses. The present work employs strategies to generate a synthetic extranodal immunoplatform that can harbor both exogenously provided and endogenously recruited immune cells (primed against tumor cells), at the same time providing immuno-factors that support these cells and counter immunosuppressive effects from tumors. We have developed injectable self-gelling alginate formulations for this purpose, enabling sustained release of soluble immunomodulatory factors from the gels and presentation of immobilized immunostimulatory factors inside the gels. The hydrogels injected into the back flanks of mice formed a macroporous structure that allowed easy cell infiltration and migration. Modulation of the mechanical properties of self-gelling alginate was possible by varying the number of calcium-bound microspheres in the gels. During characterization of immune responses using these hydrogels, alginate gels carrying activated dendritic cells (DCs) were shown to dramatically increase the number of T cells recruited to the local injection site. When the dendritic cells were pulsed with antigen, these 'vaccination nodes' were able to initiate an antigen-specific immune response, with some of the injected DCs migrating to the regional lymph nodes and priming cognate T cells. The activated antigen-specific T cells then migrated to the injection site and infiltrated the gels, causing an effector re-trafficking phenomenon that guided both T cells and host dendritic cells to the gels. Taking advantage of this phenomenon, the ability of the vaccination nodes to serve as a peri-tumoral local therapy against established tumors was tested using an ovalbumin-expressing B16F0 subcutaneous melanoma model. When mice bearing 7-day established small tumors (~3mm^2 diameter) were immunized using alginate carrying activated DCs, a mild tumor suppression effect was observed. The anti-tumor effect was augmented by supplementing IL-15 superagonist (IL-15SA) into the gels, which caused suppression of larger tumors (~20-50mm^2), treated 14 days after tumor cell inoculation, and enhanced survival of the mice. In addition to showing therapeutic benefits against established tumors, the matrix-based approach allowed analysis of cells that trafficked locally near the tumor site. The ease of encapsulating factors and the injectable, non-invasive nature of the self-gelling alginate open up possibilities for use in other tissue engineering and regenerative medicine applications.

Thesis adviser: Darrell J. Irvine
Associate Professor

Biographical Note

EDUCATION

2004-2009 Doctor of Philosophy (Ph.D.) in Polymer Science and Technology
Department of Materials Science & Engineering.
Massachusetts Institute of Technology, Cambridge, MA

2000-2004 Bachelor of Science (S.B.) in Materials Science & Engineering
Masachusetts Institute of Technology, Cambridge, MA

2002-2003 Study abroad through Cambridge-MIT Institute exchange program
Department of Materials Science and Metallurgy
The University of Cambridge, Cambridge, UK.

1996-2000 The American School Foundation (high school), Mexico City, Mexico
Valedictorian

PUBLICATIONS

Yuki Hori, Patrick Stern, Richard Hynes, Darrell J. Irvine. "Engulfing tumors with synthetic extracellular matrices for tumor immunotherapy and analysis of local anti-tumor immune responses." (in preparation, May 2009).

Yuki Hori, Amy M. Winans, Darrell J. Irvine. "Modular Injectable Matrices Based on Alginate Solution/Microsphere Mixtures That Gel *in situ* and Co-Deliver Immunomodulatory Factors." Acta Biomaterialia 2009;5:969-982.

Yuki Hori, Amy M. Winans, Catherine C. Huang, Elizabeth M. Horrigan,, and Darrell J. Irvine. ""Vaccination nodes:" Injectable dendritic cell-carrying alginate gels for immunization and immunotherapy." Biomaterials 2008;29(27):3671-82.

Darrell J. Irvine, Agnieszka N. Stachowiak, and **Yuki Hori**. "Lymphoid tissue engineering: Invoking lymphoid tissue neogenesis in immunotherapy and models of immunity." Seminars in Immunology, 2008, 20(2):137-46.

Hyungbin Son, **Yuki Hori**, S.G. Chou, D. Nezich, Ge. G. Somsonidze, G. Dresselhaus, M.S. Dresselhaus, and Eduardo B. Barros. "Environment effects on the Raman spectra of individual single-wall carbon nanotubes: suspended and grown on polycrystalline silicon." Applied Physics Letters, Vol.85, No.20. November, 2004.

ORAL & POSTER PRESENTATIONS

Yuki Hori, Amy M. Winans, Catherine C. Huang, Elizabeth M. Horrigan, and Darrell J. Irvine. "In Vivo Generation of "Vaccination Nodes" for Anti-Tumor Immunotherapy Using Injectable Hydrogels." BMES meeting fall 2008 (St.Louis). [Oral]

Yuki Hori and Darrell J. Irvine. "Immune Cell Recruitment To Injectable Matrices Containing Lymphoid Stromal Cells, Chemokines, or Dendritic Cells *In Vivo.*" Society for Biomaterials Meeting, spring 2007 (Chicago). [Poster]

HONORS/AWARDS

Fitness Member of the Year Award from MIT Zesiger & Alumni Centers (fall 2007)
Best 3B Internship Report (equivalent of senior thesis) Award (from DMSE; spring 2004)
Most Outstanding Student Award (from DMSE; spring 2004)
Certificate of Honor: Cumulative GPA 5.0/5.0 (from DMSE; spring 2004)
Most Outstanding Junior Award (from DMSE; spring 2003).

Acknowledgment

I would first like to thank Darrell for letting me join the Irvine Lab to begin with, and for his support and guidance throughout the past 5 years. Being the first graduate student in the lab to take on an animal work, I had to start from scratch, from developing protocols to performing many of the experiments by myself. Darrell helped balance my conservative skepticism with his optimism, his passion for creating something novel, and his drive for success. Darrell's boundless knowledge from both materials science and immunology complemented many of the empirical approaches I took for pushing the project forward.

I would also like to thank my thesis committee members Professor Linda Griffith and Professor Michael Rubner. Professor Griffith provided insightful suggestions and comments that helped me design future experiments and stay better prepared to answer possible questions from paper reviewers. Professor Rubner asked many questions that encouraged me to think in a big picture, to understand where my research stand compared to the whole cancer immunotherapy and drug delivery fields. I feel very fortunate to have had a committee like this.

Surviving through many of the rough times would not have been possible without the support and encouragement from the members of the Irvine Lab. Agnieszka (Agi) Stachowiak was a senior member of the lab when I first joined the group, and she taught me a lot of laboratory skills, including tissue culture, epifluorescence and confocal microscopy, inverse opal scaffold fabrication, flow cytometry preparation, cell isolation, and many other skills that ended up very useful throughout the whole research experience at MIT, even after my initial project (*in vitro* work involving lymphoid stromal cells) completely changed to a new one (*in vivo* cancer immunotherapy work) at the beginning of my 3rd year in graduate school. I want to thank her patience, time, and effort in teaching me and other members of the lab. I would also like to thank Siddhartha Jain and Junsang Doh, who were also the first members of the lab along with Agi, as well as Heejae Kim, for helping me to get oriented in the lab and for answering questions related to research. Sid also was a great mentor in helping me with job searches during my last year of the graduate school. I am more than thankful to Yana Wang and Maria Foley for their warm friendship and support during the entire graduate school experience. Yana and I joined PPST (Program for Polymer Science and Technology) in the same year, and we went through almost every step of the graduate school life together, from taking classes, studying for the qualifying exams, and writing thesis proposal and performing research. The whole grad school experience would have been very different if it were not for her company and constant encouragement for me to keep going. Maria joined the lab a few months after I did, and her background in biology and her experience in industry brought a lot of positive elements to the lab. On top of being an exemplary scientist for me, she always stayed supportive and encouraging during many of the tough times I have experienced. Special thanks goes to Amy Winans who was my lab technitian for a year, and mainly helped with the *in vitro* characterization of self-gelling alginate as well as with tasks that were painful for my arms which was undergoing constant episodes of inflammation. Cathy Huang also helped me with alginate microsphere synthesis and characterization during a summer as a UROP student. It was also a great experience to have mentored an MEng student Andy Song. It was also nice to have Bonnie Huang and Brandon Kwong as lab mates: Bonnie was very thoughtful and considerate of my arm conditions and Brandon shared with me a lot of reagents and cells. Yuhua Hu and I went through some of our rough times together, and we helped each other de-stress together over

meals and by going exercising. I would also like to thank the past and present post-docs – Yen-Chen Huang, Anurag Maheshwari, Matthias Stephan, James Moon, and Soong-Ho Um as well as the rest of the Irvine lab (past and present) – Anna Bershteyn, Marc Natter, Xingfang Su, Adrienne Li, Prabhani Atukorale, Andy Miller, and Vinay Mahajan for their help and for being great labmates. I would also like to thank Sheree Bean for keeping the lab organized and placing product orders for me, as well as Erin Morehouse especially for her help with processing spleens for some of my tumor experiments.

Without the enormous help from Elizabeth Horrigan (from DCM), all of the *in vivo* mouse work would not have been possible. She anesthesized and shaved the back flanks of mice to prepare them for gel injections, helped with retro-orbital, intradermal, and intraperitoneal injections, and performed retro-orbital bleeding for me. Kathy Cormier and Chakib Boussahmain from the DCM Histology Lab and Denise Crowley and Weijia Zhang from the Koch Institute Histology Lab for their help with histology sections. Philip Erni and Randy Ewoldt from the Hatsopolous Microfluidics Laboratory offered me an immense of assistance with rheometry. Discussions with Philip was extremely helpful in setting up parameters during measurements and analyzing the data in the end.

I would also not have survived the ordeal if it were not for the understanding, help, and encouragement from the people from MIT Medical (especially Jackie Sherry), MGH Occupational Therapy (especially), MGH Physical Therapy (Diana Czulada), and the MIT Disabilities Office (Kathleen Monagle). The staff and friends from Alumni and Zesiger Sports and Recreational Centers provided me with a space and time for relaxation and fun, which was a critical part of my graduate school experience.

It does not suffice just to say "thank you" to my family and friends for always being there for me and providing me with necessary resources to go through hardships. Besides painful experience, we have also shared a lot of fun memories while my past 8-9 years at MIT, starting from my undergraduate education.

Many thanks goes to all the mice that contributed their lives (involuntarily) for my experiments. I hope their lives will add to discoveries and inventions that will help a number of people (and perhaps animals too) in the future.

All the funding agencies that supported the work are acknowledged at the end of chapters 2, 3, and 4.

Table of Contents

Appendix D: Experimental Protocols For *In Vivo* Gel Immunization And Analyses

List of Figures

List of Tables

Chapter 1
Introduction and Motivation

Standing at the interface of materials engineering and immunology, the thesis work presented here seeks to fill in some of the gaps that currently exist in cancer immunotherapy, by using injectable polymeric hydrogels to create a synthetic inflammatory milieu to foster anti-tumor immunity. An efficient immune response requires a fine-tuned orchestration of factors and immune cells at the right moments in the right sequence. By providing a synthetic inflammatory microenvironment that cells can utilize to mount an anti-tumor immune response directly at tumor sites, via delivery of key immune cells (i.e. dendritic cells) and sustained release of anti-tumor factors, we hope to support and guide the responses against malignant tumor cells. This thesis work describes the development and characterization of the injectable hydrogel materials, their role in generating and modulating antigen-specific immune responses when encapsulating and delivering dendritic cells, and their application to tumor thepary.

1.1 Cancer Immunotherapy

1.1.1 Conventional treatments of cancer

Cancer is an uncontrolled and abnormal growth and alterations of otherwise healthy, normal cells in the body, and such malignant neoplasms consist one of the leading causes of deaths in the United States as well as all over the world (1). Conventional methods of treatments for cancer so far have mostly involved external interventions, such as surgery, radiation therapy, and chemo-therapy, in an attempt to remove and reduce cancerous cells and surrounding tissues as well as lymph nodes that may be affected. For example, taking advantage of the tumor's high chemosensitivity, multiple drugs have been developed against ovarian cancer (2). Treatment of colon cancer often involves surgical removal of polyps in the colon (2). Solid tumors are usually responsive to radiation therapy (3), which is also used for late stage melanoma patients as a palliative treatment(4). However, despite the increased detection accuracy and application of the above mentioned treatments, the battle against cancer still remains a war not yet won (5). One of the limitations of cancer therapy based on conventional interventions is that the body itself is unprotected from future recurrences, and treatment of primary as well as metastatic tumors becomes difficult when tumors are not easily accessible by surgery. As a result, cancer immunotherapy, utilizing the body's own immune system to reject cancer and create a systemic protective immunity within the host's body, has become an intensively researched cancer therapy

strategies in recent years. Ideally, immunotherapy not only treats the existent, detectable tumors but also generates a systemic memory of tumor antigens to protect against recurrence as well as to eradicate metastatic malignancies.

1.1.2 Role of the immune system in responses against tumors

Tumor immunotherapy relies on the ability of the body's immune system to recognize cancerous cells as a danger. The potential of the immune system to fight against cancer was first observed in 1890 by William Coley, when inoperable sarcoma patients were successfully treated by injection of *Streptococcus erysipelas* bacterial cultures (6). Increased incidences of cancer in immunocompromised hosts (7-9) as well as mice lacking specific sets of immune cells, including T cells, natural killer (NK) cells, and NK T cells (10-12), and other immune-related factors, such as interferon-γ (IFN- γ; a cytokine that increases the killing capacity of cytotokic $CD8^+$ T cells) (11, 13-16) and perforin (a cytolytic granule in T cells and NK cells that participate in cytolytic killing of target cells) (17-19) , and spontaneous disappearance of malignancies in immunocompetent patients also point to the importance of the immune cells in controlling cancerous growths (20). The idea that components of the immune system are capable of fighting against cancer is called cancer immunosurveillance (21-23). The presence of tumor-infiltrating lymphocytes (TILs), such as $CD8^+$ T cells (24, 25) and NK cells (26-28), in cancer patients has been demonstrated to be a favorable prognosis of the survival of the patients. Other cell types that are known to be important for tumor suppression and eradication include dendritic cells (29, 30), $CD4^+$ T cells (31), and interferon-producing killer dendritic cells (IKDCs) (32, 33).

Under ideal situations, an anti-tumor immune response would involve antigen presenting cells (APCs), particularly dendritic cells, recognizing the tumors as a danger and activating the cognate oncoantigen-specific T cells (Figure 1-1). Tumor antigens are believed to either drain to the lymph nodes via lymphatics or be picked up by dendritic cells and brought to the lymph nodes (34). $CD8^+$ cytolytic T-cells (CTLs) activated in the lymph nodes by dendritic cells would then migrate to the tumor site and kill the tumor cells, mainly via degranulation of cytotoxins such as perforin and granulysin. $CD4^+$ T cells both help regulate and maintain the $CD8^+$ T cell response (35, 36) as well as actively participate in the anti-tumor immune response by secreting cytokines that activate both Th1 (proinflammatory response against intracellular pathogens) and Th2 responses (allergic responses that mainly involve eosinophils) (31). The innate arm of the immunity also plays an important role in responses against cancer; immunosurveillance by NK cells involves degranulation of perforin, expression of Fas Ligand (inducer of apoptosis), and TRAIL (TNF-related apoptosis-inducing ligand)-mediated effector functions (37, 38). NK cells, upon proper activation, can also provide help to dendritic cells during anti-tumor responses (39). NK T cells recognize self- and foreign lipids and glycolipids in the context of CD1d molecules on target cells, and rapidly secrete cytokines such as IL-4 and IFN- γ (40). Macrophages infiltrating the tumor bed can produce IL-12, which causes more IFN- γ production by NK cells; macrophages themselves, upon exposure to IFN- γ, can also exert tumoricidal mechanisms (41, 42). The cells of the innate immunity, through cytokine secretion and non-specific killing of tumor cells, facilitate release of tumor antigens from dead tumor cells and recruit tumor antigen-specific effectors of the adaptive immunity, leading to the activation of antigen-specific T cells.

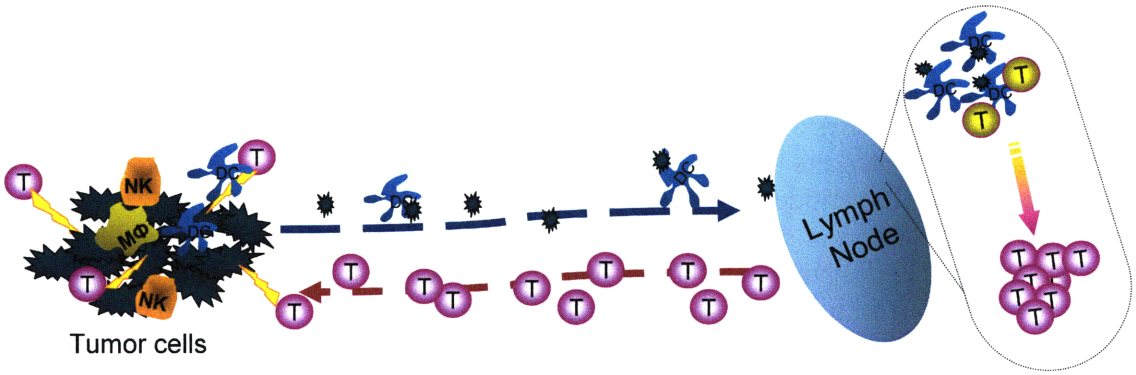

Figure 1-1: Schematic of an anti-tumor immune response. An ideal anti-tumor response is initiated when cells of the innate immunity, such as NK cells and macrophages, liberate tumor antigens. The tumor antigens can either drain to the lymph nodes themselves, or be picked up by dendritic cells for transport to the regional lymph nodes, where antigen-specific T cells are activated. The activated effector T cells then migrate to the tumor site and attack the tumor cells.

Ironically, however, these effectors in both innate and adaptive immune responses against cancer in reality also have the potential of promoting tumor development. In the recently-refined notion of immunosurveillance, called the immunoediting hypothesis, immunosurveillance consists of the 'elimination' phase of an anti-tumor response (43). With the increased immune pressure on the tumors, mutations occurring in the surviving tumor cells select for tumors resistant to immune elimination. Tumor cells downregulate their antigen as well as MHC I expressions (44), upregulate anti-apoptotic signals (45), and become insensitive to IFN- γ (15). In the 'equilibrium' phase that follows after any tumor variant survives the initial elimination phase, lymphocytes are able to control tumor growth but not completely eliminate them. The tumor cells that selectively survive the equilibrium phase then enter the 'escape' phase and continue to grow, showing resistance to immune responses (43). It is usually in this escape phase when tumors become clinically detectable. The immune system thus inadvertently takes the dual task of generating a response that is supposed to be a beneficial, tumor-eliminating response, and one that sculpts the tumors to become more aggressive and uncontrollable. Cancer vaccines are thus being developed to overcome the growing and resistant tumor cells to push the tumor-immune system dynamics back towards the elimination phase.

1.1.3 Existing cancer vaccines and those in development

With the recognition of the ability of the immune cells to fight against tumor cells, cancer vaccines have been in development in hope to boost and support the immune responses against tumors. Traditional vaccines that are already in clinical use are prophylactic, or preventive, vaccines against viruses, bacteria, or fungi to prevent future infection, whereas cancer vaccines can either be prophylactic or therapeutic (targeting to treat existing cancers). Despite the amount of research in the development of cancer vaccines, only a few cancer vaccines have been approved by the US Food and Drug Administration, including vaccines against hepatitis B (which can lead to certain types of liver cancer) and human papillomavirus (HPV; which can

cause cervical cancer), which are both prophylactic against viruses that may cause cancer (46). Therapeutic vaccines that are under investigation and in clinical trials can be divided into several categories: 1) monoclonal antibodies; 2) peptide vaccines; 3) whole cell tumor vaccines; 4) dendritic cell vaccines; 5) viral vectors and DNA vaccines; and 6) idiotype vaccines (46, 47). Monoclonal antibody vaccines are passive immunotherapy strategies; monoclonal antibodies are directed against surface markers that are over-expressed on tumor cells, which can keep the tumor growth on hold. In peptide vaccines, peptides, or protein fragments of tumor antigens, that are shared amongst the same type of cancer or isolated from patients, are directly injected into patients along with adjuvants (substances that help stimulate the immune system to produce a sufficient response to eliminate the target). Collections of tumor lines or tumor cells taken from patients themselves can also be used as a whole cell tumor vaccine to present a mixture of antigens that can potentially stimulate an immune response. Dendritic cell vaccines are autologous cell vaccines that involve isolation of patients' dendritic cells from peripheral blood. The dendritic cells are then expanded, matured, and loaded with tumor antigens *ex vivo*, after which they are injected back into the patients in hope to activate the antigen-specific T cell population. Tumor antigen proteins can also be generated using viral vectors and DNA to transduce dendritic cells to express the tumor antigens. If generated successfully, the immune response can be directed against dendritic cells expressing the onco-antigens and subsequently attack the tumor cells. Idiotype vaccines target the B-cell receptor of B-cell malignancies as a unique antigen, and recombinant forms of these receptor proteins can be injected into patients like peptide vaccines.

Despite the many forms cancer vaccines take, the essential components of cancer vaccines generally include the antigen that the specific target tumor expresses, and an adjuvant that stimulates the immune system to produce a sufficient response to eliminate the target. The antigen used should ideally be expressed only on the tumor cells and not on normal cells, and should be carefully selected, depending on whether humoral or cellular immune responses are to be induced (48). There are many adjuvants used in cancer as well as other types of vaccines, including cytokines (49), dendritic cells (which are considered to be physiological adjuvants) (50), alum (51), MPL (monophosphoryl lipid A) (52), and MF59(53).

Since efforts from individual scientists and researchers trying to find a cure for cancer using monotherapies have generally been unsuccessful, cancer immunotherapy is now entering a new era of combination therapies, combining different vaccine strategies as well as combining immunotherapy with the traditional cancer therapy strategies like chemotherapies.

1.2 Challenges in Cancer Vaccines

Despite much of the effort that has gone into finding therapeutic vaccines for cancer, tumor cells exert multiple mechanisms to survive anti-tumor immune responses and hamper the generation of effective anti-tumor response. Tumor cells are derived from the host's own cells, and they mostly express self-antigens that the host immune system is tolerant against, making the tumor antigens very weakly immunogenic (54). Even when a successful immune response is initiated in the host, the tumor cells evade (immune evasion) or locally suppress (immunosuppression) the immune responses (47). Mechanisms of immune evasion by tumor cells include stromal barrier formation and secretion of factors that prevent efficient DC maturation and attainment of proper effector functions (55-57); tumors also establish a positive

pressure gradient to hinder lymphocyte infiltration into the tumors (47). Even when antigen-specific effector cells are generated, the infiltration of these cells into the tumors has been limited (58-61). In addition, tumor cells also actively suppress the immune responses via secretion of factors, such as those that impair the functions and proper maturation of dendritic cells, causing local accumulation of immature myeloid-derived suppressor cells (62). These myeloid suppressor cells disable antigen recognition by $CD8^+$ T cells by nitration of TCR-CD8 T cell receptor complex, inducing $CD8^+$ T cell anergy (63). Tumor cells also downregulate the production of TNF-α and nitric oxide from macrophages inside the tumors, making the macrophages less tumoricidal than the ones that participate in non-tumor related inflammatory activities, while the tumors cause an increase in the level of nitric oxide, which is known to suppress lymphocyte activity, distal to the tumor site, suppressing the anti-tumor effector functions of circulating lymphocytes (64). Recruitment of regulatory T cells, cells that normally regulate the extent of inflammation to prevent autoimmune diseases and overly activated immune responses, to the tumor bed further inhibits anti-tumor immune responses (65, 66).

Both immune evasion, preventing therapeutic agents to circulate into the tumor core using the tumor barrier, and immunosuppression by tumors play a large role in why effective cancer vaccines have not been developed yet. Currentt attempts in finding an effective cancer vaccine thus focus on countering immunosuppression from tumors, rescuing the dormant, immunosuppressed effector cells.

1.3 'Vaccination Nodes': Motivation and Significance

1.3.1 Hypothesis

In order to address some of the challenges that have faced cancer immunotherapy, we have hypothesized that by providing a synthetic microenvironment as a 'military base,' for both exogenously injected and endogenously recruited effector cells right next to the tumor cells, but possibly protected from multiple negative effects of the tumor itself, we would be able to mount a vigorous response against cancer cells (Figure 1-2). Many of the current vaccine strategies seek to promote the robust infiltration of tumors with functional immune cells to promote tumor destruction. However, defects in tumor vasculature, suppressive signals produced by tumor cells or co-opted tumor-resident immune cells, and rapid tumor growth can limit the ability of activated and competent immune cells from accumulating. Peri-tumoral provision of an inflammatory milieu using injectable hydrogels could potentially concentrate immune effector functions at the tumor site and maintain a continuous infiltration of effectors, thus maintaining the adaptive phases of anti-tumor responses, which usually fail to take place in many of the immunotherapy strategies explored so far.

Furthermore, in addition to providing a scaffold for anti-tumor immune cells, we hypothesized that the injectable matrix could also enable delivery of immunoregulatory factors that can facilitate anti-tumor immune responses. Systemic administration of high dosages of factors that have anti-tumor properties, such as Interleukin-2 (IL-2), are known to be toxic to patients (49, 67). Thus, sustained release of immunocytokines and other immunomodulatory factors from gels or microparticles at a tumor site has been explored and demonstrated to enhance local immunotherapies by reducing systemic exposure to these potent factors and

provide more sustained local concentrations of these factors at the tumor site (49, 67-69). Local application of certain combinations of cytokine, chemotherapy, and/or immunostimulatory ligand treatments to treat established tumors has shown promise in not only eliminating treated tumors but also generating systemic immunity capable of destroying large distal tumors (49, 69). Thus, the use of biomaterials to deliver local combinatorial immunotherapies may lead to further enhancements in the potency and safety of such treatments.

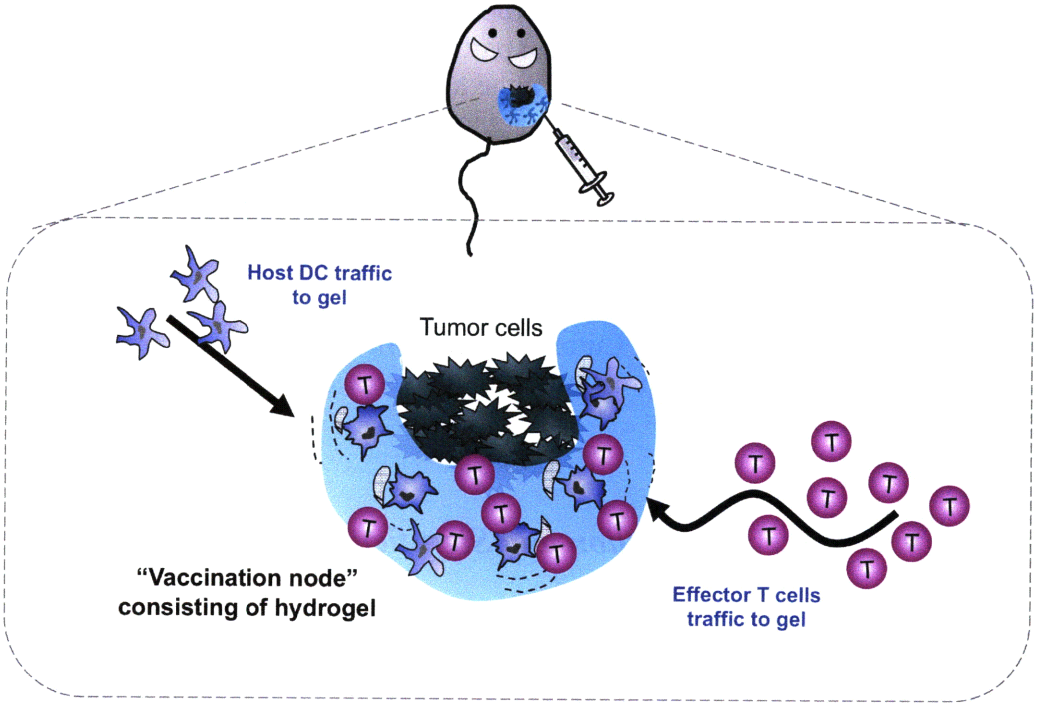

Figure 1-2: Schematic of the concept of our 'vaccination node' hypothesis. We hypothesized that by creating a synthetic immunoplatform that can attract a number of effector cells equipped to fight against cancer cells to the injection site, we would be able to concentrate and direct the effector functions against tumors at the tumor site. The hydrogel material would act like a 'military platform' that the endogenous cells can use to mount a response against the tumor cells.

Matrix-based immunotherapy moreover allows for examination of cells that traffic around the tumors. Several studies have suggested that events that occur systemically and locally during anti-tumor responses are not correlated (64, 70); for example, systemic generation of antigen-specific T cells has not always resulted in the presence of the antigen-specific effector cells inside the tumor microenvironment (58, 60, 61). The dissociation of systemic and local responses against cancer indicates a necessity for understanding what exactly happens locally at the tumor site. Tumor-infiltrating cells (TILs) have provided valuable insight into the prognosis of cancer patient survival (29, 71-73). However, tumor-free survivors do not have any tumors to be analyzed, and local anti-tumor mechanisms that have taken place in these patients cannot be studied. Matrix-based immunization, therefore, allows for identification and analyses of cells that are attracted to the peripheral site even for tumor-free survivors. The preliminary studies

conducted to select an injectable matrix material appropriate for our applications are shown in Appendix A.

1.4 Outline of thesis work

The battle against cancer involves an intricate and often delicate balance between cancerous cells evading and suppressing anti-tumor responses and immune cells, both specific and non-specific for onco-antigens, attempting to control and eliminate the malignant, abnormally growing cells. In this thesis work, we demonstrate that providing a scaffold, or a 'military base,' for endogenous effector cells near tumor masses to mount a vigorous response against cancer cells, and concentrating effector functions of the anti-tumor response at the tumor site, help tip the balance in favor of the fighting effector immune cells in controlling tumor growths and survival time of the mice. In Chapter 2, we show the development and characterization of injectable self-gelling alginate hydrogels. Since alginate forms gels almost instantaneously from the point of contact with soluble calcium ions, addition of calcium ions makes the gel difficult to be injected using regular syringes. By way of providing an internal source of calcium uniformly throughout the alginate matrix precursor solution, using 'calcium reservoir microspheres' (CRMs), also synthesized with alginate, the alginate becomes injectable. In Chapter 3, 'vaccination nodes' consisting of self-gelling alginate encapsulating activated, mature bone-marrow derived dendritic cells (BMDCs) are shown to mediate an antigen specific response and re-traffic the effector T cells and dendritic cells to a desired peripheral injection site. The phenomenon was a product of a synergistic effect between the activated dendritic cells and alginate and not of dendritic cells alone. Studies using these vaccination nodes as an immunotherapy against established tumors are shown in Chapter 4. We demonstrate that co-delivery of IL-15 superagonist (receptor-cytokine complex) improves the tumor growth inhibition effect and the survival length of the mice treated. Incorporation of IL-15 complex, furthermore, obviated the need for *ex-vivo* expanded dendritic cells, and improvement of tumor growth control and survival was achieved by giving a second immunization to the mice at the tumor site. The injectable alginate hydrogel, in addition, not only allowed for a sustained release of immunomodulatory factors and production of a local inflammatory milieu, but also let us study the fingerprints of cells that traffic to the tumor/injection site that correlated well with the success of the vaccination. Self-gelling alginate thus is a versatile matrix material that can be used to deliver various immuno-factors and provides a robust tool for examining and modulating the effect of these factors as well as the cell types that participate in the local anti-tumor responses.

Chapter 2
Development and Characterization of Self-Gelling Alginate

In this chapter, we describe the development and characterization of injectable alginate formulations via self-gelation strategy. The injectable nature of the hydrogel renders the material suitable for clinical applications and friendly to patients receiving potential cancer treatments using the self-gelling alginate system.

2.1 Introduction

Alginate is a natural polysaccharide commonly obtained from brown seaweed, which forms a physical hydrogel in the presence of divalent cations such as calcium. Due to its biocompatibility, mildness of gelation conditions, and low immunogenicity, purified alginate has been widely used in food and pharmaceutical industries, as well as for many biomedical, biomaterial, and therapeutic applications (74-78). Alginate chains are multiblock copolymers consisting of poly-D-mannuronic acid (M) blocks, poly-L-guluronic acid (G) blocks, and alternating G/M blocks. The size, proportions, and the distribution of each block influence both the physical and chemical properties of alginate, with G units contributing to the crosslinking capacity through stereocomplexation in an "egg-box" conformation(79), while M and G/M blocks provide flexibility to the resulting networks. Alginate is stable against breakdown by mammalian enzymes but dissolves and can be eliminated through the kidneys *in vivo*; alternatively, partial oxidation of uronic units of sodium alginate can be used to make alginate susceptible to hydrolytic breakdown *in vivo*(80-82).

Because of the cooperative nature of crosslinking by G units and the small size of the crosslinking ions, gelation of alginate can occur very rapidly. For example, aqueous alginate solutions added dropwise into a calcium-containing aqueous bath form gel beads via rapid diffusion of calcium into the alginate. Such 'external gelation' methods have been employed for entrapment of cells or macromolecules into microbeads for therapeutic agent delivery (75, 76, 83). Alternatively, 'internal' gelation methods have been developed, in which the gelling ions are supplied from within an initially soluble alginate solution. For example, calcium salts with low water solubility, such as carbonate, sulfate, and phosphate (74, 84-87) can be mixed with alginate precursor solutions; slow dissolution of these inorganic calcium sources controllably crosslinks the surrounding alginate solution. Since many calcium salts and complexed ions show

pH-dependent solubility, molecules such as polyphosphate or ethylenediamine tetraacetic acid (EDTA) (84, 88, 89) or chloride compounds such as ammonium chloride(88) may be added to alginate solutions to promote gradual release of calcium by changing the pH of the release medium.

To achieve non-invasive delivery of alginate gels for biomedical applications, variations on the concept of internal gelation have been employed to create 'self-gelling' formulations of alginate that facilitate injection of alginate followed by *in situ* crosslinking *in vivo*. Melvic et al (90) lyophilized calcium alginate gels and milled these dried solids to form calcium alginate particles, which were used as a source of slowly-released calcium ions when mixed with soluble alginate solutions. Thermally triggered release of calcium from phospholipid vesicles mixed with alginate solutions, employing liposomes that rupture at a physiological temperature, has also been demonstrated as a method for *in situ* formation of alginate hydrogels (91). Alternatively, for applications where soft gels are suitable, alginate with low levels of calcium added can be formulated as a viscous solution that is still injectable (92).

In this chapter, we show characterization of the mechanical properties and structure of gels formed from self-gelling alginate formulations, utilizing internal calcium source from calcium reservoir alginate microspheres, *in vitro* and *in vivo*. Compositions were chosen such that the gels form low-viscosity solutions amenable to mixing/drawing in a syringe, and set to fstable gels following injection via crosslinks contributed by ions in the interstitial fluid *in vivo*. A similar strategy of injecting low-viscosity calcium-crosslinked alginate (via homogenization and dispersion of calcium gluconate in a sodium alginate solution) followed by gelation *in situ* has also been successfully employed for repair of myocardial infarction in rats in a recent study by Landa, et al(93). In addition, we explored strategies to enhance the function of these gels in immunotherapy, via the co-delivery of the immunomodulatory factors interleukin-2 (IL-2) and CpG oligonucleotides in the matrix. We thus demonstrate two different strategies for incorporating factors into these injectable matrices, encapsulation within the bulk matrix (IL-2), or electrostatic anchoring to the surfaces of embedded alginate microspheres (CpG oligos). By variable combination of these strategies, a flexible platform for cell delivery and supporting factors is obtained. This modular approach to augmenting an injectable, biocompatible gel that supports cellular infiltration with slow release of cytokines or presentation of factors immobilized within the matrix may be useful in a range of soft tissue regenerative medicine applications, in addition to our particular interest in immunotherapy of cancer.

2.2 Materials and Methods

2.2.1 Materials

Sterile alginates Pronova SLM20 (MW 75,000 – 220,000 g/mol, >50% M units; endotoxin level <25EU/g) and Pronova SLG20 (MW 75,000 – 220,000 g/mol, >60% G units; endotoxin level <25EU/g) were purchased from Novamatrix (FMC Biopolymers, Sandvika, Norway). All antibodies were purchased from BD Biosciences (San Jose, CA). 2, 2, 4-trimethylpentane (isooctane, ChromAR grade, 99.5% purity) was obtained from Mallinckrodt Baker (Phillipsburg, NJ). Poly-L-lysine hydrobromide (MW 30,000-70,000 g/mol), FITC-poly-L-lysine hydrobromide (MW 30,000-70,000 g/mol), and 6-aminofluorescein were obtained from Sigma-Aldrich (St. Louis, MO). Mag-fura-2 tetrapotassium salt, was purchased from Invitrogen (Carlsbad, CA). CpG oligonucleotides with a phosphorothioate backbone (CpG 1826, sequence

5'-/5AmMC6/TCC ATGACGTTCCTGACGTT-3') and FITC-CpG (FITC-CpG 1826, sequence 5'-/5AmMC6/ TCC ATGACGTTCCTGACGTT/36-FAM/-3') were synthesized by Integrated DNA Technologies (Coralville, IA). Recombinant murine IL-2 was purchased from Peprotech Inc (Rocky Hill, NJ). Hilyte Fluor™ 647 amine was purchased from Anaspec, Inc (San Jose, CA), and Slide-A-Lyzer Dialysis Cassettes (7000MWCO) from Pierce Biotechnology (Rockford, IL). All other chemicals were purchased from Sigma and used as received unless otherwise stated.

2.2.2 Fluorescent labeling of alginate

SLM20 alginate (0.02g/mL) was mixed with 9 mM EDC (1-Ethyl-3-[3-dimethylaminopropyl]carbodiimide hydrochloride) and 9 mM sulfo-NHS (*N*-hydroxysulfo succinimide) in PBS at 20°C for 2 hrs. An equal volume of 6-aminofluorescein (4.5 mM in 70% ethanol) or Hilyte Fluor 647 (0.32 mM in water) was added to the alginate solution containing EDC/Sulfo-NHS and reacted at 20°C for 18 hrs while rotating. The resulting solution was then dialyzed (7 KDa MWCO) against 1 L PBS at 4°C for 3 days with 3-5 changes of the dialysis bath. Labeled alginate solution was adjusted to a concentration of 0.01g/mL in PBS, sterile-filtered and stored in the dark at 4°C until use.

2.2.3 Calcium reservoir microsphere synthesis and self-gelling alginate

Alginate microspheres were synthesized (see Appendix C.1 for detailed protocol), with 1.5 mL sorbitan monooleate, 0.5 mL polyethylene glycol sorbitan monooleate, and 35 mL isooctane, homogenized for 3 min using an UltraTurrax T25 homogenizer (IKA Works, Wilmington, NC) at a speed of 8x1000/min. Pronova SLG20 solution (0.01 g/mL in PBS, 400 μL) was added and homogenized for 3 min, followed by addition of 25 μL aq. $CaCl_2$ (0.05 g/mL) with homogenization for 4 min. The resulting particles were washed once with 30 mL isooctane and 3X with 1 mL of deionized, distilled (95) water, then resuspended in DD water for a final volume of 1 mL and stored at 4°C until use. Microsphere sizes were determined from optical micrographs taken with a Zeiss Axiovert 200 epifluorescence microscope at 40X and analyzed with MetaMorph software (Molecular Devices, Downingtown, PA). Endotoxin levels in the microspheres were assessed using the QCL-1000® Endpoint Chromogenic LAL Assay (Lonza, Basel, Switzerland) according to the manufacturer's instructions. This measurement on high-G alginate microspheres yielded 0.000615EU/ug particles, well below levels stimulatory for innate immune cells (96-98).

Self-gelling alginate gels were formulated by pelleting calcium reservoir SLG20 microspheres (quantities as noted in the text), resuspending the particles in a minimal residual volume of water with a bath sonicator for 2 min, and adding Pronova SLM20 (0.01g/mL in PBS) alginate matrix to a constant final volume (i.e. 170 μL microspheres+alginate), dispersing microspheres throughout the solution. For delivery of self-gelling alginate *in vivo*, 150μL of microspheres/solution mixture was immediately drawn by an insulin syringe (28gauge, BD Biosciences) and injected *s.c.* in anesthetized mice.

2.2.4 Ca^{2+} quantification in alginate microspheres and self-gelled alginate

Alginate microspheres (100 μL of stock suspension) were pelleted and dissolved with EDTA (ethylenediaminetetraacetic acid disodium salt dehydrate; 100 μL, 2.5mM in water) and 890 μL PBS, with 10 min of sonication. Mag-fura-2 dye (5 μg/mL) was added to the dissolved microsphere solution and fluorescence was recorded on a SpectraMax M2 Microplate Reader (Molecular Devices, Sunnyvale, CA) at 340ex/515em and 380ex/515em in a flat-bottom 96-well UV-transparent plate (BD Falcon, Franklin Lakes, NJ) alongside a series of Ca^{2+} dilution standards. Calcium levels were determined using the ratio of emission intensities recorded from 340 nm and 380 nm excitation, calibrated to calcium concentration by the standard dilutions and accounting for the fraction of calcium chelated by EDTA. In parallel, some microsphere samples were dissolved with EDTA and elemental analysis was performed using inductively coupled plasma optical emission spectroscopy by Quantitative Technologies, Inc. (Whitehouse, NJ). Elemental analysis on in vitro-formed or explanted gels was performed following digestion of gels with 100 μL of 100 mM EDTA and100 μL of 10 mg/mL alginate lyase for 24 hrs at 20°C or until dissolved.

2.2.5 Kinetics of Ca^{2+} redistribution in self-gelling formulations

For time-lapse microscopy analysis of Ca^{2+} redistribution from microspheres into alginate solutions, 200 μL of alginate matrix solution (0.01 g/mL SLM20) pre-incubated with 25 μg/mL mag-fura-2 solution for 2 hrs was imaged in a 8-well Labtek chambered coverslip (Nalge Nunc, Rochester, NY) on a Zeiss Axiovert 200 epifluorescence microscope equipped with a CoolSnap HQ CCD camera (Princeton Instruments Inc., Acton, MA). Time-lapse fluorescence images of the samples were collected at 340 nm ex/515 nm em and 380 nm ex/515 nm em at 45 sec intervals for 10 min using a 40x objective to establish the baseline fluorescence. Microspheres ($1.25x10^6$) were then mixed with the matrix solution containing the dye and time-lapse recording of mag-fura fluorescence was continued for 60 min. All data was acquired and fluorescence emission ratios (340 ex:380 ex) were analyzed using Metamorph software.

Complementary Ca^{2+} redistribution measurements were made for bulk solutions using a fluorescence plate reader: calcium reservoir microspheres were mixed with matrix alginate and at staggered timepoints following mixing, microsphere/SLM20 solutions were centrifuged at 16000*xg* for 10 min to separate microspheres from the alginate solution. The supernatant solution was mixed with mag-fura-2 dye (5 μg/mL) in a UV-transparent 96-well plate and fluorescence signals were acquired using a SpectraMax M2 Microplate Reader and analyzed as described above.

2.2.6 Shear modulus measurements

The shear moduli (G' and G'') of self-gelled alginate gels were measured using a parallel plate configuration on an AR-G2 rheometer (TA instruments, New Castle, DE) connected to a Julabo F25 Refrigerated/Heating Circulator (Seelbach/Black Forest, Germany). Self-gelling alginate containing different amounts of SLG20 microspheres were mixed and immediately pipetted onto the bottom plate and were allowed to gel for 1 hr at 25°C. A solvent trap cover was used to prevent water loss during gelation/measurements. Oscillatory shear was then applied at an angular frequency of 1 rad/s and a controlled strain of 5% with 450μm gap, a

condition that showed minimal wall slip effects. Time sweep measurements were taken for 35 min (the moduli reported are the time-averaged values), followed by frequency and strain sweeps for each sample.

2.2.7 Animals and cells

Animals were cared for in the USDA-inspected MIT Animal Facility under federal, state, local and NIH guidelines for animal care. C57Bl/6 mice and C57Bl/6 mice expressing green fluorescent protein (GFP) under the chicken β-actin promoter and cytomegalovirus enhancer were obtained from Jackson Laboratories. Bone marrow-derived dendritic cells (BMDCs) were prepared by isolating bone marrow from the tibias and femurs of C57Bl/6 mice or GFP^+ mice and culturing them *in vitro* over 6 days in the presence of 10ng/mL GM-CSF in complete medium (RPMI 1640 containing 10% FCS, 2 mM L-Glutamine, penicillin/streptomycin, and 50 μM 2-mercaptoethanol) following a modification of the procedure of Inaba (99) as previously reported (100). BMDCs were used on day 6 or 7 as resting immature DCs or stimulated with CpG overnight (~18 hrs) as activated mature DCs.

2.2.8 IL-2 release from self-gelling alginate in vitro

Alginate particles ($3x10^6$) were pelleted as above, mixed with 2 μg IL-2 (100μg/mL) for 18 hrs at 4°C, and then directly added to 1% Pronova SLM20 (140 μL of 0.01g/mL in PBS) matrix to form a gel. All samples were allowed to gel at 37°C for 2 hrs while gently shaking, followed by a gentle wash with 1 mL of complete medium. Release studies were conducted by adding 1mL of the complete medium to gels at 37°C; 950 μL of supernatant was removed at each time point over 7 days and fresh medium added to replace that withdrawn. The supernatants were stored at 4°C until all the time points were collected, and on day 7 the alginate gels were digested with 10mg/mL alginate lyase for ~20 min at 37°C to recover all remaining cytokine. The amounts of cytokine in supernatants from each sample were quantified by sandwich ELISA according to the manufacturer's instructions (R&D Systems, Minneapolis, MN). The bioactivity of IL-2 released from alginate was tested by measuring proliferation induced in the IL-2-dependent cell line CTLL-2 (generously provided by Laboratory of Prof.Dane Wittrup at MIT) compared to solution standards of IL-2, using the WST-1 proliferation assay (Roche Applied Science, Mannheim, Germany) according to the manufacturer's instructions, with 10,000 CTLL-2 cells/well in a 96-well plate and 48-hour incubation before adding WST-1.

2.2.9 CpG/Poly-L-Lysine-coated alginate particles and BMDC stimulation

Alginate microspheres synthesized under sterile conditions were incubated with 2 mg/mL poly-L-lysine in sterile DD H_2O for 2 hr at 20°C while rotating with a Labquake rotator, washed 3X with 1 mL of sterile DD H_2O, followed by incubation with 50 μM CpG or FITC-CpG (in PBS) solution (5 nmoles CpG/FITC-CpG per 10^6 particles) overnight at 4°C while rotating. The microspheres were washed 3X again with sterile DD H_2O and resuspended at a concentration of $10x10^6$ particles/mL.

Microspheres (10^6 or $0.5x10^6$ unmodified, Poly-L-lysine coated, or CpG/PLL-coated) or control soluble CpG were added to day-5 BMDC cultures containing 10^6 cells/mL and incubated

at 37°C for 18 hrs. Treated or control BMDCs were harvested from culture plates, blocked with 10 μg/mL anti-CD16/CD32 antibody for 10 min at 4°C, and stained with fluorescent antibodies against surface markers (CD11c, I-A^b, and CD40) for 20 min on ice. Stained cells were analyzed on a BD FACSCalibur flow cytometer (BD Biosciences).

2.2.10 FITC-CpG release from FITC-CpG/PLL alginate microspheres

FITC-CpG/PLL-coated alginate microspheres were prepared as described above, and 10^6 particles were either aliquotted into Eppendorf tubes by themselves or encapsulated into self-gelled alginate (140 μL 0.01 g/mL SLM20 in PBS + $3x10^6$ calcium reservoir microspheres) containing 11 mM calcium. Samples were washed once with 1 mL of phenol-red free RPMI 1640 with 10% FCS. Release measurements were initiated by adding 300 μL of complete medium (phenol-red free); at each timepoint the supernatant was collected and 300 μL fresh medium added to the samples over a 7-day period. The amount of FITC-CpG released into the media was quantified by the intensity of FITC fluorescence in the supernatant using a Perkin-Elmer HTS 7000 Plus Bio Assay Reader (Waltham, MA) with 492 nm ex and 535 nm em, calibrated by a serial dilution of FITC-CpG standard solutions.

2.2.11 Fluorescence and reflectance-mode confocal microscopy

For *in vitro* samples, SLM20 alginate labeled with 6-aminofluorescein (130μL of 0.01g/mL in PBS) was mixed with $4x10^6$ calcium reservoir microspheres (~14.8mM Ca^{2+}). For injected gels, C57Bl/6 BMDCs ($2x10^6$) were washed 3X with PBS and mixed with 160 μL fluorescently-labeled SLM20 (0.01 g/mL in PBS) and 10^6 calcium-reservoir microspheres, then 150μL of the alginate/cell suspension was injected *s.c.* into the flanks of anesthetized C57Bl/6 or GFP^+ mice with a 28 gauge insulin syringe (BD Biosciences). Animals were euthanized and gels were explanted from mice 22-48 hrs after inoculation and imaged using a Zeiss LSM 510 confocal microscope (Thornwood, NY). Reflectance mode imaging was obtained by collecting back-scattered light using a 488nm laser for illumination. 3D reconstructed images were obtained through 100-300 μm depths in 1-2 μm *z*-steps using a 40x water-immersion objective. 3D reconstruction and projections over multiple *z*-planes were processed using Volocity software (Improvision Inc, Waltham, MA).

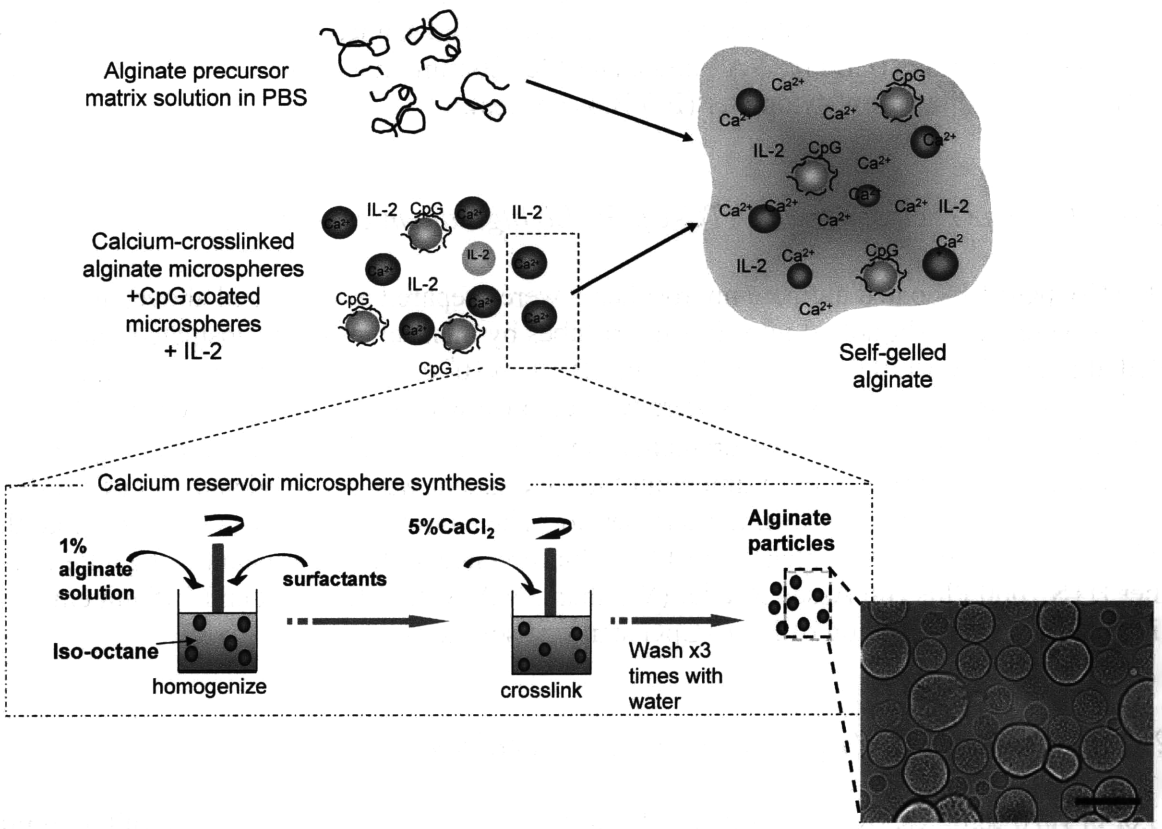

Figure 2-1: Schematic of self-gelling alginate formulations based on calcium reservoir alginate microspheres. Calcium-crosslinked alginate microspheres and microspheres modified with CpG oligonucleotides are mixed with soluble 'matrix' alginate in PBS containing soluble IL-2 (which may also contain cells or other factors). Diffusion of calcium ions in the microspheres into the surrounding solution induces crosslinking of the soluble alginate and gel formation. The inset figure outlines the process of calcium reservoir alginate microsphere synthesis via a water-in-oil emulsion of alginate in isooctane in the presence of surfactants. The micrograph shows the brightfield optical micrograph of as-synthesized calcium-crosslinked alginate microspheres (scale bar:50 μm).

2.3 Results and Discussion

2.3.1 Characterization of calcium-reservoir microspheres

Prior studies have demonstrated that alginate microspheres of sizes 1-250 μm diameter can be prepared using water-in-oil emulsions (101, 102). Similarly, we synthesized calcium-loaded alginate microspheres by emulsification of an aq. solution of alginate in isooctane containing surfactants, followed by crosslinking of alginate droplets via addition of aqueous calcium to the emulsion (Figure 2-1). In order to form microsphere reservoirs that could bind substantial amounts of calcium, particles were formed from high-G alginate (Pronova SLG20, >60% G unit), based on the higher affinity of G units of alginate for calcium compared to M units (79, 103, 104). Each synthesis produced ~$10x10^6$ calcium reservoir microspheres (CRMs) and the resulting microspheres had mean diameters of 12 μm ± 9 μm with a pellet volume of ~10 μL per

10^6 microspheres. Calcium loading was measured by dissolving the microspheres with EDTA and PBS, followed by measurement of released ions using the calcium-sensitive fluorescent dye mag-fura-2 (105-107). Using this technique, the microspheres were found to contain an average of 1.5 ± 0.2 μmol of Ca^{2+} per mg alginate ($n > 10$ independent batches of particles). Elemental analysis of these samples yielded an average of 1.6 ± 0.2 μmoles of Ca^{2+} (n=6), consistent with the fluorescence assay. The microspheres exhibited no swelling over the course of a week and were stable for at least 7 days in water. Analysis of the supernatant from CRM suspensions using mag-fura-2 indicated that the concentration of free Ca^{2+} in the supernatant was effectively zero and little Ca^{2+} was released into the aqueous phase during storage.

2.3.2 Gelation of alginate solutions using calcium-reservoir microspheres

The concept of self-gelling alginate using calcium-loaded microspheres is illustrated in Figure 2-1. Upon mixing of alginate microspheres with an alginate aqueous solution in PBS, calcium ions rapidly diffused from the microspheres into the solution to form a stable alginate gel, facilitated by sodium ion exchange. Alginate with a high M content (Pronova SLM20, >50% M units), which forms a mechanically less rigid gel than G-rich alginate (84, 103, 108), was used as the solution matrix component to favor cell infiltration into gels in their ultimate *in vivo* application. To measure the kinetics of calcium redistribution upon mixing CRMs with matrix alginate for self-gelation, we used the same microsphere/matrix composition applied for *in vivo* injections described later ($9x10^5$ CRMs mixed with 150μL SLM20 alginate (0.01 g/mL in PBS)). As described below, this composition does not form a stable gel *in vitro* but forms a low-viscosity alginate solution (additional calcium from the surrounding tissues contributes in *vivo*); we used this sub-gelation condition as a strategy to allow calcium redistribution followed by rapid separation of microspheres from the still-fluid alginate matrix solution (via centrifugation), in order to measure the amount of calcium released into the matrix solution. First, calcium redistribution kinetics was characterized using a calcium-sensitive dye, mag-fura-2, tracking the ratio of fluorescence emission following excitation at wavelengths of 340 nm vs. 380 nm over time by time-lapse fluorescence microscopy. Figure 2-2A shows a representative temporal trace of calcium levels detected in the alginate solution by mag-fura-2 following addition of CRMs, illustrating the extremely rapid release of calcium into the PBS/alginate matrix. Taking into account the physical act of mixing (~3 min), the microspheres released Ca^{2+} within the first several min of mixing of the particles with the matrix solution. Bulk fluorescence measurements on a fluorescent plate reader following separation of microspheres from the matrix alginate after 12 min showed 2.3-2.6 mM Ca^{2+} in the alginate solution (data not shown), consistent with the data from time-lapse microscopy, a concentration that was constant for up to 1 week. Since the total calcium concentration in the alginate matrix + microspheres (as determined by elemental analysis) was 3.7±0.3 mM for this composition, approximately 70% of calcium initially present in the CRMs was released within the first few minutes, and the remaining calcium remained sequestered within the particles for at least 7 days. Consistent with the rapid ion redistribution kinetics measured by the calcium-sensitive dye reporter, when fluorescent polystyrene nanoparticles (500 nm diam.) were mixed with self-gelling alginate containing a greater total content of calcium by adding 4-fold more CRMs to alginate matrix solutions (14.8 mM total calcium), time-lapse fluorescence imaging showed a cessation of nanoparticle Brownian motion within 5 min, indicating gelation on short timescales when sufficient calcium-reservoir

microspheres were present (data not shown). This data is also consistent with a prior study, which reported an increase of the shear elastic modulus of alginate within the first several minutes of mixing of alginate with alginate-associated calcium (90).

The microscale structure of self-gelled alginate was visualized by employing fluorescein-labeled SLM20 as the matrix mixed with unlabeled SLG20 microspheres (net calcium concentration ~14.8 mM). Examination of the structures of the resulting gels by confocal microscopy showed a random distribution of the polydisperse calcium-reservoir microspheres (indicated by the non-fluorescent spherical voids) throughout the alginate matrix (Figure 2-2B).

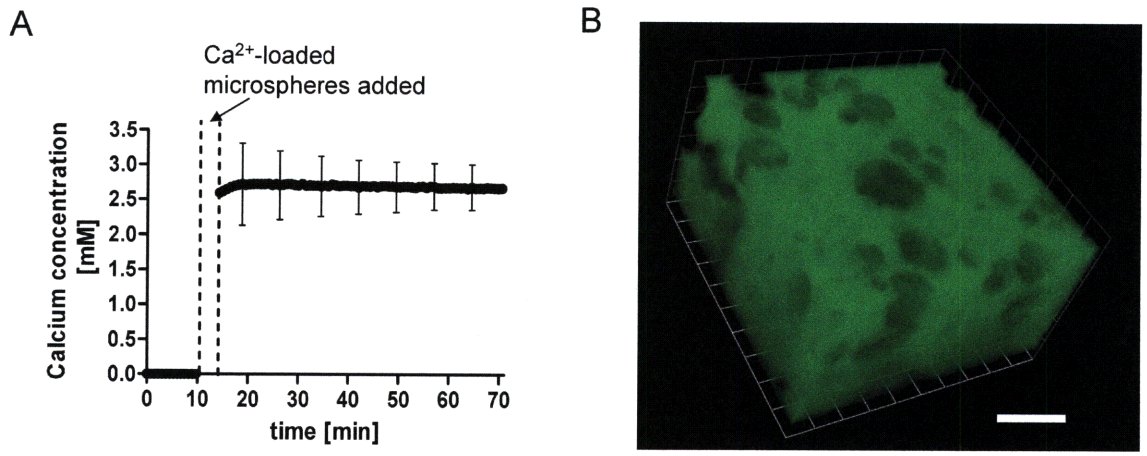

Figure 2-2: Calcium ions are rapidly released from calcium reservoir microspheres into the matrix alginate. (A) Temporal trace of calcium concentration in 'matrix' alginate determined by fluorescence microscopy using the calcium-sensitive dye mag-fura-2. Calcium reservoir microspheres (1.25×10^6) were mixed with 200 µL SLM20 alginate in PBS (composition used for injection *in vivo*) and immediately imaged in time-lapse microscopy. (Error bars = SD, every 10^{th} timepoint). (B) 3D reconstruction of a self-gelling alginate formulation containing 4×10^6 calcium reservoir microspheres in 130µL SLM20 matrix (14.8 mM Ca^{2+} overall), showing alginate microspheres (nonfluorescent voids) distributed throughout the fluorescent matrix. (scale bar: 50µm).

2.3.3 Mechanical properties of self-gelled alginate hydrogels

Because the concentration of CRMs directly determines the amount of calcium in self-gelling formulation, the mechanical properties of the resulting gels were directly modulated by the amounts of particles added. Figure 2-3A shows the shear moduli of self-gelled alginate containing different amounts of SLG20 microspheres, as measured by parallel plate rheometer. Each gel composition was allowed to set on the rheometer plate for 1 hr at 25°C before small oscillatory shear was applied. Figure 2-3B shows the shear modulus over a range of angular frequencies for gels with ~8.6mM calcium concentration, showing the dominance of elastic behavior over two decades of angular frequency. Similar behavior was seen for gels with calcium concentrations above ~6mM (data not shown). The amplitude of the strain (5%) used for all the measurements fell within the linear region of the viscoelastic spectrum as shown in Figure 2-3C (for the case of ~8.6mM calcium concentration). Prior studies have generally reported elastic moduli measured for gels containing substantially higher calcium concentrations (> 50-100 mM) and are on the order of 10^3 Pa (109-112). However, direct comparison is

difficult since the mechanical properties of alginate are affected by the alginate block structure, molecular weight, G/M ratio, and concentration. The mechanical properties are also dependent on the electrolyte composition of the gelling medium, since monovalent ions will compete for binding sites despite the high affinity of calcium ions with alginate G units(113). Such a mechanism is clearly involved in the present case where the matrix alginate was in PBS solution (0.14M NaCl, 3mM KCl, 10mM K_2HPO_4, pH=7.4), leading to mechanically soft gels as observed by LeRoux et al. for alginate gelled in the presence of 0.15M NaCl (114), and as Khromova observed for alginate gelled in the presence of KCl (88).

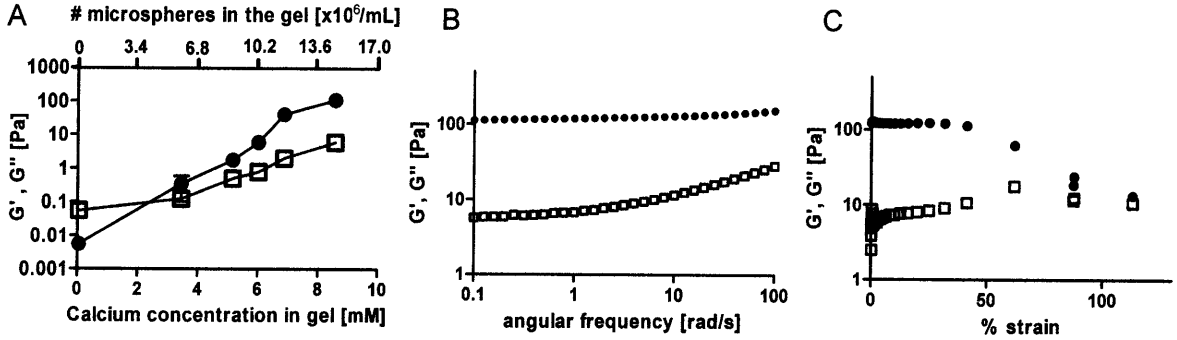

Figure 2-3: Mechanical properties of self-gelling alginate gels are controlled by the amount of calcium reservoir microspheres in the formulation. (A) Shear storage (G' (●)) and loss (G" (□)) moduli of self-gelled alginate containing different amounts of SLG20 microspheres were measured by parallel plate rheometer, showing an increase in the elastic shear moduli with the number of calcium reservoir alginate microspheres for a fixed total volume of the final gels. (B) Frequency sweep of self-gelling alginate gel with 8.6mM total calcium content shows the elastic component of the modulus G' (●) dominating the mechanical behavior of the gel over the viscous component G" (□) over two decades of angular frequency. (C) The magnitude of strain (5%) applied to the modulus measurement in fig 3A was in the linear region of the viscoelastic spectrum. The plot shown is for the case of 8.6mM Ca^{2+} in a self-gelling alginate formulation ((G' (●)) and loss (G" (□)).

Ionically crosslinked alginate is easily displaced from equilibrium by mechanical forces, and its behavior is heavily influenced by kinetics despite its elastic behavior at low strains (113). In addition, alginate is a shear-thinning fluid (103). Thus, even for matrix/microsphere mixtures providing > 6 mM total Ca^{2+}, gels with constant and stable shear moduli were not achievable when shear was applied immediately after loading onto the rheometer stage (data not shown); precluding measurement of the change in shear modulus with time. However, this behavior facilitated mixing of the matrix solution and microspheres; despite rapid ion release, uniform mixing of the calcium-loaded microspheres and the matrix was feasible even at relatively high CRM concentrations because application of shear during mixing disrupted crosslinking. The self-gelling system is thus suitable for applications in which mechanically soft yet uniform and stable gels are desired.

2.3.4 Sustained release of IL-2 from self-gelling alginate

Due to its mild gelation conditions, alginate has become an attractive candidate for encapsulation and delivery of proteins and other drugs in recent years (94, 115-118). We are

particularly interested in the application of self-gelling alginate for co-delivery of immune cells and immunoregulatory factors at tumor sites to promote anti-tumor immune responses. We previously demonstrated that dendritic cells (DCs) are readily encapsulated in subcutaneously-injected self-gelling alginate (94), and in order to augment their functions, we sought to co-deliver immunoregulatory factors in these gels that could play complementary roles in supporting anti-tumor immune responses: the immunocytokine interleukin-2 (IL-2) and CpG oligonucleotides. To build on the self-gelling system already described, we encapsulated IL-2 into the gels, and used alginate microspheres as modular components to immobilize CpG on their surfaces and mix them along with CRMs into matrix alginate solutions (Figure 2-1).

IL-2 is a cytokine that supports proliferation and effector functions of lymphocytes(119-123). It is FDA-approved for treatment of metastatic melanoma and renal cell carcinoma via systemic injection, but is known to have dose-limiting toxicity. Thus, strategies for local delivery at tumor sites have been sought to maximize the effectiveness of this cytokine: Slow release of IL-2 has been previously demonstrated using controlled release polymers (67, 124, 125), including alginate (126). For IL-2 delivery in this self-gelling system, we mixed 2 μg of murine IL-2 with CRMs and matrix alginate solution for gelation ($3x10^6$ microspheres/140μL alginate matrix solution, giving ~11mM Ca^{2+}). Release of IL-2 from the resulting gels was measured by ELISA analysis of gel supernatants over 7 days. As shown in Figure 2-4, the self-gelling alginate released IL-2 in a sustained manner over a week *in vitro*, suggesting that cytokines can be co-delivered from these gels into the surrounding microenvironment for a prolonged period following injection. The bioactivity of IL-2 released from these gels (assessed using the IL-2-dependent cell line CTLL-2) was statistically indistinguishable (95% bioactive) from control IL-2 solutions (data not shown). We have previously shown that highly cationic proteins exhibit very slow release from alginate gels due to electrostatic interactions with the matrix(127), but IL-2 has an isoelectric point near neutral pH. Thus, similar to the conclusions of other studies of cytokine release from alginate-based gels (126, 128), , we speculate that the release kinetics are mediated primarily via diffusion of IL-2 through the molecular mesh of the alginate gel.

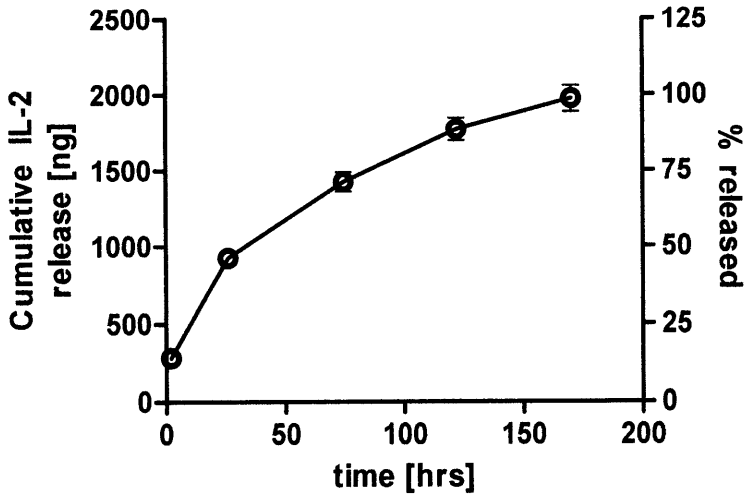

Figure 2-4: IL-2 loaded into self-gelling alginate is released in a sustained manner over a week *in vitro*. Cumulative release of IL-2, loaded into the self-gelling alginate formulation containing 11.1mM Ca^{2+}, as quantified by ELISA assay.

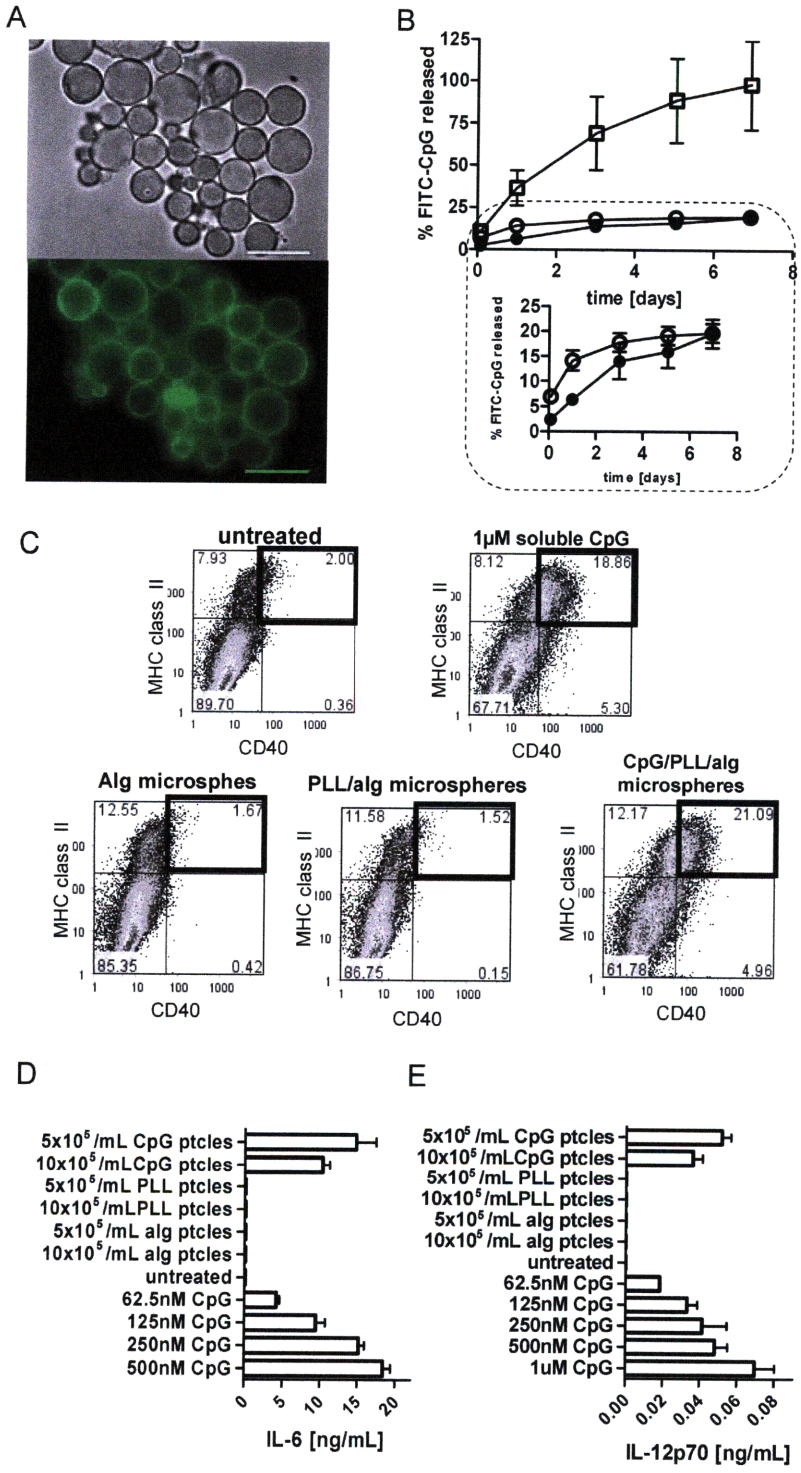

Figure 2-5: CpG oligonucleotide immobilization on alginate microspheres and activation of DCs by CpG-bearing microspheres. (A) Brightfield and fluorescence (FITC) micrographs of calcium reservoir microspheres coated with polylysine and FITC-CpG. (scale bars: 50μm). (B) Kinetics of FITC-CpG release from CpG/PLL/alginate particle suspensions (5 nmol FITC-CpG/10^6 microspheres) into serum-containing cell culture medium (O), CpG released from self-gelled alginate (11.1mM Ca^{2+}) containing the same number of CpG/PLL/alginate particles (●), or soluble CpG released from self-gelled alginate (11.1mM Ca^{2+}) encapsulating equivalent amounts of soluble CpG (□). (C) 1x10^6 bone marrow-derived dendritic cells (BMDCs) were incubated with 5-10x10^5 alginate microspheres, PLL/alginate microspheres, CpG/PLL/alginate microspheres, or 1 μM soluble CpG (positive control), or were left untreated for 18 hrs, then analyzed for surface marker expression by flow cytometry. Shown are flow cytometry scatter plots of BMDCs gated on $CD11c^+$ cells, showing CD40 and MHC class II expression. Heavy boxes highlight highly mature (activated) $CD40^{hi}MHC\ II^{hi}$ cells. CpG/PLL-coated microspheres were also able to trigger IL-6 (D) and IL-12p70 (E) secretions in BMDCs at least as efficiently as the soluble CpG did.

2.3.5 Functionalization of alginate microspheres with CpG oligonucleotides

In addition to providing IL-2 locally to recruited T-cells, we sought a strategy to provide activation signals locally to host DCs attracted to injectable alginate gels. CpG oligonucleotides, short single-stranded DNA oligos that mimic bacterial DNA strands and activate dendritic cells via Toll-like receptor-9, have been shown to potently activate DCs in cancer settings and to break tolerance to tumor antigens (129-133). Thus, we tested an approach to immobilize CpG oligos electrostatically on the surface of alginate microspheres for incorporation into self-gelling alginate formulations (Figure 2-1): the polycation poly-L-lysine (PLL) was adsorbed to the anionic surfaces of CRMs followed by electrostatic adsorption of CpG oligos (unlabeled or FITC-tagged CpG) to the PLL-modified alginate particles. Fluorescence micrographs of FITC-CpG/PLL/alginate particles (Figure 2-5A) showed clear binding of FITC-CpG to PLL-modified microspheres, and fluorescence measurements showed that ~88% of the FITC-CpG added (5 nmol FITC-CpG incubated with 10^6 particles) bound to PLL-coated microspheres. To assess the stability of CpG binding to PLL/alginate particles, we measured the release of fluorescent CpG into supernatants of CpG/PLL/alginate particle suspensions, self-gelled alginate containing the same number of CpG/PLL/alginate particles, or self-gelled alginate encapsulating equivalent amounts of soluble CpG (not immobilized). As shown in Figure 2-5B, most soluble FITC-CpG was released from self-gelling alginate by ~5 days, whereas release of CpG bound to particles was substantially slower, with only ~20% released over 1 week from either the particles alone or from the particles encapsulated in self-gelling alginate.

In order to test whether CpG bound to alginate particles was capable of eliciting DC activation, bone-marrow derived dendritic cells (BMDCs) were incubated with CpG/PLL/alginate particles, PLL/alginate particles, alginate particles, or soluble CpG as a positive control for 18 hrs. Figure 2-5C shows flow cytometry scatter plots gated on $CD11c^+$ cells for each condition: While almost no untreated control BMDCs have a highly mature (activated) MHC $II^{hi}CD40^{hi}$ phenotype, ~20% of soluble CpG-stimulated DCs show this phenotype by 18 hrs. BMDCs co-cultured with alginate or PLL/alginate microspheres showed similar phenotypes as untreated immature DCs, whereas the CpG-coated particles caused upregulation of the CD40 and MHC class II molecules on the DCs comparable to the soluble CpG positive control. The viability of the cells, as assessed by PI (propidium iodide) staining, did not differ among the conditions tested, indicating no cytotoxicity of the unmodified, PLL-coated, or CpG/PLL-coated alginate microspheres (data not shown). In addition to upregulation of these molecules involved in T-cell priming, another key function of activated DCs is the production of proinflammatory cytokines. Figures 2-5D and E show that the CpG/PLL-coated microspheres triggered secretion of the pro-inflammatory cytokines IL-6 and IL-12p70 by BMDCs at least as efficiently as soluble CpG. Taken together, the above data suggests that alginate microspheres do not themselves activate dendritic cells, consistent with published data (134), but CpG oligonucleotides can be immobilized to these particles with slow release over periods in excess of 1 week, and CpG-modified CRMs mediate potent activation of DCs.

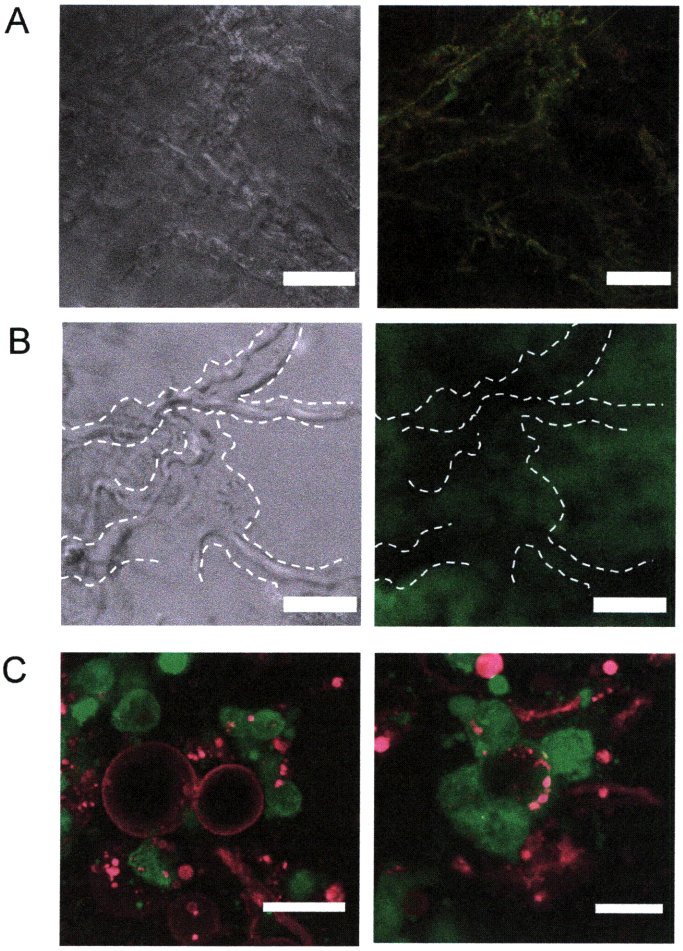

Figure 2-6: Self-gelling alginate structures and self-gelling alginate encapsulating Cy5-CpG/PLL-coated alginate microspheres *in vivo*. (A) Brightfield (left) and reflectance mode (right) images of self-gelling alginate (~$9x10^5$ microspheres in 150µL SLM20, 0.01g/mL) injected subcutaneously into back flanks of mice and explanted after 19 hrs shows micron-scale fibrils. (scale bars: 50µm). (B) Brightfield (left) and fluorescence confocal (right) images of self-gelling alginate with 6-aminofluorescein-labeled SLM20 reveals the fibrillar structures are not associated with alginate, indicating alginate forms macroporous gels when injected subcutaneously *in vivo*. (scale bars: 20µm). (C) Fluorescent Cy5-CpG (purple) on the surfaces of PLL-modified alginate microspheres was encapsulated into self-gelling alginate and injected into GFP+ mice. Cy5-CpG-coated microspheres are intact 48 hrs post-injection (left, scale bar:25 µm) and are accessible to infiltrating cells (right, shown in green, scale bar:15 µm) that can ingest the oligonucleotides. The micrographs are projections of z-planes over 6 µm.

2.3.6 Gel structure and cellular infiltration of self-gelling alginate in vivo

In order to formulate a composition of CRMs and alginate matrix suitable for injection *in vivo*, a series of compositions were tested for their ability to be readily drawn into and ejected from an insulin syringe (28 gauge). Based on this practical requirement, a composition with $6x10^3$ CRMs/ µL SLM20 solution was selected for testing *in vivo* (overall calcium concentration of 3.7±0.3 mM). Though the amount of crosslinking ions provided by the CRMs in this formulation gives weak mechanical properties *in vitro* (Figure 2-3), we hypothesized that calcium available in the interstitial fluid would contribute to crosslinking *in vivo*. Indeed, as shown in Table 2-1, when this formulation was injected *in vivo* subcutaneously in C57Bl/6 mice and explanted after 2 hrs, ~8 mM Ca^{2+} was detected in the recovered gels by elemental analysis, corresponding to gels with elastic behavior over a range of oscillatory frequencies (Figures 2-3A and B), and a Ca^{2+} contribution from the interstitial fluid of ~4.5 mM. When alginate precursor solution was injected without added CRMs and explanted after 2 hrs, 5.5 mM calcium was detected by elemental analysis, corresponding to gels with ~60-fold lower shear moduli. Thus, formulations with low concentrations of CRMs that are unable to themselves form stable gels facilitate preparation of solutions/handling, while achieving soft but stable gels following injection *in vivo* via the contribution of extracellular calcium in the tissue.

Table 2-1: Concentration of calcium ions in self-gelling alginate injected *in vivo* with or without calcium reservoir microspheres

Gel composition	Microsphere-derived Ca2+ [mM]	Total Ca^{2+} in explanted gels [mM]	Calculated Ca^{2+} contribution from interstitial fluid [mM]
no microspheres	0	5.5±0.5	5 5±0.5
with microspheres	3.7±0.3	8.1±1.3	4.5±0.2

Gels formed *in vitro* in the studies described in previous sections form under idealized conditions of pure buffer solutions, in the absence of serum or blood factors that are present *in vivo*. To determine the structure of gels formed following *in vivo* injection, we injected self-gelling alginate ($6x10^3$ CRMs/μL SLM20 solution) *s.c.* in C57Bl/6 mice, explanted the resulting gels 22-48 hrs after injection, and examined them in their native, hydrated state by 3D confocal microscopy. We first examined the explanted gels by reflectance-mode confocal microscopy, a technique to visualize the surface and volume architecture and topology of three-dimensional matrices including natural biopolymers such as collagen (135, 136) as well as synthetic polymer matrices (137). Nano-scale fibrils of extracellular matrix (ECM) can be resolved *in situ* through this method without the need for exogenous labeling (136). Figure 2-6A shows representative brightfield and reflectance-mode images of a self-gelled alginate matrix explanted 19 hrs after injection, showing fibrillar structures that are of micron scale. Such fibrillar structures were readily resolved within explanted alginate gels up to *z*-depths as far as reflectance could resolve (~100 μm). In contrast, self-gelled alginate matrices formed *in vitro* were generally featureless in reflectance microscopy (data not shown). To determine whether these fibrillar structures represented a morphological change induced by alginate itself *in vivo* or were instead exogenous like ECM components or blood factors such as fibrin depositing in the gels, fluorescent alginate was injected, and we examined the structure in regions where fibrillar structures were prominent enough to be observed directly in brightfield images. Figure 2-6B illustrates that fibrillar structures formed within these gels (observed in brightfield) were not associated with alginate chains (green fluorescence) but actually occupied voidspaces in the gels where alginate was absent, demonstrating that the self-gelling alginate forms a macroporous structure *in vivo*, possibly intertwined with as yet-undefined ECM components present in the serum, the interstitial fluid, and/or the blood.

To determine whether CpG-coated microspheres could maintain local depots of CpG within these gels *in vivo*, we injected self-gelling alginate carrying Cy5-labeled-CpG/PLL-coated alginate microspheres, non-coated CRMs, and activated, unlabeled BMDCs into transgenic GFP^+ mice. Gels were explanted after 24 or 48 hrs and analyzed by 3D confocal microscopy. Figure 2-6C shows that the Cy5-CpG-coated microspheres remained intact for at least 48 hrs *in vivo* (left panel). Host cells (83) were also observed clustering around CpG-bearing microspheres (Figure 2-6C right panel), and ingesting fluorescent CpG (Figure 2-6C left and right panels). We have previously shown that a large number of host DCs infiltrate alginate gels loaded with exogenous (syngeneic) activated DCs, within 48 hrs post injection (94). Availability of CpG on

the surface of alginate microspheres for a prolonged time period might thus enable sustained local activation of recruited host DCs within the matrix.

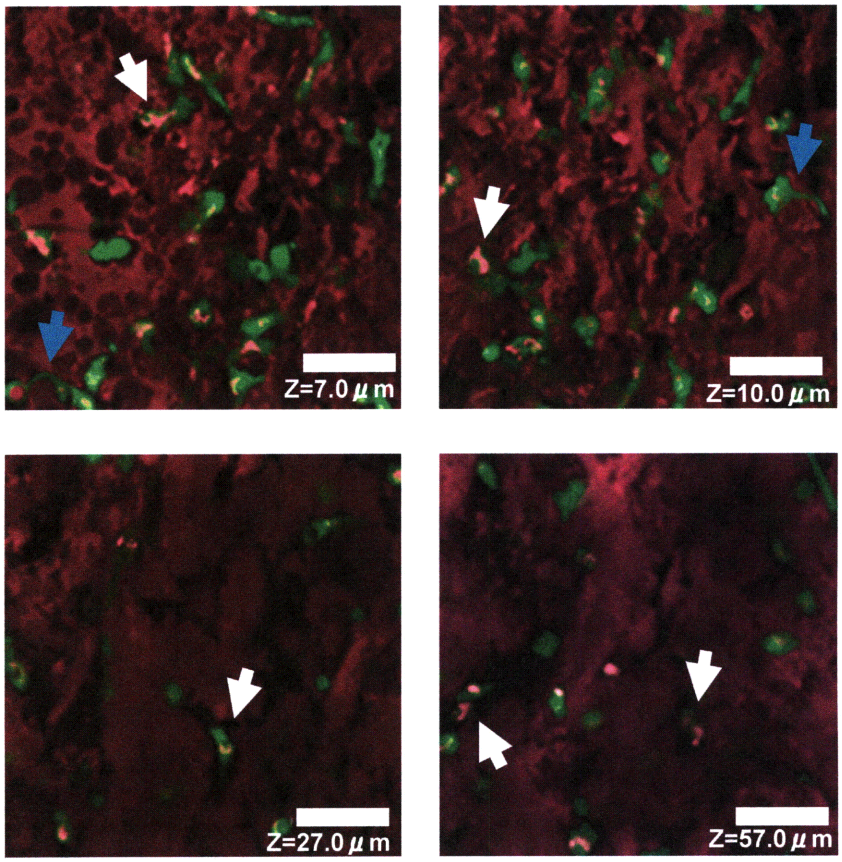

Figure 2-7: Host cells Infiltrate self-gelling alginate and preferentially occupy void spaces in the porous matrix. Fluorescence confocal microscope images of fluorescently labeled self-gelling alginate (purple) explanted from back flanks of mice 48 hrs after injection. Infiltrating GFP^+ cells occupied void spaces in the macroporous gel structure and extended lamellipodia into void spaces (blue arrows), with some phagocytic cells having ingested the matrix alginate indicated by intracellular deposits of labeled alginate (white arrows). (scale bars: 50μm).

The success of a synthetic tissue engineering scaffold as a replacement for the native tissue environment depends, among other factors, on its three-dimensional micro-architecture and mechanical integrity, and ability to support cellular migration/infiltration (104, 138). In order to visualize how host cells invade injected alginate matricesself-gelling alginate labeled with a far-red dye, Hilyte Fluor 647, and containing activated, unlabeled BMDCs was injected into transgenic GFP^+ mice. Fluorescence confocal microscopy of explanted gels at 48 hrs revealed that host cells from the surrounding tissue invade the matrix via potentially two means (Figure 2-7): cells occupied void spaces in the macroporous gel structure and extended lamellipodia into void spaces (blue arrows), suggesting they preferentially infiltrated pre-existing pores. In addition, phagocytic cells were also observed with intracellular deposits of alginate (clearly intracellular when observed in reconstructed *z*-sections, not shown), indicating ingestion of alginate by some cells as they infiltrated and made their own way through the matrix.

Examination of cell migration inside the gels under time-lapse microscopy also revealed smaller cells rapidly migrating by squeezing through small void spaces. This observation is consistent with the recent studies demonstrating that leukocytes can rapidly migrate through porous matrices in the total absence of functional integrins (139). Thus, cellular infiltration is supported by the macroporosity of *in situ*-gelled alginate, and potentially by ECM molecules deposited within the gel during injection.

2.4 Summary

We analyzed the physical properties of self-gelling formulations of alginate formed by mixing calcium reservoir alginate microspheres with a soluble alginate solution. We found that relatively stable gels were formed for matrices loaded with >~6 mM Ca^{2+}, whether provided by microspheres only *in vitro*, or by a combination of ions from the reservoir microspheres and surrounding tissue fluid *in vivo*. Redistribution of calcium ions from the reservoir microspheres was rapid, reaching equilibrium within minutes of mixing with alginate aqueous solutions. Cellular infiltration of these gels is supported by the macroporous morphology of gels formed *in situ* following injection. This alginate microsphere + alginate solution strategy for forming gels allows injectable formulations to be achieved without introducing additional compounds or components to the system (the final matrix contains only alginate). In addition, the microspheres can serve a dual function as both reservoirs for calcium and as microdepots for presentation or release of co-factors in the matrix. The ability to incorporate soluble factors like IL-2 directly into matrix and to use microspheres as modular components for augmenting these gels with slowly released factors, such as CpG oligonucleotides as demonstrated here, may provide a potent platform for immunotherapy when combined with delivery of immune cells. In addition, such non-invasively delivered gels may be of general interest for tissue engineering and regenerative medicine applications.

2.5 Acknowledgments

The work described in this chapter was supported by the Defense Advanced Research Projects agency (contract # W81XWH-04-C-0139) and the National Science Foundation (award 0348259). We would like to thank Philip Erni and Randy H. Ewoldt from the Hatsopolous Microfluids Laboratory for technical help and discussions related to rheological measurements. We would also like to thank Elizabeth M. Horrigan for assistance with animal studies.

Chapter 3
Mechanisms Behind Immune Responses Elicited By Vaccination Nodes

Using the self-gelling alginate strategy as outlined in the previous chapter, in this part of the thesis work we tested the concept of delivering DCs in an injectable hydrogel matrix, with the aim of harboring dendritic cells for prolonged time periods at a defined site and trapping/concentrating factors secreted by DCs to establish an inflammatory milieu *in situ*. The creation of such inflammatory microenvironment successfully allowed for recruitment of key immune effector cells that could potentially fight against cancerous cells near the injection site. In this chapter, we also show how these pro-inflammatory vaccination nodes could mediate antigen-specific immune responses and re-traffic the activated effector cells to a desired local site.

3.1 Introduction

Dendritic cells (DCs) are potent initiators of immune responses, acting at the interface of the innate and adaptive immune systems to activate a multitude of immune effector cells against specific antigens. They are the key antigen presenting cells (APCs) involved in priming naïve T cells during primary immune responses (140, 141). Because of their critical role in initiating immune responses, treatments based on the injection of autologous dendritic cells have become an intensively investigated vaccination strategy in preclinical and clinical studies, particularly for cancer immunotherapy (142-145). In dendritic cell vaccines for cancer, DCs derived from peripheral blood cells are loaded with tumor antigens *ex vivo* and injected in patients to promote anti-tumor T cell responses. In most studies, DCs have been injected at peripheral tissue sites (e.g., subcutaneous or intradermal sites), with the expectation that the injected cells would respond to normal homing cues and migrate to local draining lymph nodes. Upon reaching the lymph nodes where naïve T cells are concentrated, DCs can prime $CD8^+$ tumor-specific T cells that subsequently seek out and destroy tumors located elsewhere in the body. Promising data in animal models has been obtained by this approach, but results from clinical trials have been modest: even in cases where tumor specific $CD8^+$ T effector cells have been successfully generated, clinical responses have not always resulted (146-148). A limitation of such DC vaccines, and many cancer vaccines in general, is that antigen-bearing DCs in lymphoid organs have a limited ability to support the effector phase of the immune response following T cell priming, which will be carried out primarily by activated T cells that leave the lymph nodes and

migrate to sites of antigen deposition in the peripheral tissues (e.g., infection sites or tumors). This is particularly problematic in the case of anti-tumor immune responses, because tumor cells themselves exert a number of mechanisms to locally suppress the effector functions of primed T cells (63, 65, 149, 150). In addition, in many human cancers and animal models of cancer, activated T cells fail to properly home to tumors to carry out their effector functions (71, 73, 151, 152). Thus, even a vaccine that successfully primes potent anti-tumor T cells in the secondary lymphoid organs may not achieve the ultimate goal of destroying the tumor (54, 153).

To address these concerns, other studies have examined the injection of antigen-loaded dendritic cells directly into tumors (154-156). Directly delivering DCs to the site of a tumor/infection could improve immune responses by enabling DCs to prime anti-tumor T cells locally at the site where they are needed, providing the injected DCs with direct access to additional antigens, promoting attraction of additional T cells to the site through chemokine production, and allowing DC inflammatory cytokine secretion to influence the local microenvironment (157, 158). However, in the case of tumor immunotherapy, direct intratumoral or peritumoral injection of DCs inhibits tumor growth but has limited ability to cure mice of established tumors (154, 156, 159).

Although DCs delivered to tumors (or infection sites) might be well-positioned to both prime anti-tumor T cells and support the effector phase of adaptive immune responses, the known short lifespan of activated DCs (a few days) may limit the degree of success obtainable with this approach. If host dendritic cells are not recruited to the site by the initial DC injection to continue the process of antigen acquisition, T cell priming, and cytokine/chemokine production started by the vaccination, the immune response may be shut off too early or returned to a suppressed state prior to therapeutic benefit (i.e. tumor regression or infection resolution). Because activated DCs secrete chemokines and cytokines that can attract and activate other DCs (160-162), host dendritic cell recruitment following vaccination with exogenous DCs should in principle be possible. As explained briefly in Chapter 1, we hypothesized that tissue-localized recruitment of host dendritic cells and T cells to target tissue sites could be achieved if vaccine DCs were delivered in a supporting matrix chosen to (1) provide space for cellular infiltration/recruitment and to (163) promote local concentration of DC-derived chemokines and cytokines, through binding to the matrix. Here we tested this hypothesis in a murine model, utilizing a self-gelling formulation of alginate carrying dendritic cells, as described and characterized in Chapter 2. The injectable matrix was obtained by mixing calcium-crosslinked alginate microspheres with soluble alginate and dendritic cells, a formulation that gelled in a matter of minutes to obtain stable, cell-infiltratable gels that persisted several weeks *in vivo*. Using this system, we explored the concept of dendritic cell delivery in alginate gels in healthy mice, and analyzed the host response to these gels in the steady state or in response to immunization with specific antigen. In this approach, activated, antigen-loaded DCs were injected at a subcutaneous site in the *in situ*-gelling hydrogel matrix. We found that these injected DCs and alginate recruited endogenous host DCs and immune cells to the site, while simultaneously a small number of the injected cells migrated to local lymph nodes (Figure 3-1). T cells activated by these migrating DCs in the local draining lymph nodes were attracted back to the alginate matrix in response to the local inflammatory milieu established in the gel. In this way, a single injection provided antigen presenting cells to initiate naïve T cell priming in the native lymph nodes and simultaneously established a microenvironment drawing the activated T cells to the site of injection, supported by host DCs that had infiltrated the gel. These alginate 'vaccination nodes' may thus have the potential for focusing and modulating the effector phase

of an immune response at a chosen peripheral tissue site, such as a solid tumor or site of infection. In addition, these results highlight the potential interplay that may occur in a variety of implant and tissue engineering settings between the well-studied biomaterial alginate and ongoing host immune responses *in vivo*.

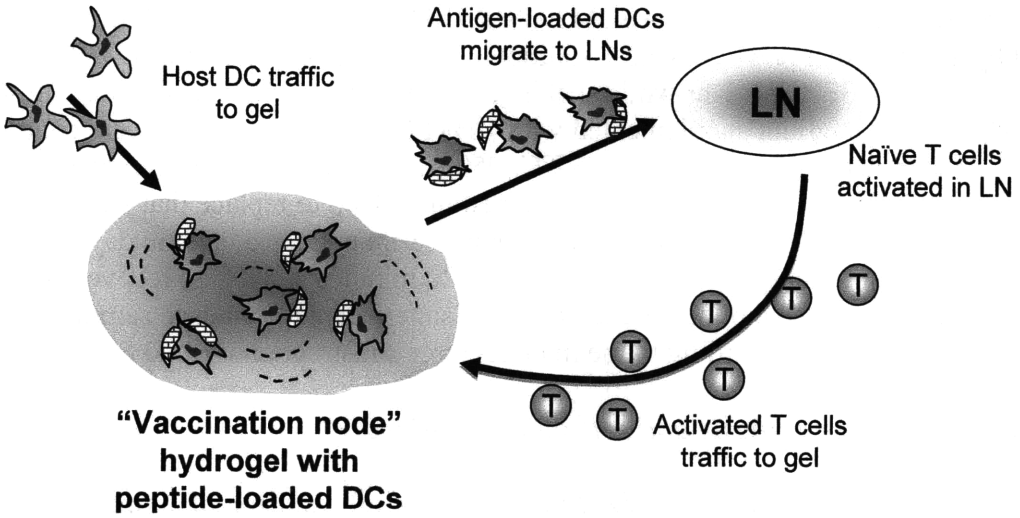

Figure 3-1: Schematic outline of DC and lymphocyte trafficking in response to injectable 'vaccination nodes.' When alginate encapsulating activated antigen-loaded DCs is injected subcutaneously into mice, a few of the inoculated DCs migrate to the draining lymph nodes, where they can prime antigen-specific T cells. Factors secreted by exogenous DCs within the alginate recruit endogenous host DCs to the gel. Once T cell priming is initiated by the lymph node-trafficking DCs, activated T cells are attracted back to the alginate matrix in response to the local inflammatory milieu established in the gel.

3.2 Materials and Methods

3.2.1 Materials

Sterile alginates Pronova SLM20 (MW 75,000 – 220,000 g/mol, >50% M units), Pronova SLM100 (MW 200,000 – 300,000g/mol, >50% M units), Pronova SLG20 (MW 75,000 – 220,000 g/mol, >60% G units), and Pronova SLG100 (MW 200,000 – 300,000g/mol , >60% G units) were purchased from Novamatrix (FMC Biopolymers, Sandvika, Norway). All antibodies, anti-mouse PE-TCRβ, anti-mouse FITC-CD19, anti-mouse APC-CD11c, anti-mouse APC-CD4, and anti-mouse APC-CD8, and Growth-Factor-Reduced Matrigel were purchased from BD Biosciences (San Jose, CA). 2, 2, 4-trimethylpentane (isooctane, ChromAR, 99.5%) was obtained from Mallinckrodt Baker (Phillipsburg, NJ). Calcium chloride dihydrate and lipopolysaccharide (LPS) from E. Coli was from Sigma-Aldrich (St. Louis, MO). CpG oligonucleotides with a phosphorothioate backbone (CpG 1826, sequence 5' - /5AmMC6/T*C*C* A*T*G* A*C*G* T*T*C* C*T*G* A*C*G* T*T - 3') were synthesized by Integrated DNA Technologies. Mouse CCL21 and CCL19 recombinant chemokines and

ELISA detection kits were purchased from R&D Systems (Minneapolis, MN). SIY peptide (SIYRYYGL) was synthesized at the MIT Biopolymers Laboratory. All the other chemicals were purchased from Sigma unless otherwise stated.

3.2.2 CCL21 and CCL19 release from alginate in vitro

Release of the chemokine CCL21 or CCL19 from alginate matrices was measured by an ELISA assay. Alginate gels were formed by mixing 2 μg mouse CCL21 or CCL19 with alginate solutions (150μL of 0.01g/mL Pronova SLM20, SLM100, SLG20, or SLG100 in PBS pH 7.4) and gelled by addition of 1% wt/vol $CaCl_2$ solution (30 μL) in Eppendorf tubes. All samples were allowed to gel at 37°C for 1 hr while shaking, followed by a gentle wash with 1mL of complete RPMI 1640 medium supplemented with 10% FCS. Release studies were conducted by adding 1mL of complete medium to gels at 37°C; 950μL of supernatant was removed for analysis at each time point over 7 days and fresh medium added to replace that withdrawn. The supernatants were stored at 4°C until all the time points were collected, and on day 7 the alginate gels were digested with 10mg/mL alginate lyase for ~20 minutes at 37°C to recover all remaining chemokine. The amounts of chemokine in supernatants from each sample were quantified using an ELISA according to the manufacturer's instructions (R&D Systems).

3.2.3 Alginate particle synthesis and self-gelling alginate

Alginate microparticles were synthesized via a water-in-oil emulsion of alginate in an organic solvent, as introduced in Chapter 2. 1.5mL of sorbitan monooleol (Span 80, Sigma) and 0.5mL of Tween-80 (Sigma) were first added to 40mL of iso-octane under magnetic stirring, and homogenized for 2 minutes using an UltraTurrax T25 homogenizer (IKA Works) at speed 8x1000/min. Pronova SLG20 solution (400 μL, 0.01g/mL in PBS) was then added drop-wise and homogenized for 3 minutes, followed by addition of 25μL 5% wt/vol $CaCl_2$ solution to crosslink the alginate. The resulting solution was homogenized for another 3 minutes, and the resulting particles were recovered by centrifugation at 2060*xg* for 5 min. The iso-octane supernatant was discarded, and the particle pellet was washed with 40mL of iso-octane. After another centrifugation, the particles were re-suspended in 1mL of deionized, distilled water and washed three times. The particles were resuspended in deionized, distilled water with a final volume of 1mL and stored at 4°C until used. Alginate particle size was determined from optical micrographs taken with a Zeiss Axiovert 200 epifluorescence microscope at 40X and analyzed with MetaMorph software (Molecular Devices).

3.2.4 Elemental analysis/quantification of Ca^{2+} ions in the alginate particles

Half a batch (500 μL) of the as-synthesized alginate microparticle suspension was centrifuged down and the supernatant removed. The pellet was resuspended with 300 μL of 100 mM EDTA (disodium EDTA dihydride) solution. Samples were analyzed using ICP-OES (inductively coupled plasma optical emission spectroscopy) by Quantitative Technologies, Inc. (Whitehouse, NJ).

3.2.5 Animals and cells

Animals were cared for in the USDA-inspected MIT Animal Facility under federal, state, local and NIH guidelines for animal care. C57Bl/6 mice and mice expressing green fluorescent protein under the chicken β-actin promoter and cytomegalovirus enhancer (GFP expressed in all cells except erythrocytes and hair follicles) were obtained from Jackson Laboratories. 2C TCR transgenic mice on a $RAG2^{-/-}$ C57Bl/6 background were a gift from Jianzhu Chen (MIT). Bone marrow-derived dendritic cells were prepared by isolating bone marrow from tibia and femurs of C57Bl/6 mice or GFP^+ mice and culturing them *in vitro* over 6 days in the presence of 10ng/mL GM-CSF in complete medium (RPMI 1640 containing 10% FCS, 2 mM L-Glutamine, penicillin/streptomycin, and 50μM 2-mercaptoethanol) following a modification of the procedure of Inaba (99) as previously reported (100). The resulting dendritic cells were activated/matured with 100 ng/mL LPS or 1μM CpG for 18 hrs and then washed thoroughly with PBS before use. For *in vivo* T cell priming studies, the dendritic cells were pulsed with 10 μM SIY peptide at the same time the maturation stimuli were added to the cultures.

3.2.6 In vivo immunization of mice

Matrix alginate Pronova SLM20 (160 μL of 0.01 g/mL alginate in PBS) was mixed with factors to be delivered (i.e. total of $2x10^6$ dendritic cells, 2 μg CCL21, or 50 μM SIY peptide in each gel) and kept on ice until injection. In the case of alginate mixed with CCL21, the chemokine was mixed with alginate at 4°C overnight to allow association of the chemokine with alginate chains. SLG20 alginate microspheres (100 μL from the microsphere stock suspension, ~$1x10^6$ microspheres) was added to an eppendorf tube and centrifuged down to obtain a pellet. The supernatant was gently removed from the tube and the microsphere pellet was vortexed and mixed with the soluble alginate + cells/chemokine solution immediately before injection into C57Bl/6 recipient mice, and 150μL total was injected with an insulin syringe (30 gauge, BD Biosciences) subcutaneously into the flanks of anesthetized mice. For intradermal and subcutaneous injections of dendritic cells alone, 50μL of PBS with or without $2x10^6$ dendritic cells was injected either s.c. or i.d. into the back flanks of mice.

3.2.7 Confocal microscopy of gels explanted from mice

GFP^+ C57Bl/6 dendritic cells were washed 3X with PBS, mixed with alginate and injected s.c. in anesthetized C57Bl/6 mice. Animals were euthanized and DC-loaded gels were explanted from mice 22 hrs after inoculation and imaged using a Zeiss LSM 510 confocal microscope. 3D Z-section images were obtained through 100-300μm depths in 4μm z-steps using a 40x objective.

3.2.8 Histology

Explanted gels were fixed with formalin for 20 hours and embedded in paraffin. Thin sections of 4μm thickness were sliced and stained with heamatoxylin and eosin (H&E).

3.2.9 Adoptive transfer of 2C cells

Splenocytes were isolated from 2C TCR transgenic mice. For labeling, the splenocytes (10^6/mL) were incubated with 10 μM carboxyfluorescein succinimidyl ester (CFSE) in serum-free RPMI for 10 min at 37°C, quenched with 5mL cold RPMI medium with FCS, and washed 3X in complete medium and PBS. Labeled cells ($5x10^6$) in 200 μL sterile PBS were adoptively transferred to anesthetized recipient C57Bl/6 mice by retrorbital injection. The mice were then immunized with alginate gels 24 hrs after adoptive transfer.

3.2.10 Flow cytometry analysis

Alginate gels, lymph nodes, and spleens recovered from immunized animals were digested with 0.28 WU/mL Liberase Blendzyme 3 (Roche Applied Sciences) for 20 min at 37°C, followed by the addition of 0.02% EDTA and 1mg/mL of alginate lyase (Sigma) or 55mM sodium citrate (Sigma) for an additional 15 min to quench the collagenase activity and digest the alginate. Digested gels were passed through 40μm nylon mesh cell strainer (BD Falcon, San Jose, CA) with 10mL of PBS. After centrifugation of the cell suspension, recovered cells were resuspended in flow cytometry buffer (1% BSA, 0.1% NaN_3 in Hank's balanced salt solution, pH 7.4) at 4°C, and blocked with 10 μg/mL anti-CD16/CD32 antibody for 10 min. The cells were then stained with fluorescent antibodies against surface markers for 20 minutes on ice, followed by three washes with flow cytometry buffer and addition of 1.25μg/mL propidium iodide (PI) for viability assessment. Stained cells were analyzed on a BD FACSCalibur flow cytometer. Enumeration of DCs/cellular infiltrates was performed by calibration of flow cytometer events to cell suspensions of known concentration. Cell losses during the multiple wash/treatment steps of gel and tissue digestions were reproducible and were accounted for in the reported recovered cell numbers.

3.3 Results

3.3.1 Self-gelling alginate as a basis for vaccination nodes

In order to deliver dendritic cells (DCs) *in vivo* in a minimally-invasive manner, we demonstrated the development of an injectable, biocompatible hydrogel that would crosslink *in situ* to form a supporting matrix in Chapter 2. An ideal material for our application would in addition be capable of reversibly binding chemokines and other supportive cytokines (either produced by DCs in the gel or exogenously added to the matrix prior to injection), to facilitate the retention of these factors in the local microenvironment and the generation of a pro-inflammatory milieu to support host T cell and DC attraction to the matrix. Because of alginate's anionic polysaccharide structure, we also hypothesized that it could support chemokine/cytokine binding in a manner mimicking cytokine binding to native glycosaminoglycans (GAGs), since many chemokines and cytokines bind to heparan sulfate and related GAGs.

To test the ability of alginate to retain and slowly release chemokines via ionic interactions with the polysaccharide chains, we first measured the *in vitro* release of two different T cell/dendritic cell chemoattractants, CCL21 and CCL19, from bulk alginate gels of different composition (alginate G:M ratio) and molecular weight. Each of these chemokines is highly

cationic, with estimated net charges of +17 and +7 for CCL21 and CCL19, respectively (163). Bulk calcium-crosslinked alginate gels (1 wt% alginate) were prepared with 2 μg chemokine per 1.5 mg alginate, and release from these gels into serum-containing medium at 37°C was recorded over 7 days. As shown in Figures 3-2A and 3-2B, only a few percent of CCL21 encapsulated in alginate gels was released over a week, whereas ~60% of the less-highly charged CCL19 was released during the same period of time. The molecular weights of these two chemokines are nearly identical (~9-12 KDa), suggesting a strong correlation between their net charge and release rates from alginate. CCL21 release rates were also more sensitive to changes in the molecular weight of the alginate and the G:M ratio of the polysaccharide compared to CCL19.

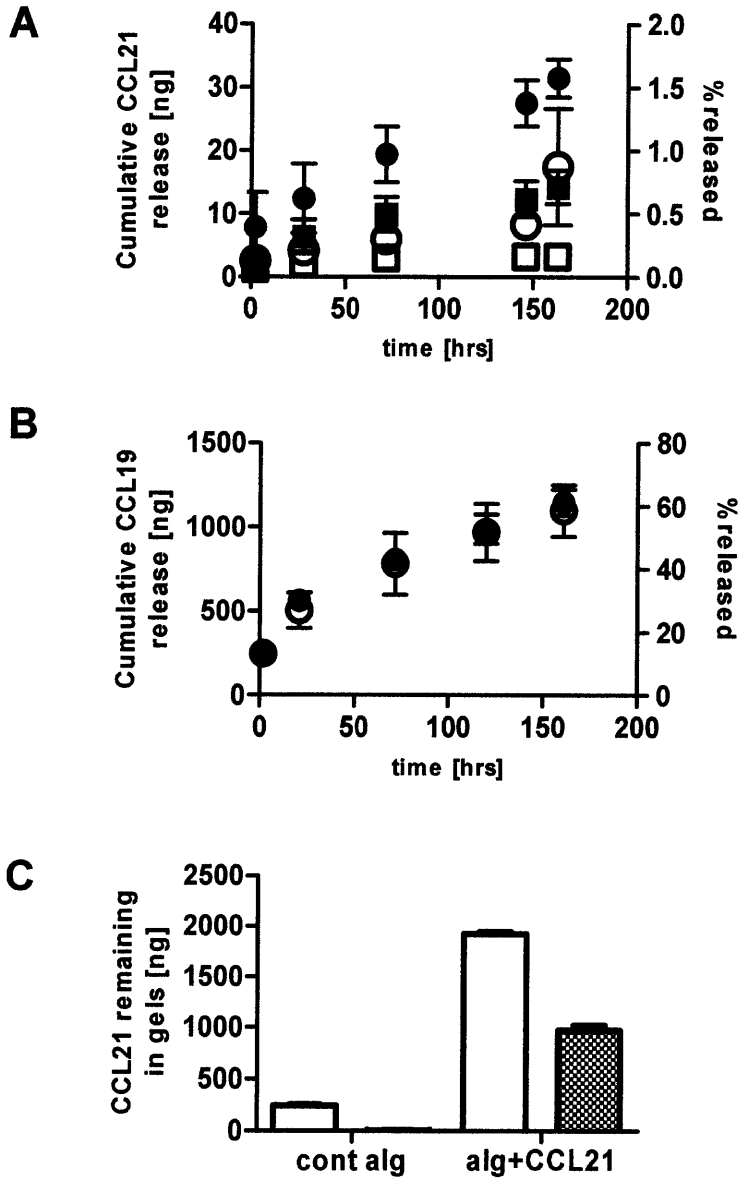

Figure 3-2: Alginate gels reversibly bind chemokines *in vitro* and *in vivo*. (A, B) In vitro release of chemokines from alginate gels: Chemokines (2 μg of CCL21 (A) or CCL19 (B)) were encapsulated in alginates with varying molecular weight and G:M ratios, and release of the protein into serum-containing medium was assessed over 7 days at 37°C by ELISA. Filled circle (•) = Pronova SLM20 (MW 75,000 – 220,000 g/mol, >50% M units), filled square (■) = Pronova SLM100 (MW 200,000 – 300,000g/mol, >50% M units), open circle (○) = Pronova SLG20 (75,000 – 220,000 g/mol, >60% G units), open square (□) = Pronova SLG100 (MW 200,000 – 300,000g/mol, >60% G units). (C) Release of CC21 from 150 μL 'self-gelled' alginate in vivo following subcutaneous injection in C57Bl/6 mice: Self-gelling alginate mixed with 2 μg CCL21 or control blank alginate was injected (150 μL) s.c. in groups of 2 C57Bl/6 mice per time point. Gels were recovered after 2 d (unfilled bars) or 7 d (dotted filled bars), digested, and chemokine remaining in the gel was measured by ELISA. Error bars = SEM.

Based on these promising initial results for sustained release of chemoattractants from alginate, we tested whether chemokines were retained/slowly released from self-gelled alginate *in vivo* too (Figure 3-2C). Self-gelling alginate mixed with 2 μg of CCL21 or control gels lacking chemokine were injected s.c. in the flanks of C57Bl/6 mice. Two or seven days post injection, the alginate gels were recovered, digested with alginate lyase/collagenase, and the amount of chemokine remaining was assessed by ELISA. As shown in Figure 3-2C, little or no CCL21 was detected in control alginate gels (confirming no substantial chemokine contribution from surrounding host tissue), but exogenously-added CCL21 was well retained over 7 days in alginate: ~90% of the chemokine initially injected was still present in the gels after 2 days, and ~50% still remained after 7 days. Thus, self-gelling alginate appears to reversibly bind and slowly release chemokines both *in vitro* and *in vivo*.

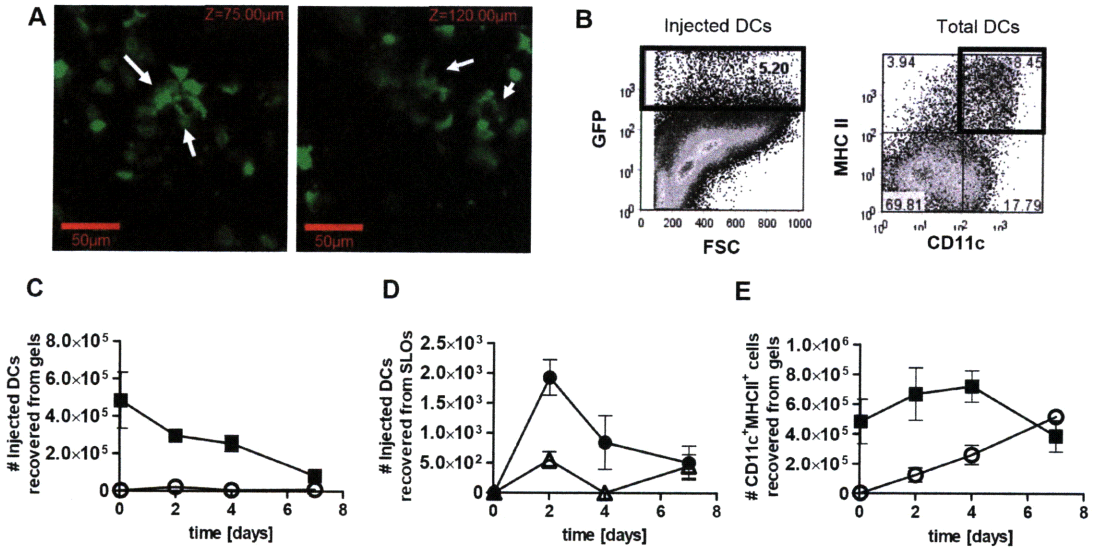

Figure 3-3: Activated dendritic cells persist several days in vivo within alginate matrices and attract host DCs to the injection site. (A) Confocal microscopy images (at two different z depths) of GFP^+ dendritic cells in self-gelled alginate matrices, explanted 22 hrs after s.c. injection in C57Bl/6 mice. DCs with spread morphologies are highlighted by white arrows. Scale bars 50μm; z positions are 75 μm (left image) and 120 μm (right image). (B) Flow cytometry scatter plots illustrating the identification of GFP^+ cells (in bold rectangle, left panel forward scatter (FSC) vs. GFP fluorescence) and dendritic cells (in bold rectangle, right panel MHC II vs. CD11c fluorescence) recovered from alginate gels. (C-E) Groups of 3 mice per timepoint were injected with control alginate or alginate carrying activated GFP^+ DCs. Gels were recovered at indicated times, digested, and recovered cells were analyzed by flow cytometry. (C) Quantification of numbers of GFP^+ cells detected in alginate gels as a function of time following injection of (○) control empty alginate or alginate carrying activated GFP^+ DCs (■). (D) GFP^+ DCs detected in draining lymph nodes (•) and spleens (Δ) over 7 d *in vivo* following injection of self-gelling alginate carrying activated GFP^+ DCs. (E) Total (endogenous + injected) $CD11c^+MHCII^+$ dendritic cells detected in self-gelling alginate matrices injected either with (■) or without (○) activated DCs, and total number of recruited endogenous DCs (▼). Error bars = SEM.

3.3.2 DC delivery

In order to determine whether self-gelling alginate is able to harbor activated dendritic cells following injection, bone marrow-derived DCs from transgenic GFP^+ mice were prepared. GFP expression serves both as a fluorescent marker of the identity of the injected DCs as well as a marker of their viability (164). GFP^+ DCs were activated by treatment with CpG oligonucleotides (ligands for the DC-activating receptor Toll like receptor-9), washed thoroughly, then mixed with alginate solution and Ca^{2+}-loaded microspheres and injected s.c. into the flanks of C57Bl/6 mice ($2x10^6$ DCs in 150 μL alginate). Twenty-two hours post injection, the gels were explanted and examined by confocal fluorescence microscopy. As shown in Figure 3-3A, GFP^+ dendritic cells were able to adhere and spread within the gel over this timeframe *in vivo*. Some cells were also observed to be actively migrating through the gel when observed in time-lapse (data not shown). Activated DCs are known to have a short lifespan of only a few days (165, 166), and many fewer GFP^+ cells were detectable by confocal microscopy in gels explanted after 7 days (data not shown).

Previous studies investigating the fate of dendritic cells following administration as DC vaccines have shown that following bolus s.c. or intradermal injection of free cells, many DCs remain at the injection sites for several days, even though activated DCs express the chemokine receptor CCR7 that guides homing to lymphatics and draining lymph nodes (157, 167-169). In order to track the lifespan and location of DCs injected in alginate vaccination nodes, GFP^+ dendritic cells were activated with LPS for 18 hrs, then $2x10^6$ cells were mixed with self-gelling alginate and injected s.c. in C57Bl/6 mice. The gels, spleens, and draining lymph nodes of injected mice were isolated on days 2, 4, or 7, digested, and recovered single cell suspensions were stained with antibodies for cell surface markers and analyzed by flow cytometry. Injected DCs at each location were detected via GFP fluorescence, while the total number of recovered dendritic cells (both injected cells and endogenous host DCs) present at the site/organ was identified on the basis of CD11c and MHC II co-expression, as shown in Figure 3-3B. At 1 hr following injection, ~25% of the injected DCs could be recovered from gels (Figure 3-3C). By two days post-injection, about ~15% of the inoculated dendritic cells were still present in the alginate gel and their numbers continued to decline to ~0 by day 7 (Figure 3-3C), due to death of the short-lived activated cells and/or emigration from the matrix. The total number of GFP^+ cells detected in the draining lymph nodes or in the spleens peaked on day 2, and declined over the ensuing 5 days (Figure 3-3D). The relatively low numbers of exogenous DCs detected migrating from gels to draining lymph nodes were comparable to findings in prior studies in which purified mouse dendritic cells were injected s.c. as free cell suspensions (168). Importantly, even such low numbers of DCs have been implicated in initiation of potent immune responses (167-169).

Dendritic cells can transfer membrane, antigen, and even intact peptide-MHC complexes to other DCs through direct contact or through release of vesicular structures known as exosomes (170, 171); thus host DCs can play a major role in the immune responses elicited by injected DC vaccines. Strikingly, though the number of exogenous DCs in alginate gels quickly decayed over 1 week following injection, host DCs were rapidly recruited to the alginate matrix in response to the presence of the injected cells and alginate. As shown in Figure 3-3E, the infiltrate of the host $CD11c^+MHCII^+$ dendritic cells (injected and endogenous) was sustained over 7 days, by which time nearly all of the DCs present in the alginate were host cells, constituting ~6% of the

total cellular infiltrate in gels at this timepoint. While the initial presence of exogenous DCs facilitated the recruitment of $CD11c^+MHCII^+$ DCs during the early time points, the steady immigration of host $CD11c^+MHCII^+$ in empty alginate also elucidates the importance of alginate, acting synergistically with the exogenous DCs, in the host DC recruitment. To determine if this increased number of host DCs attracted to activated-DC-carrying gels was limited to accumulation of host cells at the edge of gels in a classic foreign body-type response or involved direct migration of cells into the matrix, we injected gels loaded with unlabeled mature DCs into GFP^+ mice. 3D optical sectioning of gels explanted 2 or 7 days after injection showed that GFP^+ host cells (some with obvious dendritic morphology) had infiltrated into the gels as far as confocal imaging could clearly resolve (~100 μm into gels, data not shown). Thus, injected activated DCs are rapidly lost from the alginate vaccination nodes, with a small number trafficking to lymph nodes, while host DCs rapidly replace these cells and remain in the gels over at least 7 days.

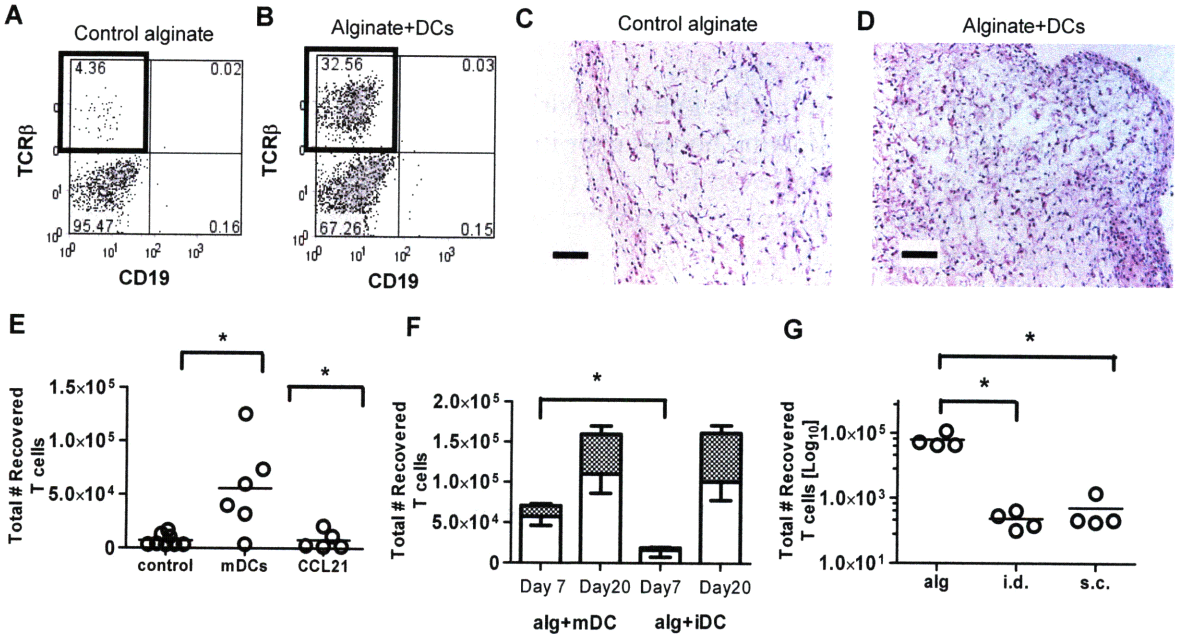

Figure 3-4: Alginate matrices carrying mature DCs chemoattract T cells *in vivo*. Self-gelling alginate carrying dendritic cells or control 'empty' gels were injected s.c. in C57Bl/6 mice (groups of 5-8 mice per timepoint), recovered at different time points, and analyzed by flow cytometry and histology. (A, B) Flow cytometry analysis of cells recovered from gels after 7 d in vivo and stained with antibodies against the T cell receptor (TCR□) or CD19 (a B cell marker). Control 'empty' alginate elicited minimal T cell infiltration (A) but alginate carrying CpG-matured dendritic cells attracted a substantial T cell infiltrate (B). (C, D) H&E-stained histological sections of gels 7 d following injection: (C) control empty alginate, (D) alginate carrying mature dendritic cells. (scale bars 100μm). (E) Quantification of total T cell infiltrate after 7 d in vivo in control empty alginate gels, gels loaded with mature DCs (mDCs) or gels loaded with 2 μg CCL21 (CCL21). Each open circle represents the response in an individual mouse (* statistically significant differences, $p<0.05$, Dunn's multiple comparison test). (F) Quantification of CD4 T cell (open portion of bars) and CD8 T cell (hatched portion of bars) infiltration of alginate gels carrying immature (alg+iDC) vs. mature DCs (alg+mDC) at 7 and 20 d post-injection. (* statistically significant differences $p<0.05$ by one-tailed unpaired Student's t test). Error bars = SEM. (G) Comparison of T cell attraction to different sites of DC injection: alginate gels carrying mature DCs (alg), intradermal injection of free mature DCs (i.d.), or subcutaneous injection of free mature DCs (s.c.). (* significant differences $p<0.05$ by one-tailed unpaired Student's t test).

3.3.3 T cell recruitment

For alginate vaccination nodes to be effective in directing the physical locale of an immune response, the attraction of both DCs and host T cells to alginate gels would be a key event. Activated DCs secrete several chemokines known to attract T cells (172-174), and thus we hypothesized that DCs would promote T cell infiltration of alginate vaccination nodes. In order to investigate T cell attraction to alginate matrices, self-gelling alginate gels with or without CpG-matured DCs were injected s.c., and gels were recovered and digested after 2 or 7 days for analysis of cellular infiltrates. Cells recovered from gels were antibody stained to detect expression of T cell receptor (TCR), CD11c (as a marker of DCs), and CD19 (as a marker for B cells) and analyzed by flow cytometry. As shown in Figures 3-4A and 3-4B, by day 7 alginate containing CpG-matured dendritic cells elicited a greatly increased infiltration of T cells relative to control alginate lacking DCs, making up ~30% of the total infiltrate. Few if any B cells were detected in either case. Hematoxylin/eosin-stained histological sections of alginate gels recovered after 7 days showed a substantially increased cellular infiltrate within gels injected with activated DCs (Figure 3-4D) compared to control alginate (Figure 3-4C). Quantification of total T cells attracted to gels (Figure 3-4E) showed an 8-fold increase in the total number of T cells present in mature DC-carrying gels vs. 'blank' alginate. This increase in T cells in the gels was not simply a nonspecific increase in all inflammatory cells, as the total number of cells recovered from alginate gels carrying mature DCs was only 2-fold over 'blank' alginate gels on day 7 (data not shown). Interestingly, delivery of the strong T cell chemoattractant CCL21 by mixing 2 μg CCL21 with alginate prior to injection as a non-cellular alternative could not substitute for activated DCs in driving T cell attraction to the gels (Figure 3-4E). Although the number of T cells recruited to alginate gels carrying CCL21 was increased compared to control blank alginate on day 2 (data not shown), the effect of the chemokine alone was not statistically significant by day 7 (Figure 3-4E). We also compared alginate gels injected with activated DCs or immature (non-activated) DCs to determine whether DC maturation was important for the T cell recruitment response. Injection of immature DCs in alginate attracted few T cells by 7 days (not statistically different from blank alginate), but by 20 days post injection, T cell infiltration into gels that had initially harbored immature (iDC) or mature DCs (mDCs) was essentially identical and T cells made up nearly 50% of the total cellular infiltrate (Figure 3-4F and data not shown). On day 7, about 19% of the total T cells recovered were $CD8^+$ T cells in alginate + mDC gels; $CD8^+$ T cells increased to ~31% of the total T cell population by day 20. Altogether, alginate vaccination nodes carrying activated dendritic cells rapidly recruited both host T cells and dendritic cells to the matrix, and these cellular infiltrates were sustained over more than three weeks *in vivo*.

To determine whether the alginate matrix and activated DCs have a synergistic role in the attraction of host T cells, we compared T cell infiltration into DC-loaded alginate gels with T cell infiltration into s.c. or intradermal tissue sites where activated DCs were injected alone in saline. Intradermal injection of activated DCs, which is one of the most promising routes of DC administration in dendritic vaccines, has been reported to elicit some T cell attraction to the injection site detectable by histology (157). Figure 3-4G shows that at least 125-fold more T cells were recovered from DC-carrying alginate gels than from s.c. or i.d. sites of DC-only injection. Moreover, the T cell recruitment phenomenon observed in gels carrying DCs was not a result of a nonspecific response against massive dead cells at the injection site, as confirmed by injection of apoptotic and necrotic DCs in the gels that showed inferior attraction of T cells to the

gel site (Figure S2, Appendix B.1). This result illustrates the unique T cell recruitment response elicited by dendritic cell vaccination using alginate gels.

3.3.4 T cell priming and re-trafficking

The data shown above demonstrate the attraction of host T cells and dendritic cells to activated DC-loaded alginate matrices. Once T cells and DCs are brought together, the key function of activated DCs is to present antigenic peptides to T cells and initiate T cell priming. To determine whether antigen-loaded dendritic cells delivered in alginate gels could initiate priming of naïve T cells and to track the evolution of a T cell response initiated by alginate vaccination nodes, we used an adoptive transfer model to create a defined antigen-specific T cell population in host mice (schematically described in Figure 3-5A). In these experiments, CFSE-labeled T cell receptor (TCR)-transgenic 2C splenocytes, whose T cells express a TCR that recognizes the peptide sequence SIYRYYGL (SIY peptide) bound to H-2K^b class I MHC, were adoptively transferred into syngeneic C57Bl/6 mice, allowing the labeled T cells to take up residence in the lymph nodes and spleen of the recipient animals and recirculate through the blood along with the endogenous T cell population. The adoptively-transferred cells can be identified *ex vivo* by staining with the antibody 1B2 (a monoclonal antibody that specifically recognizes the 2C TCR (175)) and by CFSE fluorescence. As shown in Figure 3-5B, flow cytometric analysis of cells recovered from lymph nodes of animals receiving 2C T cells reveals a clearly detectable population of 1B2$^+$CFSE^{hi} cells, representing naïve, undivided 2C T cells (~0.3% of the CD8$^+$ T cell population in lymph nodes). Activation and proliferation of these T cells *in vivo* leads to halving of the CFSE fluorescence level on each cell division, such that divided cells are distinguished by steadily decreasing levels of CFSE fluorescence (illustrated in Figure 3-5B, right panel).

To assess antigen-specific T cell priming in this system, CFSE-labeled 2C cells were transferred to groups of recipient C57Bl/6 mice. Twenty-two hours later, these recipient mice were immunized s.c. on the flank with alginate containing activated dendritic cells that had been loaded with SIY peptide *in vitro*. Control gels lacking DCs were injected on the opposite flanks of the same mice (Figure 3-5A). Gels, draining lymph nodes, and spleens of the mice were harvested on day 3, day 5, or day 7 following immunization to analyze the kinetics and localization of the SIY-specific 2C T cells over time.

Figure 3-6A shows representative flow cytometry plots of 1B2 expression vs. CFSE fluorescence levels for cells recovered from the secondary lymphoid organs and alginate gels following immunization with DC-loaded alginate, summarizing the timecourse of 2C T cell responses. The scatter plots show events gated on live cells (propidium iodide^{low}) for gel samples and gated on CD8$^+$ cells for secondary lymphoid organs; CD8$^+$ cells constituted ~30% of the LNs and ~20% of the spleens. 1B2$^+$ 2C T cells detected in each sample are highlighted by overlaid bold rectangles on the scatter plots. By day 3 following immunization with alginate gels, adoptively transferred 2C cells were readily detected in lymph nodes (LNs) and spleen, but few, if any, cells had entered alginate gels (with or without injected DCs); the 2C T cells had not yet begun to undergo cell division in response to the immunizations. (The few 1B2$^+$CFSE^{low} cells in the day 3 plots from lymph nodes and spleens arise from a low nonspecific background staining, as confirmed by control staining of wild-type, non-adoptively transferred spleens and lymph nodes (data not shown)). Five days post immunization, priming and proliferation of 2C cells was strongly evident in the draining LNs and activated CFSE^{low} 2C T cells were detected in the

spleens of immunized mice. Still very few 2C cells were detected in the alginate gels; these results indicate that priming of the antigen-specific T cells is initiated by DCs in the draining lymph nodes– either injected SIY-DCs that migrated from the alginate gel to the LNs, or SIY peptide carried to LNs by host DCs attracted to the injection site.

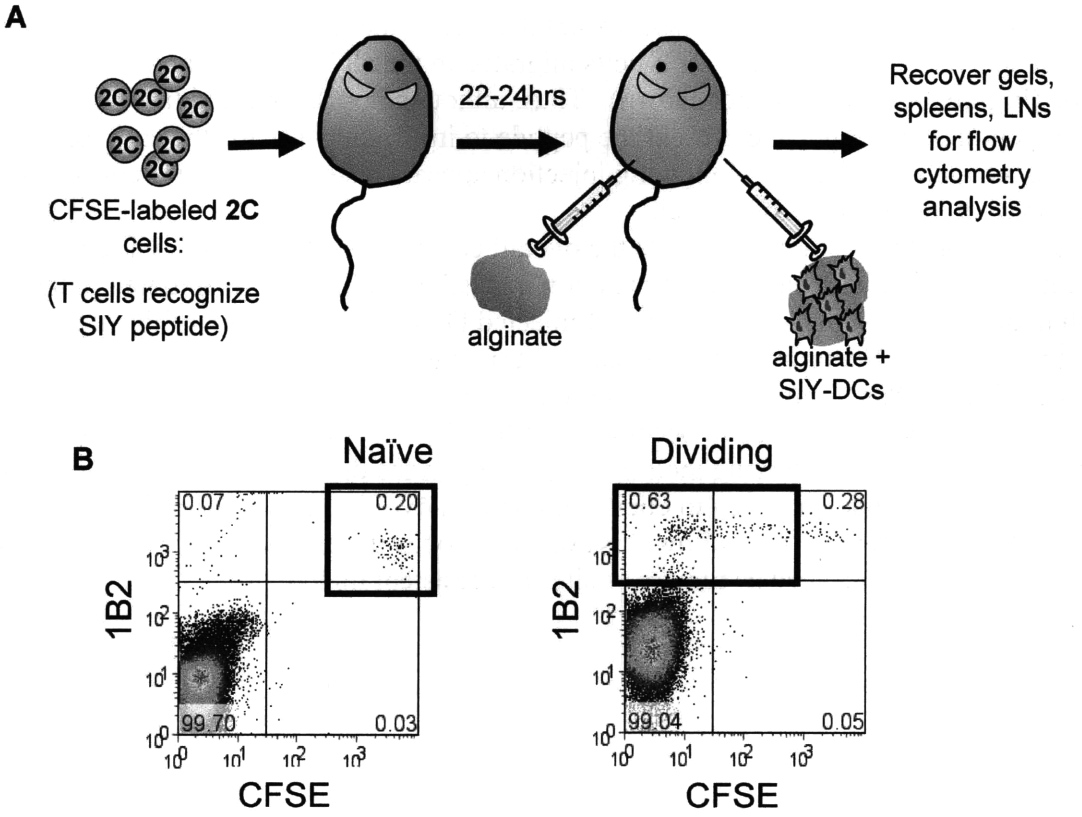

Figure 3-5: Adoptive transfer model for tracking antigen-specific T cell responses following vaccination node immunization. (A) CFSE-labeled 2C splenocytes were retro-orbitally injected into wild type C57BL/6 mice, and 22 hrs later the mice were immunized with control alginate on the left flank and alginate containing activated, SIY peptide-pulsed DCs on the right flank. The gels, inguinal lymph nodes, and spleens were then isolated at various timepoints after immunization for flow cytometry analysis. (B) Flow cytometry scatter plots (gated on $CD8^+$ cells) illustrating detection of naïve$1B2^+CFSE^{bright}$ 2C cells in lymph nodes following adoptive transfer (before immunization), and dividing $1B2^+$ $CFSE^{low\text{-}intermediate}$ 2C cells which are in the process of being primed/activated following immunization.

Seven days post immunization, a robust $CFSE^{low}1B2^+$ 2C effector T cell population was detected in alginate gels that had been initially injected carrying SIY-pulsed DCs, but not in control 'blank' gels from the opposite flanks of immunized mice. Figure 3-6B shows the percentage of $CD8^+$ T cells and 2C T cells that infiltrated the control alginate and alginate+SIY-DC samples by day 7, showing that a large fraction of the $CD8^+$ T cells that infiltrate the gels are 2C T cells. The lack of activated 2C T cell recruitment to the control gels indicates that 2C T cell homing to the alginate+SIY-DC gels is not a nonspecific attraction as part of the host response to alginate alone, but is rather dependent on the presence (initially) of the activated

exogenous DCs, the SIY antigen, or both. To distinguish between these possibilities, a control experiment was performed where mice with adoptively-transferred 2C T cells were immunized on one flank with alginate carrying activated DCs (but lacking SIY peptide) and on the opposite flank with alginate carrying free SIY peptide but no DCs. In these animals, T cell priming had already initiated in the LN by day 2 as some of the soluble SIY peptide drained to the lymph nodes (data not shown). By day 7, a few 2C T cells migrated to alginate containing activated (antigen-free) DCs, but to a much lesser extent than when the DCs had been loaded with SIY (data not shown). Likewise, few 2C T cells migrated to the alginate gels carrying free SIY peptide (Figure 3-6C and data not shown). Thus, although host DCs could theoretically infiltrate the SIY peptide-loaded gel and present the peptide to infiltrating T cells, the early presence of activated, antigen-bearing DCs following injection appears to set the stage for enhanced attraction of effector T cells to the gel.

The data from these studies suggests the overall chain of events outlined in Figure 3-1 for a single immunization with alginate 'vaccination nodes:' T cell priming is initiated in the draining lymph nodes, either by the small number of injected DCs that migrate out of the alginate and reach the draining LNs, or by host DCs that infiltrate the alginate and pick up antigen from live or dying injected DCs. Importantly, the presence of activated antigen-pulsed DCs in the gels conditions the vaccination node to become a site for directed homing/accumulation of activated antigen-specific T cells following their initial priming in the draining lymph nodes. The ability of this vaccination node approach to elicit priming of naïve T cells and then direct their trafficking to a defined site may allow this system to focus the effector phase of the immune response at a target site, such as tumors or sites of persistent infections.

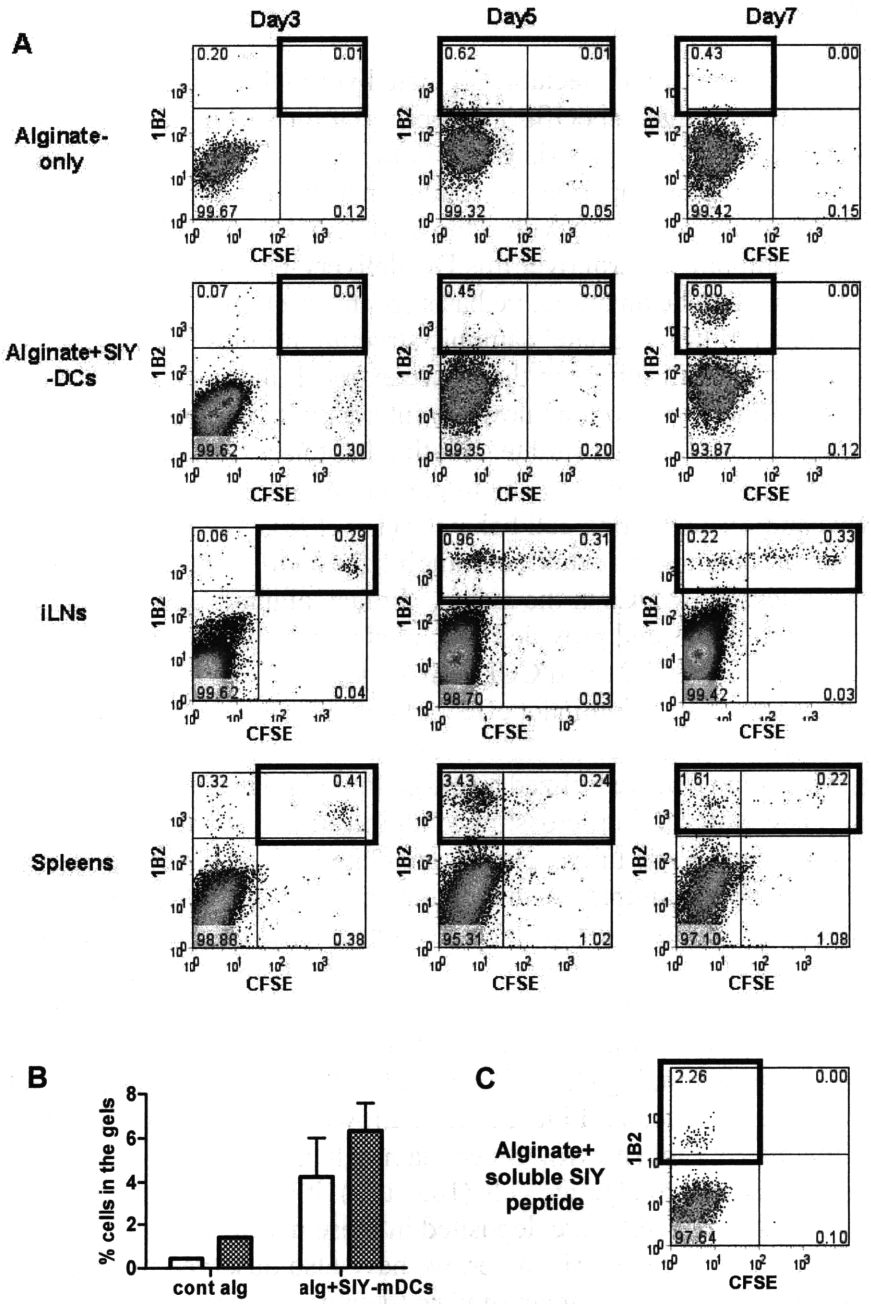

Figure 3-6: Dendritic cells delivered in alginate gels initiate T cell priming in draining lymph nodes and recruit activated T cells to the alginate matrix. (A) Flow cytometry scatter plots (CFSE vs. 1B2) tracking the temporal evolution of 2C T cell activation and trafficking following immunization with alginate gels. Shown are analyses of cells recovered from control alginate, alginate carrying peptide-pulsed mature DCs, inguinal lymph nodes, and spleens show the biodistribution and cell division on days 3, 5, or 7 after gel injection. Heavy boxes highlight $1B2^+$ 2C T cells recovered from each sample. (B) Quantification of 2C T cells as a percent of all live cells recovered (open bars) and total $CD8^+$ T cells as a percent of all live cells recovered (dotted bars) in control alginate and alginate carrying SIY-pulsed mature DCs on day 7 (n = 2 mice per condition). (C) In a control experiment, mice that had received CFSE-labeled 2C T cells were injected on one flank with alginate carrying SIY-pulsed DCs and on the other flank with alginate carrying SIY peptide alone. Error bars = SEM. Data are from one representative of two independent experiments.

3.4 Discussion

In this chapter, the ability of an injectable alginate hydrogel to support the delivery of dendritic cells and initiate antigen-specific T cell priming for vaccination or immunotherapy was demonstrated. The choice of an appropriate matrix to deliver DCs in this application was dictated by the desire for a biocompatible, injectable material capable of binding factors secreted by DCs to promote their concentration within the matrix, but which would eventually dissolve over time to provide temporal control over this DC delivery-based therapy. Based on these criteria, we found alginate to be an attractive basis for this system, as described in Chapter 2. In addition to its biocompatibility, alginate's anionic structure mimics the presence of negatively charged sugars such as heparan sulfate in the native extracellular matrix environment. Chemokines (and cytokines) *in vivo* are known to interact with and bind cell surface and ECM glycosaminoglycans such as heparan sulfate, creating haptotactic gradients of immobilized chemokines. Matrix binding is thought to be important in the cell-guiding properties of many chemokines *in vivo* and for regulating cell behavior (176-178). We hypothesized that alginate matrices would support chemokine/cytokine immobilization to favor the concentration and retention of factors released by DCs in the matrix. In fact, alginate gels reversibly bound positively charged chemokines and provided sustained release of leukocyte attractant molecules (Figure 3-2). The release of CCL21 and CCL19 from alginate was strongly dependent on their effective net charge, indicating a dominant effect of charge-charge interactions on the release rate of these molecules.

To apply this system *in vivo*, we utilized a self-gelling alginate formulation obtained by mixing soluble alginate with calcium-crosslinked alginate microspheres. Alginate with a high G content (SLG20) was used for the microspheres, enabling high levels of calcium ions to be loaded into each microsphere; alginate with a high M content (SLM20), which forms mechanically softer gels, was used for the matrix alginate to favor cell infiltration. When compared with other injectable biopolymers such as collagen and Matrigel in pilot studies, alginate demonstrated substantially greater mechanical stability, which allowed reproducible quantitative analysis of cellular infiltrates (data not shown).

In addition to reversibly binding chemokines, self-gelling alginate was able to harbor exogenously injected dendritic cells (Figure 3-3A), allowing them to spread and adhere as well as migrate inside the matrix (not shown). Since mammalian cells have been previously reported to exhibit little or no adhesion to alginate gels (103, 179), it is possible that adhesion proteins (e.g., secreted by local stromal cells) are deposited in these matrices *in vivo* over time, enhancing cell adherence and migration *in situ*. However, we have also observed that freshly isolated splenocytes migrate in self-gelling alginate *in vitro* (data not shown), which may imply that leukocytes possess the ability to migrate through alginate gels via a mechanism independent of integrins or other common adhesion molecules. Along these lines, T cells have been observed to migrate through fibrillar collagen gels even in the presence of blocking antibodies against the known lymphocyte integrins (180, 181) or in the total absence of functional integrins (139).

One of the factors determining the efficacy of dendritic cell vaccines is the route of administration of antigen-loaded DCs, and studies of DC immunization have suggested that the majority of inoculated cells remain at the injection site (167-169). Of the few DCs that do migrate away from the injection site, Eggert et al. (164, 167) showed that subcutaneously or intradermally injected DCs migrate preferentially to the draining lymph nodes. In order to track the trafficking of DCs following injection in our alginate gel system, we generated and injected

GFP^+ mature dendritic cells. In agreement with earlier studies (164, 168), the total number of inoculated DCs detected in draining lymph nodes peaked 2 days after s.c. injection (Figure 3-3D). Many dendritic cells also remained within the gels over several days (Figure 3-3C). One of the challenges of DC vaccines is to prolong the period of time MHC-peptide-complexes are displayed by short-lived activated DCs (182), and if alginate can act as a local depot for protein antigen or peptide-MHC complexes which can be transferred to attracted host DCs, this might sustain stimulation of effector cells. Notably, despite the steady loss of injected DCs, the total number of $CD11c^+MHCII^+$ cells in DC-carrying gels remained nearly constant over the first week *in vivo* (Figure 3-3E).

In addition to recruiting a large number of host antigen presenting cells, we examined whether dendritic cells delivered with self-gelling alginate *in vivo* recruit T cells to the injection site, as the generation of antigen specific effector T cells and their proper trafficking are crucial to successful dendritic cell vaccines. Activated DCs secrete a number of chemoattractants for T cells (172-174), and histological analysis of human patients receiving intradermal injections of DCs has shown evidence for specific attraction of T cells to sites of DC injection (157). Alginate by itself elicited minimal T cell infiltration, but in the presence of mature dendritic cells, large numbers of T cells were attracted to these matrices, with both $CD4^+$ (~70-80%) and $CD8^+$ (~20-30%) T cells present (Figure 3-4). Compared to standard immunization regimens where free DCs are injected in s.c. or i.d. sites, more than 100-fold greater levels of T cells were drawn to alginate matrices loaded with DCs relative to free DC injection at native tissue sites. The T cell infiltrate in the presence of DCs persisted for over 20 days *in vivo* (Figure 3-4F) until the alginate gels dissolved (data not shown). Because the time for dissolution of alginate gels can be readily manipulated by changes in the crosslinking and molecular weight of the alginate chains (80, 103), it should be possible to specifically design these gels to last for requisite time periods and maintain T cell localization at chosen peripheral tissue sites for defined periods.

Given that mature dendritic cells were able to attract both T cells and host dendritic cells to alginate gels, we examined whether antigen-pulsed dendritic cells delivered in alginate could initiate an immune response and redirect effector T cell trafficking to the gels. Analysis of the cell division profile of a labeled, adoptively-transferred clonal T cell population over time *in vivo* indicated that T cell activation following alginate gel/DC immunization was initiated in the draining lymph nodes, followed by migration of primed T cells to the spleen and alginate matrix site which initially contained exogenous mature dendritic cells. Whether further priming and proliferation of T cells take place within the gels is yet to be verified, though we have detected elevated levels of interferon-γ in these gels (data not shown). The majority of T cells that homed to alginate gels containing SIY-pulsed DCs were $1B2^+$ 2C cells (Figure 3-6C), demonstrating the antigen-specific nature of the effector cell retrafficking to these sites.

Based on these findings, we hypothesize that attraction of primed, antigen-specific T cells to DC-loaded alginate gels can be used to redirect the physical locale of the effector phase of an immune response. For example, injection of DC-loaded alginate gels around solid tumors may allow host DCs and anti-tumor T cells to be concentrated in the tumor microenvironment. Factors can be delivered from alginate matrices to counter immunosuppressive factors secreted from the tumor microenvironment. The feasibility of co-delivering supportive factors (e.g., inflammatory cytokines, Toll-like receptor ligands, etc.) in the alginate matrix provides numerous means to locally foster an anti-tumor immune response using this system.

3.5 Summary

The overall efficacy of dendritic cell vaccines depends on multiple factors, including the state of dendritic cell maturation, the dose of antigens, the choice of adjuvant, the route of immunization, effector cell re-trafficking, etc. Here in this part of the thesis work we have shown that 'vaccination nodes,' injectable alginate gels carrying dendritic cells, are able to initiate an immune response with DCs acting as a physiological adjuvant for antigen delivery, while simultaneously conditioning the alginate matrix to guide effector immune cells to migrate to the gel. We thus believe vaccination nodes combine the T cell priming potential of dendritic cell vaccines with the ability to guide the traffic of effector cells to desired tissue sites.

3.6 Acknowledgements

The work presented in this chapter was supported in part by the Defense Advanced Research Projects Agency and the 3M Innovation Fund. We would like to thank the Division of Comparative Medicine Histology Lab at MIT for helpful discussions/advice and assistance with histological analyses.

Chapter 4
APPLICATION OF VACCINATION NODES TO TUMOR THERAPY

With the understanding that self-gelling alginate can deliver immunostimulatory/immunomodulatory factors of different nature in a sustained manner both *in vitro* and *in vivo*, and allows easy cellular infiltration, together with the observations that the synergy between alginate and activated dendritic cells can generate and re-focus immune responses to a desired peripheral injection site, we examined the application of these vaccination nodes to tumor settings. In order to augment the efficacy of the vaccine, the delivery of IL-15 superagonist complex from the self-gelling alginate was explored. The robust nature of self-gelling alginate also allowed us to study the types of cells at the local tumor sites that contribute to efficient and successful control of tumor growth.

4.1 Introduction

Local therapies for cancer are of interest for treating unresectable metastases and/or for treating sites of resection to combat local recurrence (183-185). Most immunotherapy strategies seek to promote the robust infiltration of tumors with functional immune cells to promote tumor destruction. However, defects in tumor vasculature, suppressive signals produced by tumor cells or co-opted tumor-resident immune cells, and rapid tumor growth can limit the accumulation of activated and competent immune cells (186, 187). Recently, combinations of cytokine, chemotherapy, and/or immunostimulatory ligand treatments used to locally treat established tumors have shown promise in not only eliminating treated tumors but also generating systemic immunity capable of destroying large distal tumors (49, 69, 133, 188-190). However, such powerful treatments may need to be coupled with methods to control delivery of these potent immunoregulatory factors and limit systemic toxicity (191, 192) . Prior work has demonstrated that controlled release of immunocytokines from gels or microparticles at a tumor site can enhance local immunotherapies, by sustaining the intratumoral concentration of these factors while reducing systemic exposure following a single injection (67, 124, 193). Thus, the use of biomaterials to deliver local combinatorial immunotherapies may lead to further enhancements in the potency and safety of such treatments.

In the previous chapters, we described an injectable gel formulation of alginate, which can be loaded with exogenous immune cells, proteins, or immunoregulatory factors. Alginate

has been studied extensively as a matrix for cell therapy and tissue engineering, and has been shown to be safe for use in patients (194-196). We found that injection of alginate gels with embedded activated dendritic cells in healthy mice elicits a sustained infiltration of host T-cells and dendritic cells into the matrix, and that these matrices can release encapsulated cytokines over a period of 7-14 days (197, 198). We hypothesized that a similar recruitment of lymphocytes and DCs to alginate gels surrounding established tumors could promote local antigen presentation and provide a local reservoir of immune cells for tumor invasion supported by immunoregulatory factors released from the gel. To test this concept, we surrounded established melanoma tumors with DC/cytokine/TLR ligand-loaded gels, and analyzed tumor growth and the recruitment of leukocytes to the tumor-engulfing gels and the tumors themselves. A single injection of alginate ECMs carrying DCs and the immunoregulatory cytokine IL-15 superagonist (IL-15SA) concentrated the cytokine within the tumor and led to prolonged control/regression of established melanomas. Importantly, immune cell recruitment into peritumoral gels correlated with infiltration of the adjacent tumor. Because these gels were stable at least one month *in vivo*, they were readily recovered post-treatment to monitor the composition of the tumor-local cellular infiltrate. We found that immune cell accumulation within these peritumoral ECMs was substantial only under conditions where tumor growth was strongly suppressed, and was completely lacking in mice where tumor growth was progressing.

4.2 Materials and Methods

4.2.1 Materials

Sterile alginates Pronova SLM20 (MW 75,000–220,000 g/mol, >50% M units) and Pronova SLG20 (MW 75,000–220,000 g/mol, >60% G units) were purchased from Novamatrix (FMC Biopolymers, Sandvika, Norway). Anti-mouse FITC-TCRβ, anti-mouse PE-I-A^b, anti-mouse APC-CD11c, anti-mouse APC-CD8α, anti-mouse APC-CD4, anti-moue FITC- and PE-NK1.1 were purchased from BD Biosciences (San Jose, CA). APC-tetramer ova-MHC I was from Beckman Coulter (Fullerton, CA), anti-mouse PE-CD8α antibody was from Invitrogen (San Diego, CA), and anti-mouse foxp3 staining kit was from eBioscience (San Diego, CA). Isooctane was obtained from Mallinckrodt Baker (Phillipsburg, NJ). Calcium chloride dihydrate and alginate lyase were from Sigma-Aldrich (St. Louis, MO). CpG oligonucleotides with a phosphorothioate backbone (CpG 1826, sequence 5'-/5AmMC6/TCCATGACGTTCCTGACGTT-3') were synthesized by Integrated DNA Technologies. Mouse IL-15 and mouse IL-15Rα-human Fc chimera recombinant proteins and ELISA detection kits were purchased from R&D Systems (Minneapolis, MN).

4.2.2 Animals and cells

Animals were cared for in the USDA-inspected MIT Animal Facility under federal, state, local and NIH guidelines for animal care. C57Bl/6 mice were obtained from the Jackson Laboratory. Bone marrow-derived dendritic cells were prepared following a modification of the procedure of Inaba (99) as previously reported (100). DCs were activated/matured with 1μM CpG and pulsed with 1 μg/mL each of ova class I and ova class II peptides (Anaspec, San Jose, CA) for 18 hrs and washed 3X with PBS before use. B16-ova cells based on the B16F0 parental melanoma line were transfected with ovalbumin expressed as an MSCV vector with puromycin

resistance, followed by an IRES and Ovalbumin-2A-green fluorescent protein (GFP). The ova expressed in these cells lacks the first 55 amino acids (deleting the secretion signal) and is soluble in the cytoplasm.

4.2.3 Calcium reservoir microsphere synthesis and self-gelling alginate

Alginate microspheres were synthesized as described in the previous chapters, by emulsifying a 1% solution of SLG20 alginate in isooctane followed by the addition of aq. $CaCl_2$ to crosslink the alginate. The resulting particles were washed with water and stored at 4°C until use.

4.2.4 Tumor inoculation and alginate gel therapy

Except where noted otherwise, anesthetized C57Bl/6 mice were inoculated with $3x10^4$ B16-ova cells s.c., which were allowed to establish for 14 days. IL-15 superagonist (IL-15SA) was prepared by incubating 5 μg IL-15 and 31.7 μg IL-15Ra/Fc (equimolar amounts) at 37°C in 15.9 μL PBS for 30 min. Matrix alginate (160 μL of 0.01 g/mL SLM20 alginate in sterile PBS at 4°C) was mixed with factors to be delivered (e.g., $2x10^6$ dendritic cells, 36.7 μg IL-15 SA, and/or 80 μg CpG in 150 μL gel) and kept on ice until injection. Calcium-loaded alginate microspheres were synthesized as previously described (94, 198). Endotoxin levels in the alginate preparations were well below levels stimulatory for innate immune cells (97), as described previously (198). The Calcium-loaded microspheres (~$1x10^6$) were mixed with the matrix alginate solution and 150 μL of the mixture immediately injected s.c., surrounding tumors. For i.p. injections, 36.7 μg of IL-15SA was injected in 200 μL of PBS, and for i.t. injections, the same amount of IL-15SA and 2 x 10^6 dendritic cells were injected into tumors in 30μL of PBS.

4.2.5 Flow cytometry analysis

Alginate gels, lymph nodes, and spleens recovered from treated animals were digested with 0.28 WU/mL Liberase Blendzyme 3 (Roche Applied Sciences, Indianapolis, IN) and 1 mg/mL of alginate lyase (Sigma) for 20 min at 37°C. Digested gels and tissues were passed through a 40 μm nylon mesh cell strainer (BD Falcon) with 9 mL complete RPMI medium. Recovered cells were resuspended in FACS buffer (1% BSA, 0.1% NaN_3 in Hank's balanced salt solution, pH 7.4) at 4°C, blocked with anti-CD16/32 antibody for 10 min, then stained with fluorescent antibodies for 20 min on ice, followed by 3 washes with FACS buffer and addition of 1.25μg/mL propidium iodide (PI) for viability assessment. For foxp3 staining, cells were first stained with Live/Dead Fixable Dead Cell Stain Kit (Invitrogen), and then fixed, permealized, and stained according to the manufacturer's instructions (eBioscience). Stained cells were analyzed on a BD FACSCalibur flow cytometer. Enumeration of cellular infiltrates was performed by calibration of flow cytometer events to cell suspensions of known concentration, and cell frequencies determined from a live cell gate with low PI staining. Cell losses during the multiple wash/treatment steps of gel and tissue digestions were reproducible and were accounted for in the reported recovered cell numbers.

4.2.6 IL-15Rα release in vitro and in vivo

Soluble IL-15Rα/Fc (15.9 μg, 2 mg/mL in PBS) was mixed with 80 μL of alginate matrix solution (0.01g/mL in PBS), and then gelled with $5x10^5$ calcium-loaded alginate microspheres to crosslink the alginate in an epppendorf tube for 2 hrs at 37 °C. RPMI medium with 10% FCS was added (500 μL) and cytokine release was assessed by ELISA analysis quantifying IL-15Rα in the supernatant at staggered time points. The release of the IL-15SA was quantified *in vivo* by injecting alginate gels carrying 36.7 μg IL-15SA (31.7 μg IL-15Rα-Fc + 5 μg IL-15) around 14 day-old B16-ova tumors in C57Bl/6 mice. Gels and tumors were recovered from independent mice at staggered times, digested using the same digestion protocol as used for flow cytometry analyses, or by using T-Per Tissue Protein Extraction Reagent (Pierce, Rockford, IL) supplemented by Halt Protease Inhibitor Cocktail (Pierce) according to the manufacturer's instructions. The digestion supernatants were collected and the amount of IL-15SA was quantified by using IL-15Rα ELISA kit or two-site IL-15Rα/IL-15 ELISA. Loss of a fraction of IL-15SA due to the digestion process was accounted for using control digestions with known quantities of IL-15SA added and were accounted for in the analysis.

4.2.7 IL-15 superagonist immobilization on protein A-coated beads

The cytokine (5 μg per gel) and the receptor alpha chain (31.7 μg per gel) were pre-complexed (at 2 mg/mL in PBS) for 30 min at 37 °C, after which the solution was mixed with 1 million Protein A-coated beads (Bangs Laboratories, Rockford, IL) in order to partly mimic the presentation of IL-15 by IL-15Rα on cell surfaces (199). The Protein A-coated polystyrene beads (~10 μm diameter) captured the Fc portion of the IL-15Ra/Fc chimera to present the superagonist complex on the surface of the beads (see Supplemental Figure S3, Appendix B.2). Protein A-coated beads bound about 8% of the IL-15 complex added, leaving the rest of the complex in a soluble form in the self-gelling alginate. The Protein A beads themselves did not cause any activation of BMDCs *in vitro*, i.e. no upregulation of CD40 (a costimulatory molecule which is upregulated upon DC maturation) and MHC class II (upregulation of which is a sign of DC maturation) and no TNF-α (a proinflammatory cytokine) secretion, and the number of Protein A-coated beads (1 million per gel) injected was determined by keeping the endotoxin level to be below 0.1EU. More detailed protocols regarding handling of Protein A –coated beads and IL-15/IL-15Rα complex conjugation to the beads are in Appendix D.6.

4.2.8 Statistical Analysis

All data are shown as mean±S.E. Comparisons of two experimental groups was performed using two-tailed Mann-Whitney tests using GraphPad Prism software (GraphPad Software Inc., La Jolla, CA). Comparisons of Kaplan-Meyer survival curves were made using a log-rank test.

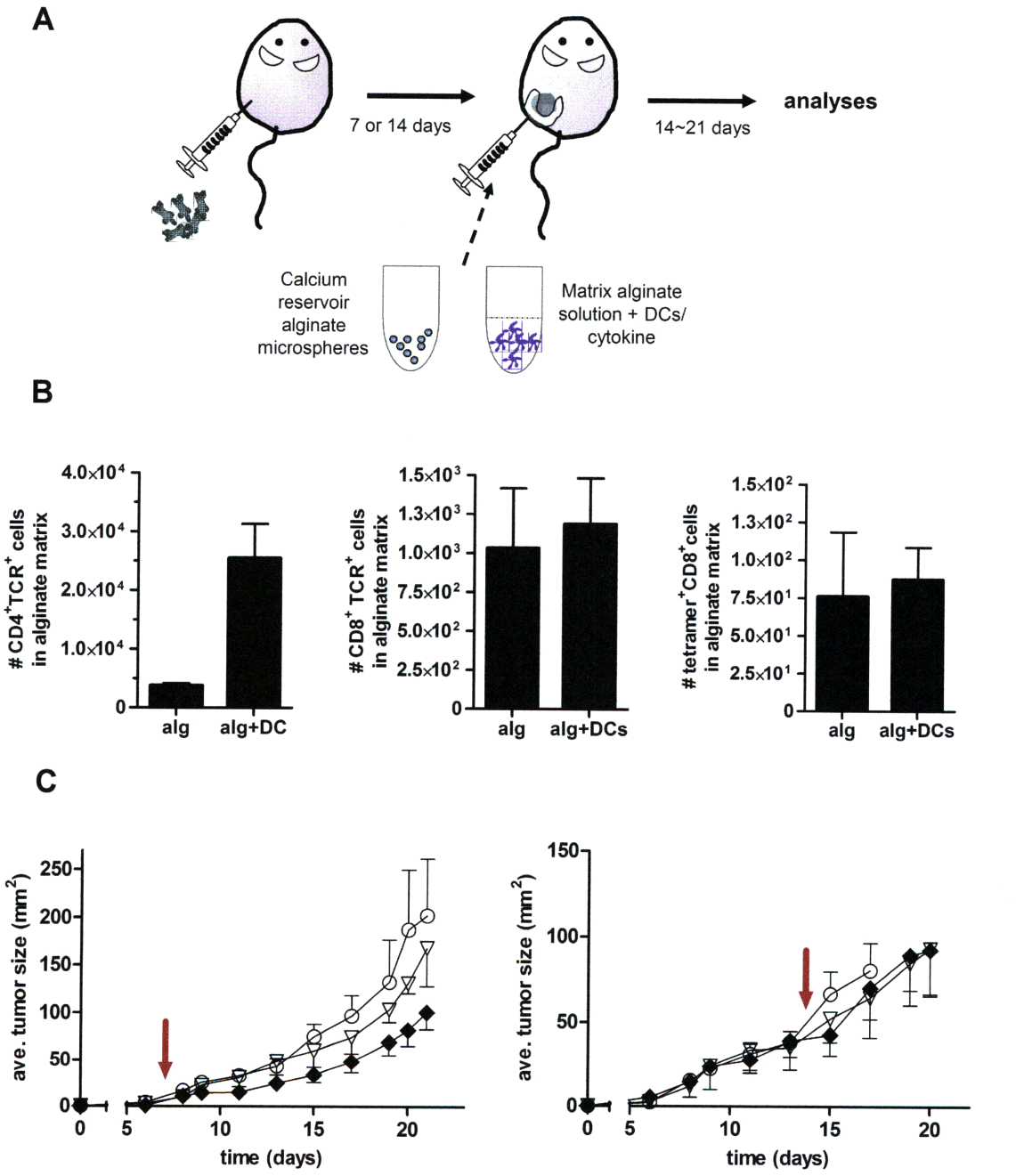

Figure 4-1: Dendritic cell-loaded alginate gels injected around established melanoma tumors elicit peritumoral accumulation of $CD4^+$ T-cells but fail to attract $CD8^+$ T-cells and have limited therapeutic efficacy. (A) Schematic of therapeutic approach. (B, C) C57Bl/6 mice were inoculated with $5x10^4$ B16-ova tumor cells, and 7 or 14 days later, mice received a single peritumoral injection of either empty alginate matrices or alginate carrying $2x10^6$ activated, ova peptide-loaded DCs. (B) Numbers of gel-infiltrating T-cells recovered 14 days after injections (n = 4-5 mice per group, bars: s.e.m.). (C) B16-ova tumor growth following treatment of 7-day- or 14-day-established tumors with alginate gels alone (▽) or alginate loaded with antigen-pulsed DCs (◆) compared to untreated tumors (○) (n = 10 mice per group).

4.3 Results

4.3.1 Immunizations with alginate carrying tumor-antigen pulsed DCs.

In Chapter 3 we showed, in non-tumor-bearing animals, that s.c. injection of alginate gels carrying activated, antigen-loaded dendritic cells elicited priming of naïve $CD8^+$ T-cells in the local draining lymph nodes (supported by migration of a small number of DCs from the gel to the lymph nodes), followed by accumulation of primed antigen-specific T-cells in the gels. To determine whether DCs delivered in alginate gels could similarly promote accumulation of antigen-specific T-cells at solid tumor sites, we analyzed the response of established B16F0 melanoma tumors transduced with GFP and the model antigen ovalbumin (B16-ova tumors) to peritumoral injections of activated, ova peptide-loaded DCs in alginate gels. B16-ova cells were inoculated s.c. in C57Bl/6 recipients and allowed to establish for 7 or 14 days. Mice then received a single injection of alginate (150 μL) to surround tumors with gels carrying activated bone marrow-derived dendritic cells loaded with class I- and class II-restricted ova peptides (Figure 4-1A). Tumor growth was monitored and gels were recovered 14 days after injection for digestion and analysis of the local immune cell infiltrate accumulating at the tumor site. As shown in Figure 4-1B, empty alginate gels injected around 14-day-old tumors contained few $CD4^+$ or $CD8^+$ T-cells. In contrast, gels carrying ova-pulsed, activated DCs elicited a substantial accumulation of $CD4^+$ T-cells. However, in contrast to responses in healthy mice (197), DC-loaded gels did not recruit many $CD8^+$ T-cells or endogenous ova-specific $CD8^+$ T-cells to the peritumoral matrix (Figure 4-1B). Further, the net therapeutic effect of this $CD4^+$-rich T-cell recruitment to the tumor-surrounding gels was limited: DC-carrying gels elicited a minor suppression of 7-day established melanomas and were ineffective for treating 14-day established tumors (Figure 4-1C). Thus, peritumoral gels carrying activated DCs supported the recruitment of $CD4^+$ T-cells to the matrix, but attraction of $CD8^+$ T-cells was poor and the effect on established tumor growth was limited.

4.3.2 Sustained release of IL-15 superagonist from alginate gels.

The poor therapeutic effect of DC delivery in tumor-surrounding gels might have reflected insufficient recruitment of $CD8^+$ T-cells (or other immune effector cells such as NK cells) to the matrices, failure of peritumoral immune cells to actually infiltrate/attack the surrounded tumor, suppression of recruited immune cell function at the tumor site, or a combination of these factors. Thus, we next tested the ability of alginate gels to carry both DCs and immunocytokines, for slow release of signals that would support $CD8^+$ T-cell accumulation and sustained effector functions in the tumor-local environment. Recent studies have demonstrated that IL-15 is capable of reverting anergy in tumor-infiltrating T-cells (200, 201), and that IL-15/IL-15Rα chain complexes function as a superagonist (IL-15SA) that potently expands $CD8^+$ T-cells and NK cell populations *in vivo* (199, 200, 202, 203). Motivated by these prior studies, we mixed pre-formed complexes of IL-15 and recombinant murine IL-15Rα-Fc fusion protein in alginate gels, to obtain sustained release of this cytokine into the tumor environment. In some experiments, $1x10^6$ protein-A-conjugated 10 μm-diameter beads were included in the gel, which immobilized ~8% of the IL-15SA via high-avidity binding of the Fc portion of the IL-15SA complex, in an attempt to mimic cellular presentation of IL-15 within the alginate matrix (Figure S3, Appendix B.2). However, we found that inclusion of the protein-A beads had no detectable

effect on the anti-tumor response at the amount immobilized in these experiments. Self-gelled alginate released encapsulated IL-15SA over ~2 weeks *in vitro* (Figure 4-2A). *In vivo*, IL-15SA-loaded alginate gels injected peritumorally around d14 B16-ova tumors released cytokine for ~5-7 days (Figure 4-2B). In agreement with prior studies of local cytokine delivery (67, 92), the level of cytokine detected in the systemic circulation following tumor-local gel release was substantially lower than levels achieved for the same total quantity of cytokine injected as a bolus i.p., particularly over the first 4 days following injection (Figure 4-2C). In addition, local release of IL-15SA from peritumoral matrices led to peak concentrations of cytokine in the tumor on day 3 post injection that were ~40-fold greater than that achieved by systemic cytokine injection (Figure 4-2D). Thus, IL-15SA delivered locally from peritumoral alginate ECMs lowered systemic exposure to the cytokine and greatly concentrated the dose achieved within the tumor itself compared to i.p. injection.

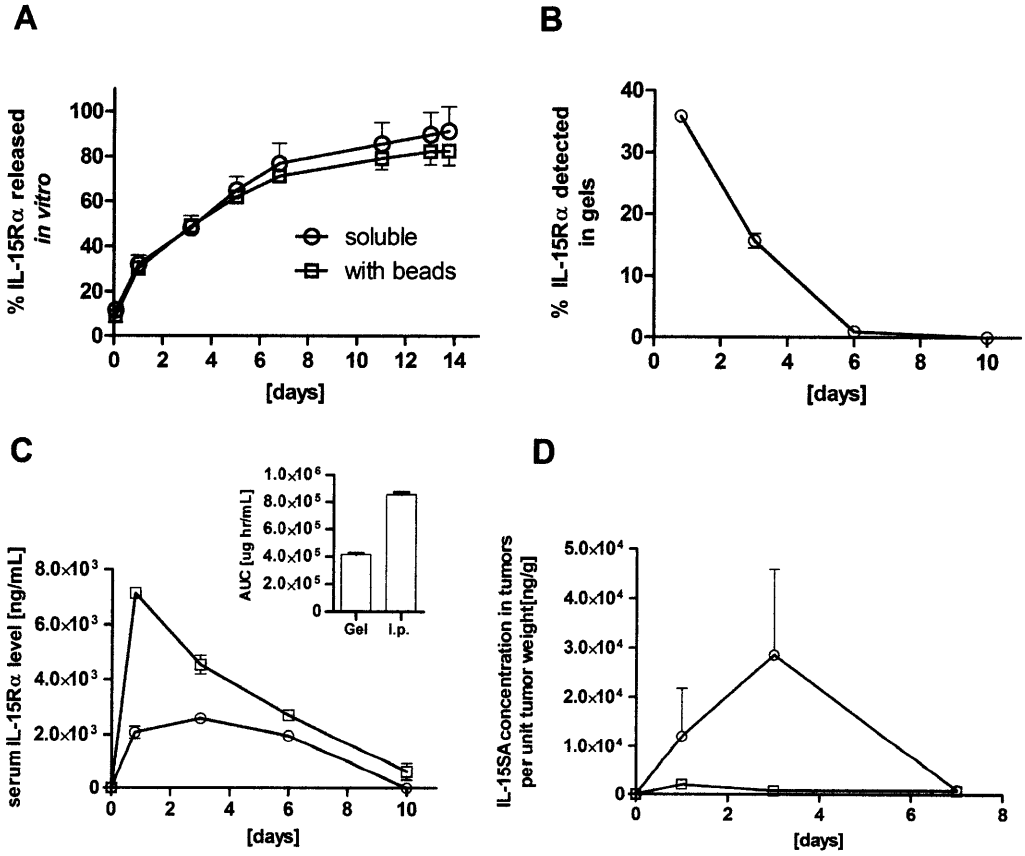

Figure 4-2: IL-15SA loaded in alginate matrices concentrates cytokine in the tumor over several days and lowers systemic exposure relative to systemic injection. (A) 15.9 μg IL-15Rα/Fc was mixed with 80 μL self-gelling alginate *in vitro* and release into RPMI medium with 10% fetal calf serum at 37°C was measured over 2 weeks by ELISA. (B-D) 36.7 μg IL-15SA was mixed with 150 μL self-gelling alginate and injected peritumorally around 14-day-old B16-ova tumors (O). For comparison, the same quantity of IL-15SA was injected i.p. as a separate group (□). Cytokine present in the gels (B), serum (C), and tumor itself (D) was monitored by ELISA over 7-10 days (n = 3-4 samples per time-point). Inset of (C) shows the integrated area under the curve quantifying total cytokine exposure in serum for gel vs. i.p. delivery of IL-15SA over the 10 day timecourse, using IL-15Rα ELISA.

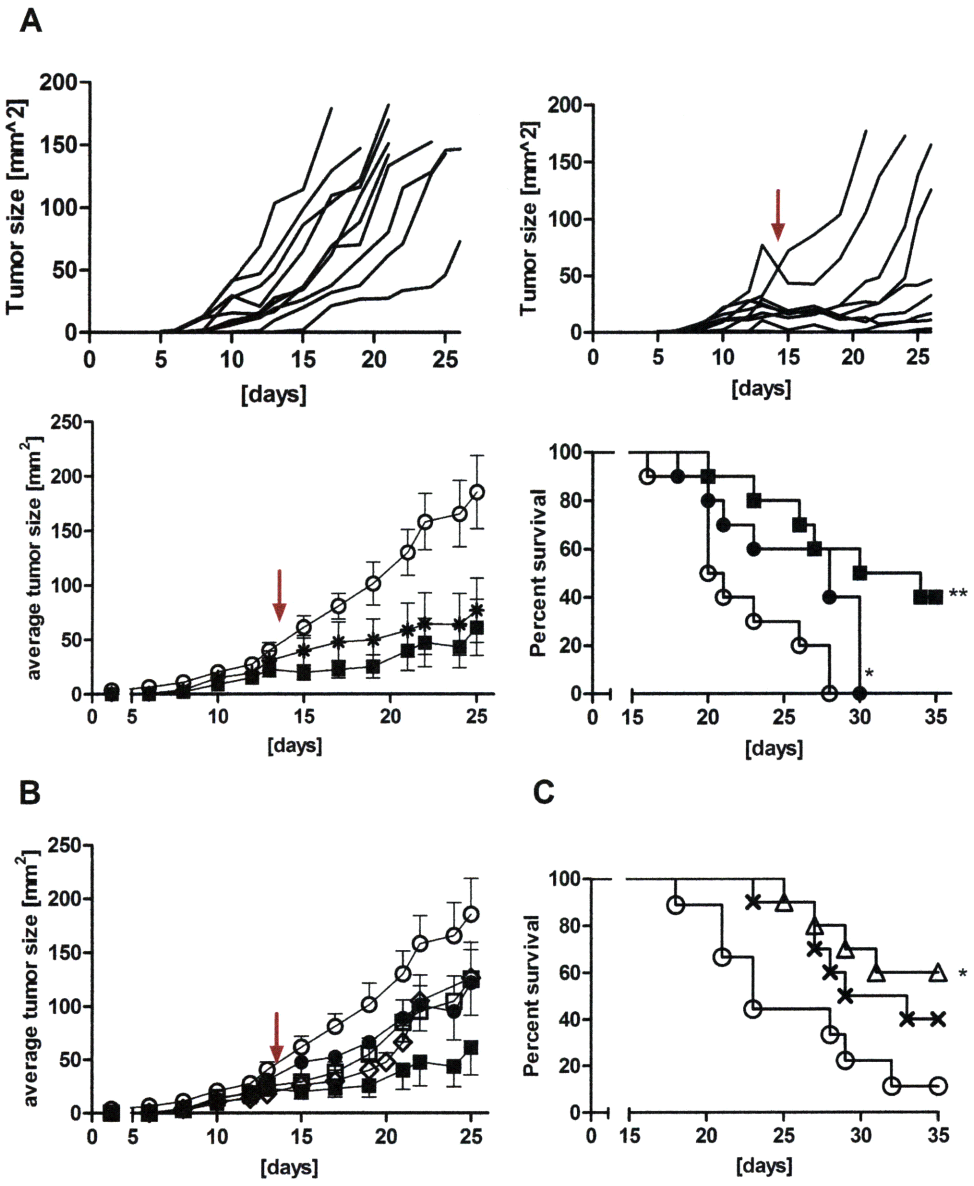

Figure 4-3: Dendritic cells combined with IL-15SA released from peritumoral alginate matrices elicit prolonged control of established tumor growth and enhance survival. C57Bl/6 mice were inoculated s.c. with $3x10^4$ B16-ova cells and left untreated or received peritumoral injections of 150 µL alginate gels carrying $2x10^6$ antigen-pulsed DCs and/or 36.7 µg IL-15SA on d14 (*n* = 10 per group). (A) Tumor growth curves are shown for untreated mice (upper left) or mice treated with alginate carrying DCs+IL-15SA (upper right). (Lower left) Average tumor growth for mice treated with alginate carrying DCs+IL-15SA (■) or IL-15SA alone in gels (✱), or left untreated (○). (Lower right) Survival of mice treated with alginate carrying DCs and IL-15SA (■), intratumoral injection of DCs and IL-15SA (●), or left untreated (○). (B) Tumor growth for untreated mice (○) vs. mice treated with alginate carrying DCs+IL-15SA (■), i.t. injection of free DCs and IL-15SA (●), s.c. injection of alginate carrying DCs and IL-15SA on flank opposite the tumor (◇), or peritumoral injection of alginate carrying DCs while IL-15SA is given i.p. (□). (C) Survival of mice left untreated (○) or receiving a single peritumoral injection on day 14 of alginate carrying IL-15SA and 80 µg CpG (✕), or receiving two injections of alginate carrying 36.7 µg IL-15SA on days 14 and 21 (△).

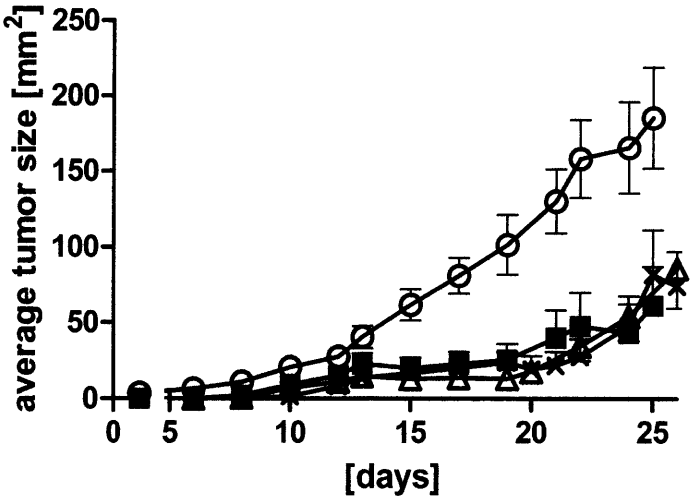

Figure 4-4: Dendritic cells combined with IL-15SA released from peritumoral alginate matrices elicit prolonged control of established tumor growth and enhance survival. C57Bl/6 mice were inoculated s.c. with $3x10^4$ B16-ova cells and left untreated or received peritumoral injections of 150 µL alginate gels carrying $2x10^6$ antigen-pulsed DCs and/or 36.7 µg IL-15SA on d14 (*n* = 10 per group). (A) Tumor growth curves are shown for untreated mice (upper left) or mice treated with alginate carrying DCs+IL-15SA (upper right). (Lower left) Average tumor growth for mice treated with alginate carrying DCs+IL-15SA (■) or IL-15SA alone in gels (✱), or left untreated (O). (Lower right) Survival of mice treated with alginate carrying DCs and IL-15SA (■), intratumoral injection of DCs and IL-15SA (●), or left untreated (O). (B) Tumor growth for untreated mice (O) vs. mice treated with alginate carrying DCs+IL-15SA (■), i.t. injection of free DCs and IL-15SA (●), s.c. injection of alginate carrying DCs and IL-15SA on flank opposite the tumor (◇), or peritumoral injection of alginate carrying DCs while IL-15SA is given i.p. (□). (C) Survival of mice left untreated (O) or receiving a single peritumoral injection on day 14 of alginate carrying IL-15SA and 80 µg CpG (×), or receiving two injections of alginate carrying 36.7 µg IL-15SA on days 14 and 21 (△).

4.3.3 Enhancement of anti-tumor response by IL-15 superagonist in alginate

To test the therapeutic effect of combining DCs and IL-15SA in tumor-surrounding matrices, 14-day established B16-ova tumors were treated with a single peritumoral injection of alginate matrices carrying ova-pulsed dendritic cells and IL-15SA, and tumor growth was monitored for 21 days. Compared to untreated controls, a single peritumoral immunization with alginate carrying DCs and IL-15SA substantially retarded tumor growth in the majority of animals, and enabled mice with tumors smaller than ~50 mm^2 at the time of treatment to control tumor growth for at least 1 week following gel injection (Figure 4-3A). Larger tumors also occasionally showed substantial reductions in size transiently following injection of alginate ECMs (Figure 4-3A). Comparison of mean tumor sizes in mice receiving gels with DCs+IL-15SA vs. IL-15SA alone showed that the cytokine played a dominant role in this combination treatment, with DCs providing only a minor enhancement of the anti-tumor response (Figure 4-3A). Control of tumor growth required that IL-15SA was released locally from the peritumoral matrix, as gels carrying DCs and IL-15SA injected on the flank opposite tumors or treatment of mice with peritumoral gels carrying DCs with IL-15SA given i.p. had a much weaker anti-tumor effect than injection of the cytokine-loaded synthetic ECMs around tumors (Figure 4-3B). Further, DCs and IL-15SA in tumor-surrounding matrices were more effective than intratumoral injection of free DCs and IL-15SA (Figure 4-3B). Control of tumor growth elicited by DC/IL-15SA-carrying

gels was reflected in improved survival compared to each of these alternative treatments (Figure 4-3A and data not shown).

Because preparation of autologous DCs is a laborious and costly process for clinical implementation, we also explored whether cytokine or immunoregulatory factors alone could achieve results equivalent to tumors treated with DCs+IL-15SA. We thus tested two alternatives: first, providing two injections of alginate gel carrying IL-15SA alone, given peritumorally 7 days apart on days 14 and 21; second, giving a single injection of alginate carrying both IL-15SA and the Toll-like receptor-9 agonist CpG (204). These gel formulations elicited control over established B16-ova tumor growth similar to alginate carrying DCs and IL-15SA (Figure 4-4) and elicited prolonged survival (Figure 4-3C). Thus, optimal selection of immune-supporting factors for release from the peritumoral matrix enables this treatment to provide prolonged control of tumor growth without the need for transfer of autologous DCs.

4.3.4 Accumulation of effector cells and reduction of regulatory T-cells by IL-15SA

To begin to understand how IL-15SA alone or in combination with DCs boosted the anti-tumor response elicited by tumor-surrounding alginate ECMs, we analyzed the impact of IL-15SA delivery on the recruitment of immune cells at the tumor site following treatment of 14-day-established B16-ova tumors. As shown in Figure 4-5A, single peritumoral injections of alginate carrying DCs and IL-15SA did not increase the mean number of $CD4^+$ T-cells localizing in tumor-surrounding ECMs compared to gels carrying DCs alone, but did amplify accumulation of $CD8^+$ T-cells by ~4-fold. This $CD8^+$ T-cell infiltrate included a population of tumor antigen-specific cells detected by ova peptide-H-$2K^b$ tetramer staining (Figure 4-5A). We also quantified the frequency of $foxp3^+CD4^+$ regulatory T-cells, DCs, and NK cells attracted to the tumor site by the optimal DC-free treatment of 2 peritumoral injections of IL-15SA-loaded gels. Untreated tumors were infiltrated by low frequencies of $CD4^+$ cells, and 30-50% of these cells were $foxp3^+$ (Figure 4-5B). In response to IL-15SA/gel therapy, both the frequency of $foxp3^+$ cells and the ratio of $foxp3^+$ T-cells to total T-cells (205) within tumors were significantly reduced. In addition, the frequencies of intratumoral NK cells and DCs were increased 16- and 4-fold respectively for IL-15SA/gel-treated tumors compared to controls (Figure 4-5B). In separate experiments, we detected substantial numbers of DCs, NK cells, and $CD11c^+I\text{-}A^{b+}NK1.1^+$ 'interferon-secreting killer' DCs (IKDCs) (33) in alginate matrices carrying IL-15SA or IL-15SA+CpG following single gel injections, and a fraction of DCs were GFP^+, suggesting that active acquisition of tumor antigen was occurring in the peritumoral matrices (Figure 4-6). Thus, immunotherapy with IL-15SA-loaded gels enhanced $CD8^+$ T-cell recruitment to the tumor site, lowered the relative frequency of regulatory T-cells, and enhanced the frequency of innate immune cells, all factors expected to augment the anti-tumor response.

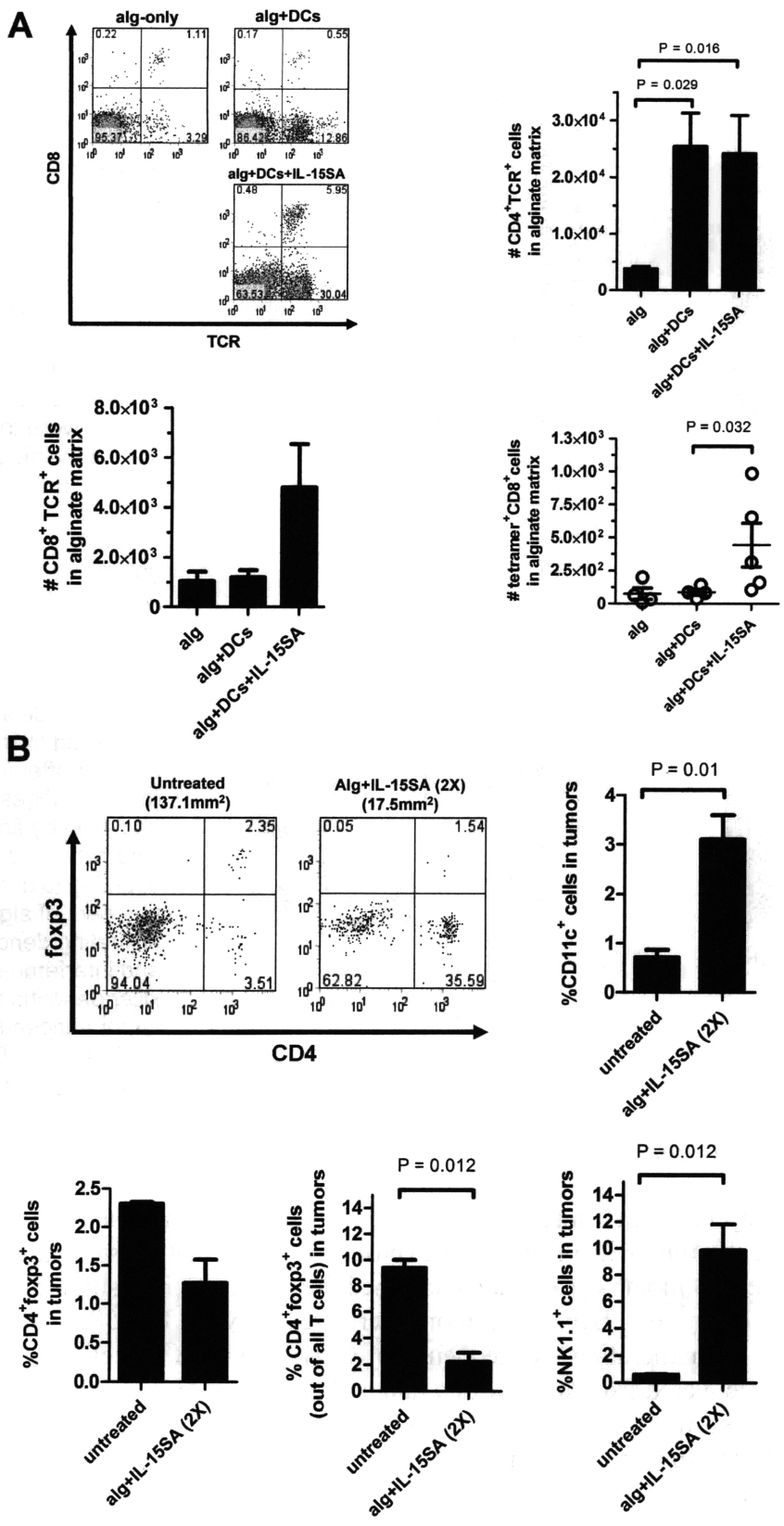

Figure 4-5: Alginate gels carrying IL-15SA elicit accumulation of $CD8^+$ T-cells, NK cells, and DCs at the tumor site, while frequencies of T_{regs} in the tumor are reduced. Established B16-ova tumors were treated on d14 by peritumoral injection of empty alginate gels or gels carrying antigen-pulsed DCs and/or IL-15SA (n = 4-5 per group). Gels were recovered on d28 for analysis. (A) Representative flow cytometry analyses of T-cell infiltration in gels, and mean numbers of $CD4^+$, $CD8^+$, and antigen-specific ova tetramer-stained T-cells recovered from gels. (B) B16-ova-tumor-bearing mice were left untreated or received two injections of IL-15SA-loaded alginate on days 14 and 21. On day 28, tumors and gels were recovered and frequencies of $CD4^+foxp3^+$ cells, $CD11c^+$ DCs, and $NK1.1^+$ natural killer cells were determined.

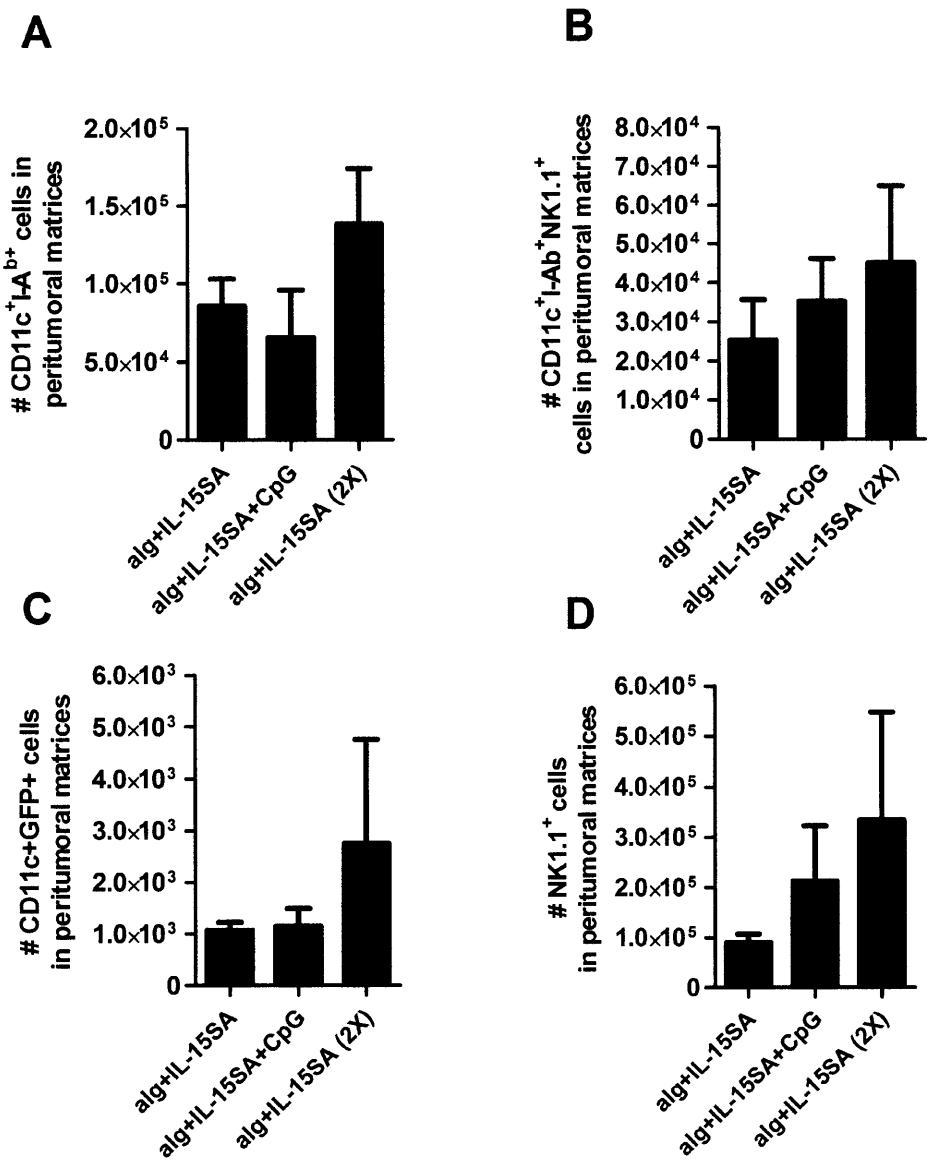

Figure 4-6: Dendritic cells and NK cells accumulate in peritumoral alginate ECMs carrying IL-15SA or IL-15SA and CpG. C57Bl/6 mice were inoculated with $3x10^4$ B16-ova cells s.c. and tumors were treated on day 14 by injection of alginate gels carrying 36.7 μg IL-15SA alone or with 80 μg CpG. One group of animals treated with IL-15SA received a second alginate injection on day 21 containing another dose of 36.7 μg IL-15SA. Gels were recovered from animals 21 days after injection (day 35), digested, and analyzed by flow cytometry and cell counting to quantify numbers of alginate-infiltrating dendritic cells and interferon-secreting killer dendritic cells (A), tumor antigen (GFP)-positive DCs (B), and natural killer cells (C).

4.3.5 Gel-tumor infiltrate correlation.

To understand the relationship between attraction of immune cells to the tumor-surrounding alginate gels and infiltration of the tumor itself, we next exploited the fact that these synthetic ECMs are stable *in vivo* for at least 3 months (197), and examined the cellular composition of the local immune response when 14-day-old B16-ova tumors were treated with IL-15SA-loaded alginate gels on days 14 and 21. Enumerating the frequency of $CD4^+$ and $CD8^+$ T-cells in both the alginate matrix and tumors recovered from mice with a range of tumor burdens on day 28, we found a strong correlation between the frequencies of $CD4^+$ and $CD8^+$ T-cells accumulated in peritumoral matrices vs. within the tumor itself (Figure 4-7A). In a similar manner, increased frequencies of $CD11c^+I\text{-}A^{b+}$ dendritic cells (DCs) and $NK1.1^+$ natural killer cells in the alginate gels coincided with increased frequencies of these cells within tumors (Figure 4-7B, C). These results suggest that immune cell attraction to the peritumoral matrix either directly promoted

infiltration of the tumor itself or served as a surrogate indicator of conditions favoring immune cell accumulation in tumors.

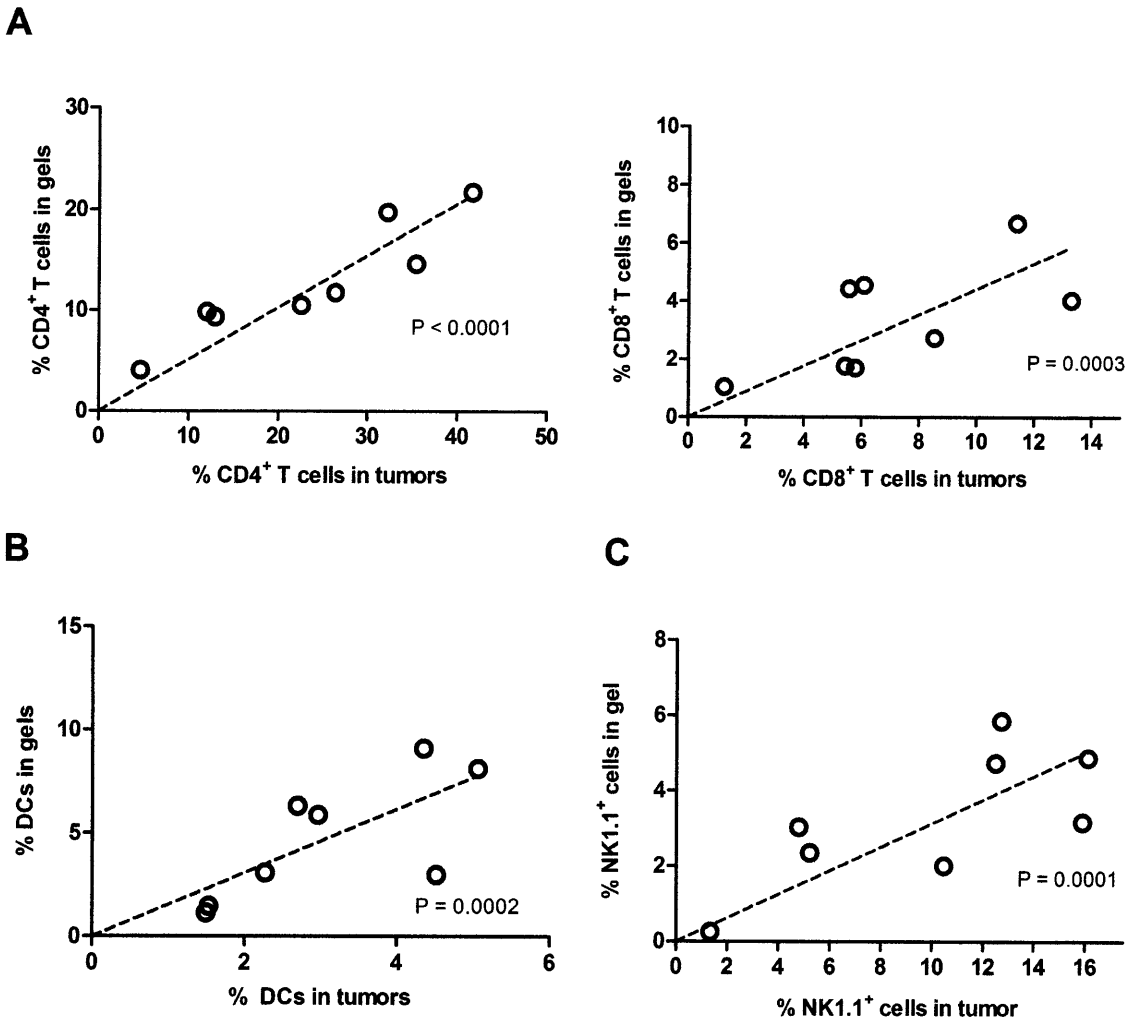

Figure 4-7: Immune cell accumulation in peritumoral alginate ECMs correlates with accumulation in tumors. Established B16-ova tumors were treated with 2 injections of IL-15SA-loaded alginate as in Figure 4-5B. Gels and tumors were analyzed by flow cytometry and shown are pooled results for gels/tumors taken from the same mice: (A) $CD4^+TCR^+$ and $CD8^+TCR^+$ T-cell frequencies; (B) CD11c+ cells; (C) $NK1.1^+$ cells. Shown is one of 3 independent experiments.

Next, we pooled flow cytometric analyses from 3 independent experiments examining different protocols of IL-15SA delivery and examined the correlation between the frequency of immune cells in the peritumoral matrix and the ultimate tumor burden present at day 28 or 35. The stability of the gels enabled examination of the infiltrates in the peritumoral matrix irrespective of the final tumor size, and our analysis included samples from mice that completely eliminated/suppressed tumors following gel therapy. Strikingly, quantification of the frequency of immune cells recovered from gels vs. final tumor size using data pooled from varied DC/IL-15SA treatments overlapped in a qualitatively common trend (Figure 4-8). The frequency of $CD4^+$ and $CD8^+$ T-cells recovered from peritumoral synthetic ECMs sharply declined with increasing final tumor size, as did the $CD4^+foxp3^-$:$CD4^+foxp3^+$ T_{eff}:T_{reg} ratio (Figure 4-8A).

(Although the quantitative number of T-cells recovered from gels varied from experiment to experiment, similar trends were also observed for total cell numbers in individual experiments (data not shown)). Elevated frequencies of peritumoral matrix-infiltrating T-cells were recovered from mice when gel therapy regressed tumors as large as ~30 mm^2 on the day of treatment and also when gel treatment prevented slow-growing tumor nuclei from ever developing (Figure 4-9). In contrast, mice where tumors had reached at least 50 mm^2 or larger by the end of the experiment uniformly lacked significant T-cell infiltrates in the tumor-surrounding matrix, even if tumor growth was transiently suppressed early in the experiment (Figure 4-9). In agreement with the data of Figure 4-7, when we examined leukocyte infiltration of tumors directly, we found a similar trend, with elevated T-cell infiltration only detected when therapy kept tumors to sizes <~25 mm^2 (Figure 4-8B). This sharply decaying relationship between T-cell recruitment at the tumor site and tumor growth contrasted with the systemic response, as tumor antigen-specific $CD8^+$ T-cells were present in the spleens of treated mice at relatively constant levels irrespective of the sizes of their tumors (Figure 4-8B). Finally, we examined whether innate components of the immune response exhibited a similar trend of localization at the tumor site following DC/IL-15SA-gel immunotherapy: The frequencies of DCs, IKDCs, and NK cells were all sharply elevated by 8-10-fold when tumors were suppressed to sizes <50 mm^2 (Figure 4-8C). Thus, control of tumor growth following gel-delivered immunotherapy coincided with elevated leukocyte recruitment to the tumor site sustained up to 3 weeks post treatment of tumors with alginate matrices. However, immune cells were present at only very low frequencies if tumors reached ~50 mm^2 in size by 2 weeks after gel therapy, suggesting that the immune response was only sustained under conditions where tumor growth was strongly suppressed.

Immune responses to tumors are limited by a number of factors developing systemically and at the tumor site directly. Two limitations in the anti-tumor immune response are insufficient recruitment of T-cells to tumors (59, 60, 206) and loss of T-cell and innate effector cell functions in the tumor microenvironment , either due to suppressive factors produced in the tumor site or via the action of regulatory T-cells (65, 150, 207). In an attempt to both stimulate T-cells and overcome immunosuppression at the tumor site, here we explored the possibility of local tumor immunotherapy by 'engulfing' established tumors with injectable synthetic ECMs carrying antigen-pulsed dendritic cells or immunoregulatory cytokines. The use of the biopolymer alginate in these studies was motivated by its known biocompatibility and extensive track record in cell transplantation and tissue engineering applications. Here we explored use of this synthetic ECM as a carrier for tumor-local delivery of dendritic cells and immunoregulatory factors, particularly IL-15 in a superagonist form. DCs have been examined in preclinical and clinical studies as possible cell-based cancer therapeutics capable of breaking tolerance to tumors (141, 144, 208), while IL-15 has been reported to trigger proliferation of anergic tumor-infiltrating T-cells (201) and revive effector functions of tumor-resident T-cells (200). Superagonist IL-15 formed by complexing IL-15 with its high-affinity IL-15Rα chain has been shown to expand $CD8^+$ T-cells, NK cells, and NK T-cells *in vivo* more effectively than IL-15 alone (199, 202), and repeated systemic injections of IL-15SA have been shown to slow tumor growth *in vivo* (200). IL-15 can also induce differentiation of monocytes into Langerhans Cell-like IL-15 DCs (209), and plays a role in maximizing APC function (210). We hypothesized that by surrounding tumors with DC/IL-15SA-loaded gels, leukocyte accumulation at the tumor site would be elevated and IL-15SA would be concentrated at the tumor site over several days, while lowering systemic exposure to the cytokine.

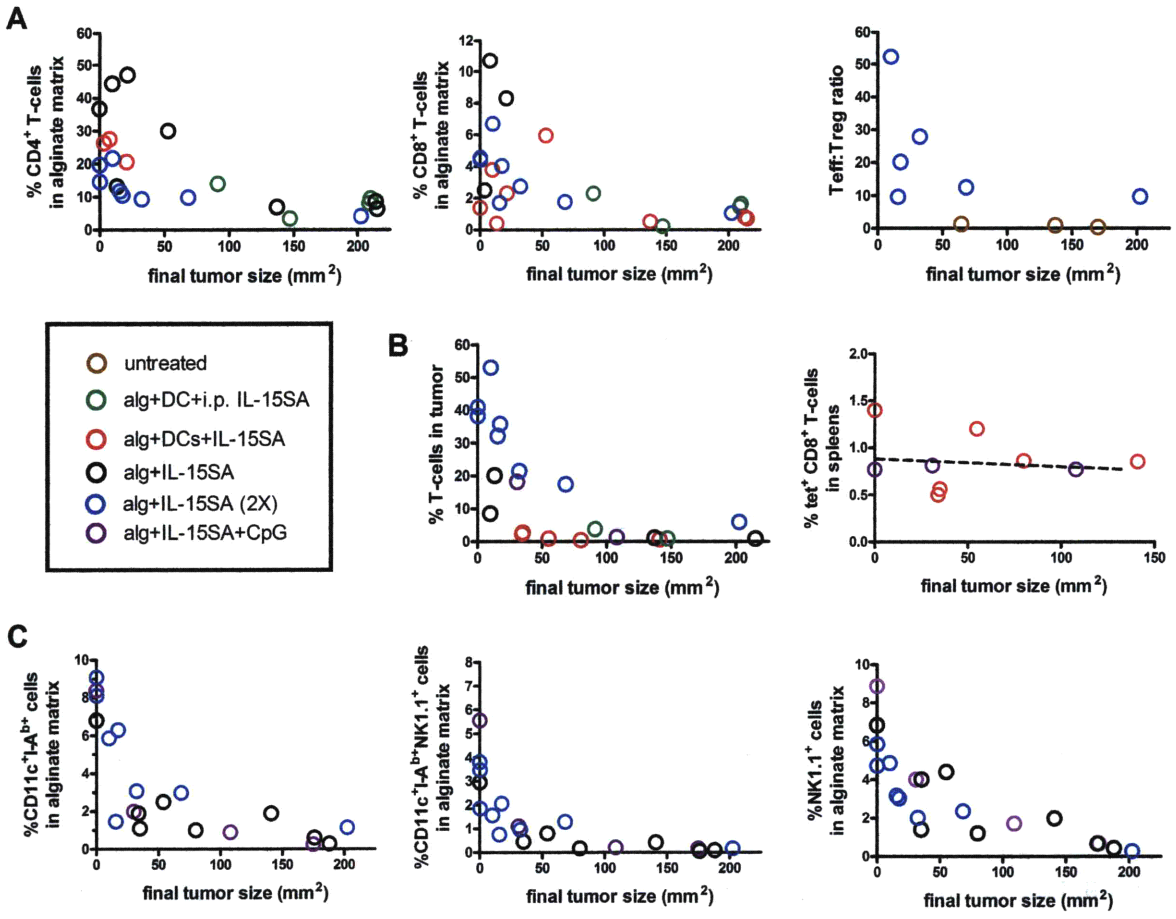

Figure 4-8: Local leukocyte accumulation in peritumoral alginate matrices is sustained in peritumoral ECMs, but only when tumor growth is strongly suppressed. Peritumoral alginate gels, tumors, and spleens were recovered at the end of peritumoral alginate gel therapy experiments performed as in Figure 4-3 and Figure 4-5, for untreated mice or mice treated with alginate carrying IL-15SA alone, DCs+IL-15SA, DCs+i.p. IL-15SA, IL-15SA+CpG, or IL-15SA (X2). Gels, tumors, and spleens were digested and analyzed by flow cytometry. Shown are frequencies of T-cells and the $CD4^+foxp3^-$:$CD4^+foxp3^+$ Teff : Treg ratio present in gels (A), total T-cells in tumors and ova-specific T-cells in spleens (B), and DCs, 'interferon-secreting killer DCs' and NK cells present in gels (C) as a function of the ultimate tumor size at d28 or d35 for pooled data from 3 independent experiments.

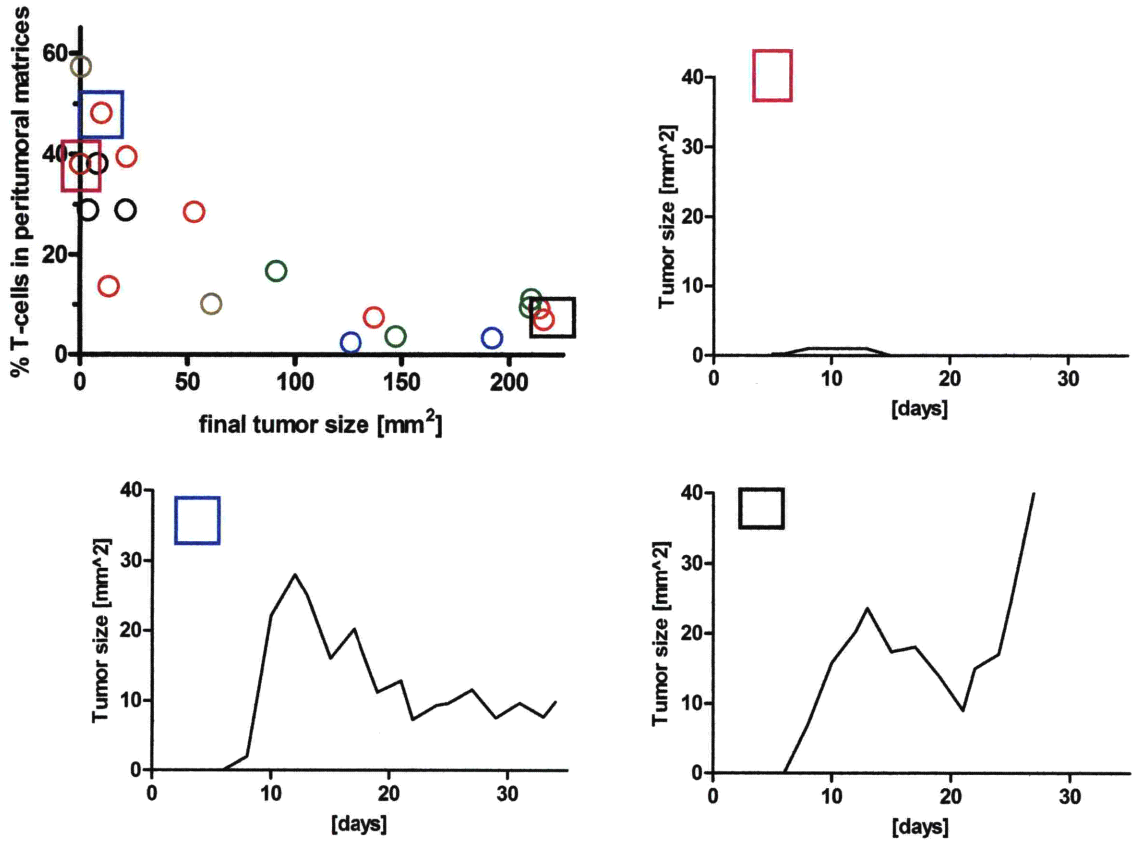

Figure 4-9: Elevated T-cell accumulation in peritumoral alginate matrices is sustained when alginate gel therapy regresses large tumors or prevents outgrowth of nascent tumor nuclei, but is completely lacking in animals that transiently regress large tumors. Example individual tumor growth curves correlated to the frequency of T-cells recovered from peritumoral alginate ECMs at the end of a gel therapy experiment on day 35. Colored boxes note the T-cell infiltrate detected on day 35 for each individual tumor growth pattern.

4.4 Discussion

We found that DCs alone in peritumoral alginate ECMs attracted $CD4^+$ T-cells to tumor sites but elicited weak $CD8^+$ T-cell recruitment and had a very limited therapeutic effect on established B16-ova tumors. However, IL-15SA delivery in the presence or absence of DCs increased the numbers of $CD8^+$ T-cells within alginate matrices (Figure 4-5A and data not shown), and increasing peritumoral accumulation of T-cells correlated with increased frequencies of lymphocytes within tumors (Figure 4-7). In contrast to gels carrying DCs alone, DCs with IL-15SA elicited anti-tumor responses that could control established melanoma growth for up to a week following a single injection, and enhanced survival of treated animals (Figure 4-3). This optimal therapeutic response from a single injection was achieved only when IL-15SA was provided locally at the tumor site and slow-released from the tumor-surrounding matrix.

Notably, exogenous DCs could be excluded from the therapy by either providing repeated IL-15SA/gel injections or by combining IL-15SA with Toll-like receptor ligands for slow release in the tumor environment, substantially simplifying this approach from a clinical standpoint. In prior studies where IL-15SA was used as a stand-alone therapy for treatment of pancreatic tumors by repeated systemic injection, the enhanced anti-tumor response appeared to be driven by 'rescued' $CD8^+$ T-cells already resident with tumors rather than by recruitment of new T-cells to the tumor site (200). Here we found that when IL-15SA was released locally at the tumor site over several days from the alginate matrix (alone or with DCs), the cytokine promoted accumulation of T-cells in both the peritumoral matrix and tumor, and reduced the relative frequency of $foxp3^+$ T_{reg}s. Whether these accumulating T-cells were expanding lymphocytes already resident in tumors at the time of treatment or represented cells recruited to the site following gel therapy remains to be determined.

In addition to providing a depot for cell/cytokine localization around tumors, alginate matrices simultaneously served as stable surrogate ECMs surrounding the tumor site, facilitating characterization of the immune response developing following tumor cell inoculation and immunotherapy. Analysis of tumor-infiltrating lymphocytes (TILs) has often been carried out in an attempt to understand the mechanisms underlying successful immune responses in preclinical models (24, 27, 59, 73, 205) and has also been used to successfully predict tumor progression and survival in patients (95, 211, 212). However, TIL analysis is by definition limited to treatments or timepoints where substantial tumor mass remains. Matrigel has been used as a synthetic ECM to inoculate tumor cells and analyze early leukocyte infiltration of nascent s.c. tumor sites (205, 213), but is steadily resorbed over a period of several weeks *in vivo* (214). Here we exploited the prolonged stability of alginate ECMs *in vivo* to analyze the makeup of immune cells locally recruited to sites where tumors were regressed or where tumor development was completely suppressed, and compared to treatments that left mice with varying degrees of tumor burden. This analysis revealed several interesting features of the immune response following gel-based delivery of dendritic cells and/or IL-15SA: First, when immune cell accumulation at tumor sites was correlated to final tumor burden for mice receiving different variations in IL-15SA local therapy, the data followed a common trend. Second, a stark contrast existed between the immune infiltrate accumulating at tumors regressed to $<\sim 50$ mm^2 vs. tumors with sizes >50 mm^2, even if tumor growth was transiently slowed by IL-15SA treatment. Frequencies of $CD8^+$ T-cells, $CD4^+$ T-cells, dendritic cells, and NK cells were all elevated at the tumor site when final tumor sizes 21 days after treatment were less than ~ 50 mm^2, but this multifaceted immune cell recruitment was absent in mice with larger tumor burdens. The lack of T-cell accumulation in progressing tumors we found here is in line with prior reports in the B16 melanoma model, where T-cell infiltration in untreated tumors has been shown to be poor due to defective expression of adhesion molecules on tumor vasculature (59). However, our studies show that in addition to suppressed lymphocyte recruitment within the tumor mass itself, T-cells also failed to accumulate with synthetic ECMs surrounding progressing tumors. Altogether, the data suggest this local gel therapy elicits an essentially "all or none" response: either established tumors are steadily regressed (or nascent tumors completely suppressed) coincident with a sustained multilineage immune cell recruitment at the tumor site, or a complete failure or collapse of this multifactorial response occurs and tumor growth progresses.

The ultimate goal of local immunotherapy is to generate a systemic immune response capable of eliminating disseminated tumors and metastases following treatment of an accessible tumor site. Several recent reports have demonstrated dramatic elimination of established tumors

via i.t. or peritumoral combination therapies with anti-CD40, IL-2, Toll-like receptor ligands, and/or chemotherapy (42, 188, 215, 216), which were accompanied by systemic immune responses destroying large distal tumors. The studies reported here suggest that injectable alginate matrices can provide a strategy for further exploring the potential of local immunotherapy with IL-15SA or other immunostimulatory factors such as these, while importantly providing a means to lower systemic exposure and frequency of dosing of these potent and potentially toxic factors.

4.5 Summary

In this part of the work, we explored the use of injectable self-gelling alginate as synthetic extracellular immunoplatform to surround tumor sites and carry therapeutic dendritic cells, cytokines, or other immunostimulatory factors for release in the peritumoral environment. Immunization of mice bearing 14-day established B16-ova melanoma tumors with alginate carrying dendritic cells (DCs) and/or IL-15 superagonist promoted immune cell recruitment to the peritumoral matrix. Single immunization with IL-15/DC-carrying gels was able to control the growth of tumors (less than $50mm^2$ in diameter) for a week or more, encouraging further improvement and use of sustained IL-15SA delivery as a local tumor therapy. The matrix-based therapy allowed us to analyze the cellular types that infiltrated the local region surrounding tumors. Matrix infiltration correlated with tumor infiltration by leukocytes, validating the significance of analyzing the gel infiltrates to understand the local cellular events that lead to either failure or control of tumor growth/better survival. Analyses conducted in this chapter demonstrated the importance of simultaneous, multilineage recruitment of T-cells, dendritic cells, NK cells, and NK T-cells elicited by treatments to successful treatment or control of tumor growth over 30 days, irrespective of the type of immunizations applied to the mice.

4.6 Acknowledgments

This part of the thesis work was supported by the Defense Advanced Research Projects agency (contract # W81XWH-04-C-0139), the NIH (EB007280-02), and the National Science Foundation (award 0348259). D.J.I. is an investigator of the Howard Hughes Medical Institute.

Chapter 5
SUMMARY AND FUTURE CONSIDERATIONS

5.1 Summary of the thesis work

Through this research work, we sought to augment existing cancer immunotherapy strategies using injectable alginate hydrogels capable of delivering various immuno-factors and to further understand the mechanisms behind successful vs unsuccessful vaccination against tumors. One of the cancer vaccines we looked into augmenting was dendritic cell vaccines, in which antigen loaded dendritic cells (DCs) are injected directly into patients to trigger immune responses. To achieve these goals, a self-gelling formulation of alginate was developed, obtained by mixing calcium-loaded alginate microspheres with soluble alginate solution and dendritic cells, a formulation that rapidly gelled in vivo. Biocompatible polymer solutions that can crosslink *in situ* following injection to form stable hydrogels also are of interest as depots for sustained delivery of therapeutic factors or cells, and as scaffolds for regenerative medicine. In the first part of this work, injectable self-gelling alginate formulations obtained by mixing alginate microspheres (as calcium reservoirs) with soluble alginate solutions were characterized for potential use in immunotherapy. Rapid redistribution of calcium ions from microspheres into the surrounding alginate solution led to rapid crosslinking and formation of stable hydrogels. The mechanical properties of the resulting gels correlated with the concentration of calcium reservoir microspheres added to the solution. Soluble factors such as the cytokine interleukin-2 were readily incorporated into self-gelling alginate matrices by simply mixing them with the formulation prior to gelation. Using alginate microspheres as modular components, strategies for binding immunostimulatory CpG oligonucleotides onto the surface of microspheres were also demonstrated. When injected subcutaneously in the flanks of mice, self-gelling alginate formed soft macroporous gels supporting cellular infiltration and allowing ready access to microspheres carrying therapeutic factors embedded in the matrix.

We then explored the use of these injectable gels for delivery of dendritic cells (DCs), key immune cells capable of initiating immune responses for vaccination or immunotherapy in cancer or infectious diseases (140-145). DCs sequestered in alginate gels elicited robust recruitment of host T-cells and dendritic cells to the matrix, while some of the inoculated DCs trafficked to the draining lymph nodes. Using an adoptive transfer model to track a defined population of T cells responding to immunization with antigen-loaded DCs, we showed that DC/alginate immunization led to recruitment of activated, antigen-specific T cells to the alginate matrix, in a manner dependent on the presence of the DC. T-cells primed in the native lymph

nodes trafficked to the alginate gels, indicating that this DC-gel immunization is capable of directing effector T-cells to defined tissue sites in large numbers.

To test the efficacy of these vaccination nodes, to accumulate immune cells at solid tumors or infection sites in the presence of supporting factors co-delivered by the hydrogel matrix, we used the B16-OVA melanoma tumor model. Local therapy of mice bearing 14-day established B16-ova melanoma tumors with dendritic cells (DCs) and/or IL-15 superagonist promoted immune cell recruitment to the peritumoral matrix, and matrix infiltration correlated with tumor infiltration by leukocytes. Single injections of IL-15/DC-carrying gels controlled the growth of tumors as large as ~30 mm^2 for a week or more. The stability of these synthetic matrices in vivo allowed us to extract the gels and analyze immune cell recruitment to the tumor locale in a consistent manner irrespective of final tumor size, even when local therapy completely prevented tumor outgrowth (i.e., no tumor was present at the completion of therapy for analysis of tumor-infiltrating lymphocytes). This analysis revealed a binary "all or none" immune response induced by local therapy, with multilineage recruitment of T-cells, dendritic cells, NK cells, and NK T-cells elicited by treatments that completely prevented tumor outgrowth over 30 days and much lower levels of all of these immune responders except NK cells elicited by treatments that failed to eliminate tumors, even if tumor growth was slowed for prolonged times.

5.2 Future Considerations and Possible Applications of Vaccination Nodes

In this work, recruitment and accumulation of effector immune cells at a local peripheral site were demonstrated. One of the future challenges for the vaccination-node assisted cancer therapy is to examine whether immune responses can be mounted against distal tumors injected away from the primary tumor being treated with the gels. Alternatively, re-challenge with the same tumor cell line or tumor cells expressing the same tumor antigens (i.e. ova-expressing EL4 tumor cell line) in mice successfully treated with vaccination nodes can be tested. Rejection of distal tumors or protection from tumor re-challenge will indicate successful induction of systemic immunity and memory, which is one of the biggest advantages and goals of cancer immunotherapy (as opposed to conventional therapies, as mentioned in Chapter 1). As cytokine delivery strategies that promote lymphoid tissue-like immune cell accumulation at tumors have also shown promising anti-tumor effects (157, 158, 217), it will also be interesting to further explore how the recruitment and self-organization of immune cells occurs in the presence of additional cytokine signals co-delivered from alginate matrices as a therapeutic strategy. Since repeated immunizations with alginate containing IL-15SA showed one of the best tumor suppression and survival enhancement (Figures 4-3 and 4-4), use of resorbable matrix to allow for multiple immunization steps can be explored. For example, alginate degradation can be controlled by selective partial oxidation of uronic units and by combining different molecular weights of alginate (80-82). We furthermore showed that the use of matrix-based therapy let us study the effect of cytokines on tumor therapy. This kind of system can be a useful screening tool for different kinds of candidate factors that need be locally released at a peripheral tissue site, without going through the problems of loading efficiencies and tuning the release profile. As nanoparticle and microsphere techonologies improve, the matrix-based delivery system may be replaced by control-release polymer nano-/microsphere vehicles.

Possible applications of self-gelling alginate as a therapy against cancer include combination therapy with other immunotherapy strategies in development, especially in the treatment of resected tumors. The in-situ forming gel can act as a bulk space-filling material at the same time

allowing the creation of local inflammatory milieu that can clean up any residual tumors at the site. Combination of the vaccination nodes with other strategies that enhance systemic protection against metastasis and future recurrences will potentially facilitate both local and systemic treatments of malignant tumors.

In addition to providing a tool for therapeutic benefits, we have demonstrated the use of matrix-based therapy to study and better understand events that occur locally near or at the tumor site. Because of the disconnection between systemic anti-tumor response and successful local tumor rejection observed in our work as well as in many previous studies (59-61, 70), it will be extremely important and useful to find a connection between the information we can acquire from systemically circulating cells and factors and the prognosis of the malignancies, especially since collection of peripheral blood is one of the most common practices used in the clinic to obtain information from cancer patients (205). Our self-gelling alginate can thus provide a valuable tool for examininig the biology of local anti-tumor responses even in tumor-free subjects.

Alginate is a material that has already found applications in a variety of applications including those outside immunotherapy (74, 78, 84, 103, 104, 218). The in-situ forming self-gelling alginate formulation introduced in this thesis work offers an alternative method of forming soft alginate gels and may easily be translated to other soft tissue regeneration and biomaterial applications, because of its many favorable tissue engineering properties including the ease of loading different types and dosages of soluble factors as well as different types of cells.

Bibliography

1. Global Cancer Facts & Figures 2007. In: American Cancer Society, Atlanta, Georgia.; 2007.
2. Alberts DS. A unifying vision of cancer therapy for the 21st century. J Clin Oncol 1999;17(11 Suppl):13-21.
3. Radiation Therapy for Cancer: Questions and Answers. In; 2004.
4. Burmeister BH, Smithers BM, Poulsen M, McLeod GR, Bryant G, Tripcony L, et al. Radiation therapy for nodal disease in malignant melanoma. World J Surg 1995;19(3):369-71.
5. Bailar JC, 3rd, Gornik HL. Cancer undefeated. N Engl J Med 1997;336(22):1569-74.
6. Coley WB. The treatment of malignant tumors by repeated innoculations of erysipelas, with a report of ten original cases. Am J Med Sci 1893;105:487-492.
7. Gatti RA, Good RA. Occurrence of malignancy in immunodeficiency diseases. A literature review. Cancer 1971;28(1):89-98.
8. Boshoff C, Weiss R. AIDS-related malignancies. Nat Rev Cancer 2002;2(5):373-82.
9. Pham SM, Kormos RL, Landreneau RJ, Kawai A, Gonzalez-Cancel I, Hardesty RL, et al. Solid tumors after heart transplantation: lethality of lung cancer. Ann Thorac Surg 1995;60(6):1623-6.
10. Girardi M, Oppenheim DE, Steele CR, Lewis JM, Glusac E, Filler R, et al. Regulation of cutaneous malignancy by gammadelta T cells. Science 2001;294(5542):605-9.
11. Shankaran V, Ikeda H, Bruce AT, White JM, Swanson PE, Old LJ, et al. IFNgamma and lymphocytes prevent primary tumour development and shape tumour immunogenicity. Nature 2001;410(6832):1107-11.
12. Smyth MJ, Crowe NY, Godfrey DI. NK cells and NKT cells collaborate in host protection from methylcholanthrene-induced fibrosarcoma. Int Immunol 2001;13(4):459-63.
13. Bach EA, Aguet M, Schreiber RD. The IFN gamma receptor: a paradigm for cytokine receptor signaling. Annu Rev Immunol 1997;15:563-91.
14. Dighe AS, Richards E, Old LJ, Schreiber RD. Enhanced in vivo growth and resistance to rejection of tumor cells expressing dominant negative IFN gamma receptors. Immunity 1994;1(6):447-56.
15. Kaplan DH, Shankaran V, Dighe AS, Stockert E, Aguet M, Old LJ, et al. Demonstration of an interferon gamma-dependent tumor surveillance system in immunocompetent mice. Proc Natl Acad Sci U S A 1998;95(13):7556-61.
16. Street SE, Trapani JA, MacGregor D, Smyth MJ. Suppression of lymphoma and epithelial malignancies effected by interferon gamma. J Exp Med 2002;196(1):129-34.
17. Street SE, Cretney E, Smyth MJ. Perforin and interferon-gamma activities independently control tumor initiation, growth, and metastasis. Blood 2001;97(1):192-7.
18. van den Broek ME, Kagi D, Ossendorp F, Toes R, Vamvakas S, Lutz WK, et al. Decreased tumor surveillance in perforin-deficient mice. J Exp Med 1996;184(5):1781-90.
19. Smyth MJ, Thia KY, Street SE, MacGregor D, Godfrey DI, Trapani JA. Perforin-mediated cytotoxicity is critical for surveillance of spontaneous lymphoma. J Exp Med 2000;192(5):755-60.

20. Blattman JN, Greenberg PD. Cancer immunotherapy: a treatment for the masses. Science 2004;305(5681):200-5.
21. Burnet FM. The concept of immunological surveillance. Prog Exp Tumor Res 1970;13:1-27.
22. Burnet FM. Immunological surveillance in neoplasia. Transplant Rev 1971;7:3-25.
23. Burnet FM. Implications of immunological surveillance for cancer therapy. Isr J Med Sci 1971;7(1):9-16.
24. Naito Y, Saito K, Shiiba K, Ohuchi A, Saigenji K, Nagura H, et al. CD8+ T cells infiltrated within cancer cell nests as a prognostic factor in human colorectal cancer. Cancer Res 1998;58(16):3491-4.
25. Schumacher K, Haensch W, Roefzaad C, Schlag PM. Prognostic significance of activated CD8(+) T cell infiltrations within esophageal carcinomas. Cancer Res 2001;61(10):3932-6.
26. Ishigami S, Natsugoe S, Tokuda K, Nakajo A, Che X, Iwashige H, et al. Prognostic value of intratumoral natural killer cells in gastric carcinoma. Cancer 2000;88(3):577-83.
27. Villegas FR, Coca S, Villarrubia VG, Jimenez R, Chillon MJ, Jareno J, et al. Prognostic significance of tumor infiltrating natural killer cells subset CD57 in patients with squamous cell lung cancer. Lung Cancer 2002;35(1):23-8.
28. Coca S, Perez-Piqueras J, Martinez D, Colmenarejo A, Saez MA, Vallejo C, et al. The prognostic significance of intratumoral natural killer cells in patients with colorectal carcinoma. Cancer 1997;79(12):2320-8.
29. Sandel MH, Dadabayev AR, Menon AG, Morreau H, Melief CJ, Offringa R, et al. Prognostic value of tumor-infiltrating dendritic cells in colorectal cancer: role of maturation status and intratumoral localization. Clin Cancer Res 2005;11(7):2576-82.
30. Satthaporn S, Eremin O. Dendritic cells (II): Role and therapeutic implications in cancer. J R Coll Surg Edinb 2001;46(3):159-67.
31. Hung K, Hayashi R, Lafond-Walker A, Lowenstein C, Pardoll D, Levitsky H. The central role of CD4(+) T cells in the antitumor immune response. J Exp Med 1998;188(12):2357-68.
32. Wang J, Xing F. A novel cell subset: interferon-producing killer dendritic cells. Sci China C Life Sci 2008;51(8):671-5.
33. Ullrich E, Bonmort M, Mignot G, Jacobs B, Bosisio D, Sozzani S, et al. Trans-presentation of IL-15 dictates IFN-producing killer dendritic cells effector functions. J Immunol 2008;180(12):7887-97.
34. Sallusto F, Mackay CR, Lanzavecchia A. The role of chemokine receptors in primary, effector, and memory immune responses. Annu Rev Immunol 2000;18:593-620.
35. Janssen EM, Lemmens EE, Wolfe T, Christen U, von Herrath MG, Schoenberger SP. CD4+ T cells are required for secondary expansion and memory in CD8+ T lymphocytes. Nature 2003;421(6925):852-6.
36. June CH. Principles of adoptive T cell cancer therapy. J Clin Invest 2007;117(5):1204-12.
37. Smyth MJ, Takeda K, Hayakawa Y, Peschon JJ, van den Brink MR, Yagita H. Nature's TRAIL--on a path to cancer immunotherapy. Immunity 2003;18(1):1-6.
38. Smyth MJ, Swann J, Kelly JM, Cretney E, Yokoyama WM, Diefenbach A, et al. NKG2D recognition and perforin effector function mediate effective cytokine immunotherapy of cancer. J Exp Med 2004;200(10):1325-35.
39. Kalinski P, Giermasz A, Nakamura Y, Basse P, Storkus WJ, Kirkwood JM, et al. Helper role of NK cells during the induction of anticancer responses by dendritic cells. Mol Immunol 2005;42(4):535-9.

40. Jerud ES, Bricard G, Porcelli SA. CD1d-Restricted Natural Killer T Cells: Roles in Tumor Immunosurveillance and Tolerance. Transfusion Medicine and Hemotherapy 2006;33:18-36.
41. Schreiber RD, Pace JL, Russell SW, Altman A, Katz DH. Macrophage-activating factor produced by a T cell hybridoma: physiochemical and biosynthetic resemblance to gamma-interferon. J Immunol 1983;131(2):826-32.
42. Nathan CF, Murray HW, Wiebe ME, Rubin BY. Identification of interferon-gamma as the lymphokine that activates human macrophage oxidative metabolism and antimicrobial activity. J Exp Med 1983;158(3):670-89.
43. Dunn GP, Old LJ, Schreiber RD. The three Es of cancer immunoediting. Annu Rev Immunol 2004;22:329-60.
44. Marincola FM, Jaffee EM, Hicklin DJ, Ferrone S. Escape of human solid tumors from T-cell recognition: molecular mechanisms and functional significance. Adv Immunol 2000;74:181-273.
45. Catlett-Falcone R, Landowski TH, Oshiro MM, Turkson J, Levitzki A, Savino R, et al. Constitutive activation of Stat3 signaling confers resistance to apoptosis in human U266 myeloma cells. Immunity 1999;10(1):105-15.
46. Cancer Vaccine Fact Sheet. National Cancer Institute. URL:http://www.cancer.gov/cancertopics/factsheet/cancervaccine. Date accessed: 02/02/2009. In; 2006.
47. Goldman B, DeFrancesco L. The cancer vaccine roller coaster. Nat Biotechnol 2009;27(2):129-39.
48. Riley LB, Agarwala SS. Melanoma vaccines. Expert Rev Vaccines 2008;7(7):937-49.
49. Pardoll DM. Paracrine cytokine adjuvants in cancer immunotherapy. Annu Rev Immunol 1995;13:399-415.
50. Gallucci S, Lolkema M, Matzinger P. Natural adjuvants: endogenous activators of dendritic cells. Nat Med 1999;5(11):1249-55.
51. HogenEsch H. Mechanisms of stimulation of the immune response by aluminum adjuvants. Vaccine 2002;20 Suppl 3:S34-9.
52. De Becker G, Moulin V, Pajak B, Bruck C, Francotte M, Thiriart C, et al. The adjuvant monophosphoryl lipid A increases the function of antigen-presenting cells. Int Immunol 2000;12(6):807-15.
53. Podda A. The adjuvanted influenza vaccines with novel adjuvants: experience with the MF59-adjuvanted vaccine. Vaccine 2001;19(17-19):2673-80.
54. Speiser DE, Miranda R, Zakarian A, Bachmann MF, McKall-Faienza K, Odermatt B, et al. Self antigens expressed by solid tumors Do not efficiently stimulate naive or activated T cells: implications for immunotherapy. J Exp Med 1997;186(5):645-53.
55. Kuppen PJ, van der Eb MM, Jonges LE, Hagenaars M, Hokland ME, Nannmark U, et al. Tumor structure and extracellular matrix as a possible barrier for therapeutic approaches using immune cells or adenoviruses in colorectal cancer. Histochem Cell Biol 2001;115(1):67-72.
56. Ganss R, Arnold B, Hammerling GJ. Mini-review: overcoming tumor-intrinsic resistance to immune effector function. Eur J Immunol 2004;34(10):2635-41.
57. Singh S, Ross SR, Acena M, Rowley DA, Schreiber H. Stroma is critical for preventing or permitting immunological destruction of antigenic cancer cells. J Exp Med 1992;175(1):139-46.

58. Buckanovich RJ, Facciabene A, Kim S, Benencia F, Sasaroli D, Balint K, et al. Endothelin B receptor mediates the endothelial barrier to T cell homing to tumors and disables immune therapy. Nat Med 2008;14(1):28-36.
59. Quezada SA, Peggs KS, Simpson TR, Shen Y, Littman DR, Allison JP. Limited tumor infiltration by activated T effector cells restricts the therapeutic activity of regulatory T cell depletion against established melanoma. J Exp Med 2008;205(9):2125-38.
60. Rosenberg SA, Sherry RM, Morton KE, Scharfman WJ, Yang JC, Topalian SL, et al. Tumor progression can occur despite the induction of very high levels of self/tumor antigen-specific CD8+ T cells in patients with melanoma. J Immunol 2005;175(9):6169-76.
61. Appay V, Jandus C, Voelter V, Reynard S, Coupland SE, Rimoldi D, et al. New generation vaccine induces effective melanoma-specific CD8+ T cells in the circulation but not in the tumor site. J Immunol 2006;177(3):1670-8.
62. Li Q, Pan PY, Gu P, Xu D, Chen SH. Role of immature myeloid Gr-1+ cells in the development of antitumor immunity. Cancer Res 2004;64(3):1130-9.
63. Nagaraj S, Gupta K, Pisarev V, Kinarsky L, Sherman S, Kang L, et al. Altered recognition of antigen is a mechanism of CD8+ T cell tolerance in cancer. Nat Med 2007;13(7):828-35.
64. Alleva DG, Burger CJ, Elgert KD. Tumor-induced regulation of suppressor macrophage nitric oxide and TNF-alpha production. Role of tumor-derived IL-10, TGF-beta, and prostaglandin E2. J Immunol 1994;153(4):1674-86.
65. Wang HY, Wang RF. Regulatory T cells and cancer. Curr Opin Immunol 2007;19(2):217-23.
66. Zou W. Regulatory T cells, tumour immunity and immunotherapy. Nat Rev Immunol 2006;6(4):295-307.
67. Hanes J, Sills A, Zhao Z, Suh KW, Tyler B, DiMeco F, et al. Controlled local delivery of interleukin-2 by biodegradable polymers protects animals from experimental brain tumors and liver tumors. Pharm Res 2001;18(7):899-906.
68. Ali OA, Huebsch N, Cao L, Dranoff G, Mooney DJ. Infection-mimicking materials to program dendritic cells in situ. Nat Mater 2009;8(2):151-8.
69. Jackaman C, Lew AM, Zhan Y, Allan JE, Koloska B, Graham PT, et al. Deliberately provoking local inflammation drives tumors to become their own protective vaccine site. Int Immunol 2008;20(11):1467-79.
70. Lee KH, Panelli MC, Kim CJ, Riker AI, Bettinotti MP, Roden MM, et al. Functional dissociation between local and systemic immune response during anti-melanoma peptide vaccination. J Immunol 1998;161(8):4183-94.
71. Clemente CG, Mihm MC, Jr., Bufalino R, Zurrida S, Collini P, Cascinelli N. Prognostic value of tumor infiltrating lymphocytes in the vertical growth phase of primary cutaneous melanoma. Cancer 1996;77(7):1303-10.
72. Clark WH, Jr., Elder DE, Guerry Dt, Braitman LE, Trock BJ, Schultz D, et al. Model predicting survival in stage I melanoma based on tumor progression. J Natl Cancer Inst 1989;81(24):1893-904.
73. Mihm MC, Jr., Clemente CG, Cascinelli N. Tumor infiltrating lymphocytes in lymph node melanoma metastases: a histopathologic prognostic indicator and an expression of local immune response. Lab Invest 1996;74(1):43-7.

74. Chang SC, Rowley JA, Tobias G, Genes NG, Roy AK, Mooney DJ, et al. Injection molding of chondrocyte/alginate constructs in the shape of facial implants. J Biomed Mater Res 2001;55(4):503-11.
75. Cirone P, Bourgeois JM, Austin RC, Chang PL. A novel approach to tumor suppression with microencapsulated recombinant cells. Hum Gene Ther 2002;13(10):1157-66.
76. Joki T, Machluf M, Atala A, Zhu J, Seyfried NT, Dunn IF, et al. Continuous release of endostatin from microencapsulated engineered cells for tumor therapy. Nat Biotechnol 2001;19(1):35-9.
77. Shang Q, Wang Z, Liu W, Shi Y, Cui L, Cao Y. Tissue-engineered bone repair of sheep cranial defects with autologous bone marrow stromal cells. J Craniofac Surg 2001;12(6):586-93; discussion 594-5.
78. Thomas S. Alginate dressings in surgery and wound management--Part 1. J Wound Care 2000;9(2):56-60.
79. Sikorski P, Mo F, Skjak-Braek G, Stokke BT. Evidence for egg-box-compatible interactions in calcium-alginate gels from fiber X-ray diffraction. Biomacromolecules 2007;8(7):2098-103.
80. Boontheekul T, Kong HJ, Mooney DJ. Controlling alginate gel degradation utilizing partial oxidation and bimodal molecular weight distribution. Biomaterials 2005;26(15):2455-65.
81. Gomez CG, Rinaudo M, Villar MA. Oxidation of sodium alginate and characterization of the oxidized derivatives. Carbohydrate Polymers 2006;67(3):296-304.
82. Kong HJ, Kaigler D, Kim K, Mooney DJ. Controlling rigidity and degradation of alginate hydrogels via molecular weight distribution. Biomacromolecules 2004;5(5):1720-7.
83. Wang T, Lacik I, Brissova M, Anilkumar AV, Prokop A, Hunkeler D, et al. An encapsulation system for the immunoisolation of pancreatic islets. Nat Biotechnol 1997;15(4):358-62.
84. Kuo CK, Ma PX. Ionically crosslinked alginate hydrogels as scaffolds for tissue engineering: part 1. Structure, gelation rate and mechanical properties. Biomaterials 2001;22(6):511-21.
85. Marler JJ, Guha A, Rowley J, Koka R, Mooney D, Upton J, et al. Soft-tissue augmentation with injectable alginate and syngeneic fibroblasts. Plast Reconstr Surg 2000;105(6):2049-58.
86. Rowley JA, Mooney DJ. Alginate type and RGD density control myoblast phenotype. J Biomed Mater Res 2002;60(2):217-23.
87. Poncelet D, Poncelet De Smet B, Beaulieu C, Huguet ML, Fournier A, Neufeld RJ. production of alginate beads by emulsification/internal gelation. II. Physicochemistry. Applied Microbiology and Biotechnology 1995;43:644-650.
88. Khromova YL. The Effect of Chlorides on Alginate Gelation in the Presence of Calcium Sulfate. Kolloidnyi Zhurnal 2006;68(1):123-128.
89. Reis CP, Neufeld RJ, Vilela S, Ribeiro AJ, Veiga F. Review and current status of emulsion/dispersion technology using an internal gelation process for the design of alginate particles. J Microencapsul 2006;23(3):245-57.
90. Melvik JE DM, Onsoyen E, Berge A, Svendsen T., inventor Self-gelling alginate systems and uses thereof patent United States Patent Application #20060159823. 2006.
91. Westhaus E, Messersmith PB. Triggered release of calcium from lipid vesicles: a bioinspired strategy for rapid gelation of polysaccharide and protein hydrogels. Biomaterials 2001;22(5):453-62.

92. Silva EA, Mooney DJ. Spatiotemporal control of vascular endothelial growth factor delivery from injectable hydrogels enhances angiogenesis. J Thromb Haemost 2007;5(3):590-8.
93. Landa N, Miller L, Feinberg MS, Holbova R, Shachar M, Freeman I, et al. Effect of injectable alginate implant on cardiac remodeling and function after recent and old infarcts in rat. Circulation 2008;117(11):1388-96.
94. Hori Y, Winans AM, Huang CC, Horrigan EM, Irvine DJ. Injectable dendritic cell-carrying alginate gels for immunization and immunotherapy. Biomaterials 2008.
95. Siddiqui SA, Frigola X, Bonne-Annee S, Mercader M, Kuntz SM, Krambeck AE, et al. Tumor-infiltrating Foxp3-CD4+CD25+ T cells predict poor survival in renal cell carcinoma. Clin Cancer Res 2007;13(7):2075-81.
96. Hu Y, Litwin T, Nagaraja AR, Kwong B, Katz J, Watson N, et al. Cytosolic delivery of membrane-impermeable molecules in dendritic cells using pH-responsive core-shell nanoparticles. Nano Lett 2007;7(10):3056-64.
97. Jotwani R, Pulendran B, Agrawal S, Cutler CW. Human dendritic cells respond to Porphyromonas gingivalis LPS by promoting a Th2 effector response in vitro. Eur J Immunol 2003;33(11):2980-6.
98. Vallhov H, Qin J, Johansson SM, Ahlborg N, Muhammed MA, Scheynius A, et al. The importance of an endotoxin-free environment during the production of nanoparticles used in medical applications. Nano Lett 2006;6(8):1682-6.
99. Inaba K, Inaba M, Romani N, Aya H, Deguchi M, Ikehara S, et al. Generation of large numbers of dendritic cells from mouse bone marrow cultures supplemented with granulocyte/macrophage colony-stimulating factor. J Exp Med 1992;176(6):1693-702.
100. Stachowiak AN, Wang Y, Huang YC, Irvine DJ. Homeostatic lymphoid chemokines synergize with adhesion ligands to trigger T and B lymphocyte chemokinesis. J Immunol 2006;177(4):2340-8.
101. Ghiasi Z, Sajadi Tabasi SA, Tafaghodi M. Preparation and *In Vitro* Characterization of Alginate Microspheres Encapsulated with Autoclaved *Leishmania major* (ALM) and CpG-ODN. Iranian Journal of Basic Medical Sciences 2007;10(2):90-98.
102. Lee HY, Chan LW, Heng PW. Influence of partially cross-linked alginate used in the production of alginate microspheres by emulsification. J Microencapsul 2005;22(3):275-80.
103. Augst AD, Kong HJ, Mooney DJ. Alginate hydrogels as biomaterials. Macromol Biosci 2006;6(8):623-33.
104. Rowley JA, Madlambayan G, Mooney DJ. Alginate hydrogels as synthetic extracellular matrix materials. Biomaterials 1999;20(1):45-53.
105. Hofer AM, Machen TE. Technique for in situ measurement of calcium in intracellular inositol 1,4,5-trisphosphate-sensitive stores using the fluorescent indicator mag-fura-2. Proc Natl Acad Sci U S A 1993;90(7):2598-602.
106. Raju B, Murphy E, Levy LA, Hall RD, London RE. A fluorescent indicator for measuring cytosolic free magnesium. Am J Physiol 1989;256(3 Pt 1):C540-8.
107. Tsien RY. Fluorescent probes of cell signaling. Annu Rev Neurosci 1989;12:227-53.
108. Smidsrod O, Skjak-Braek G. Alginate as immobilization matrix for cells. Trends Biotechnol 1990;8(3):71-8.
109. Kong HJ, Smith MK, Mooney DJ. Designing alginate hydrogels to maintain viability of immobilized cells. Biomaterials 2003;24(22):4023-9.
110. Kong HJ, Wong E, Mooney DJ. Independent Control of Rigidity and Toughness of Polymeric Hydrogels. Macromolecules 2003;36:4582-4588.

111. Ahearne M, Yang Y, El Haj AJ, Then KY, Liu KK. Characterizing the viscoelastic properties of thin hydrogel-based constructs for tissue engineering applications. J R Soc Interface 2005;2(5):455-63.
112. West ER, Xu M, Woodruff TK, Shea LD. Physical properties of alginate hydrogels and their effects on in vitro follicle development. Biomaterials 2007;28(30):4439-48.
113. Webber RE, Shull KR. Strain Dependence of the Viscoelastic Properties of Alginate Hydrogels. Macromolecules 2004;37:6153-6160.
114. LeRoux MA, Guilak F, Setton LA. Compressive and shear properties of alginate gel: effects of sodium ions and alginate concentration. J Biomed Mater Res 1999;47(1):46-53.
115. Freeman I, Kedem A, Cohen S. The effect of sulfation of alginate hydrogels on the specific binding and controlled release of heparin-binding proteins. Biomaterials 2008;29(22):3260-8.
116. Murata Y, Jinno D, Liu D, Isobe T, Kofuji K, Kawashima S. The drug release profile from calcium-induced alginate gel beads coated with an alginate hydrolysate. Molecules 2007;12(11):2559-66.
117. Wee S, Gombotz WR. Protein release from alginate matrices. Adv Drug Deliv Rev 1998;31(3):267-285.
118. Gu F, Amsden B, Neufeld R. Sustained delivery of vascular endothelial growth factor with alginate beads. J Control Release 2004;96(3):463-72.
119. Belldegrun A, Muul LM, Rosenberg SA. Interleukin 2 expanded tumor-infiltrating lymphocytes in human renal cell cancer: isolation, characterization, and antitumor activity. Cancer Res 1988;48(1):206-14.
120. Kawakami Y, Eliyahu S, Delgado CH, Robbins PF, Sakaguchi K, Appella E, et al. Identification of a human melanoma antigen recognized by tumor-infiltrating lymphocytes associated with in vivo tumor rejection. Proc Natl Acad Sci U S A 1994;91(14):6458-62.
121. Topalian SL, Solomon D, Rosenberg SA. Tumor-specific cytolysis by lymphocytes infiltrating human melanomas. J Immunol 1989;142(10):3714-25.
122. Wallace PK, Palmer LD, Perry-Lalley D, Bolton ES, Alexander RB, Horan PK, et al. Mechanisms of adoptive immunotherapy: improved methods for in vivo tracking of tumor-infiltrating lymphocytes and lymphokine-activated killer cells. Cancer Res 1993;53(10 Suppl):2358-67.
123. Rosenberg SA, Yang JC, Restifo NP. Cancer immunotherapy: moving beyond current vaccines. Nat Med 2004;10(9):909-15.
124. Bos GW, Jacobs JJ, Koten JW, Van Tomme S, Veldhuis T, van Nostrum CF, et al. In situ crosslinked biodegradable hydrogels loaded with IL-2 are effective tools for local IL-2 therapy. Eur J Pharm Sci 2004;21(4):561-7.
125. De Groot CJ, Cadee JE, Koten JE, Hennink WE, Otter WD. Therapeutic efficacy of IL-2-loaded hydrogels in a mouse tumor model. International Journal of Cancer 2002;98:134-140.
126. Liu L, Liu S, Ng SY, Froix M, Ohno T, Heller J. Controlled release of interleukin-2 for tumour immunotherapy using alginate/chitosan porous microspheres. Journal of Controlled Release 1997;43:65-74.
127. Hori Y, Winans AM, Huang CC, Horrigan EM, Irvine DJ. Injectable dendritic cell-carrying alginate gels for immunization and immunotherapy. Biomaterials 2008;29(27):3671-82.
128. Liu XD, Yu WY, Zhang Y, Xue WM, Yu WT, Xiong Y, et al. Characterization of structure and diffusion behaviour of Ca-alginate beads prepared with external or internal calcium sources. J Microencapsul 2002;19(6):775-82.

129. Kunikata N, Sano K, Honda M, Ishii K, Matsunaga J, Okuyama R, et al. Peritumoral CpG oligodeoxynucleotide treatment inhibits tumor growth and metastasis of B16F10 melanoma cells. J Invest Dermatol 2004;123(2):395-402.
130. Tokunaga T, Yamamoto H, Shimada S, Abe H, Fukuda T, Fujisawa Y, et al. Antitumor activity of deoxyribonucleic acid fraction from Mycobacterium bovis BCG. I. Isolation, physicochemical characterization, and antitumor activity. J Natl Cancer Inst 1984;72(4):955-62.
131. Vicari AP, Chiodoni C, Vaure C, Ait-Yahia S, Dercamp C, Matsos F, et al. Reversal of tumor-induced dendritic cell paralysis by CpG immunostimulatory oligonucleotide and anti-interleukin 10 receptor antibody. J Exp Med 2002;196(4):541-9.
132. Yang Y, Huang CT, Huang X, Pardoll DM. Persistent Toll-like receptor signals are required for reversal of regulatory T cell-mediated CD8 tolerance. Nat Immunol 2004;5(5):508-15.
133. Furumoto K, Soares L, Engleman EG, Merad M. Induction of potent antitumor immunity by in situ targeting of intratumoral DCs. J Clin Invest 2004;113(5):774-83.
134. Babensee JE, Paranjpe A. Differential levels of dendritic cell maturation on different biomaterials used in combination products. J Biomed Mater Res A 2005;74(4):503-10.
135. Friedl P, Maaser K, Klein CE, Niggemann B, Krohne G, Zanker KS. Migration of highly aggressive MV3 melanoma cells in 3-dimensional collagen lattices results in local matrix reorganization and shedding of alpha2 and beta1 integrins and CD44. Cancer Res 1997;57(10):2061-70.
136. Brightman AO, Rajwa BP, Sturgis JE, McCallister ME, Robinson JP, Voytik-Harbin SL. Time-lapse confocal reflection microscopy of collagen fibrillogenesis and extracellular matrix assembly in vitro. Biopolymers 2000;54(3):222-34.
137. Semler EJ, Tjia JS, Moghe PV. Analysis of surface microtopography of biodegradable polymer matrices using confocal reflection microscopy. Biotechnol Prog 1997;13(5):630-4.
138. Griffith LG, Swartz MA. Capturing complex 3D tissue physiology in vitro. Nat Rev Mol Cell Biol 2006;7(3):211-24.
139. Lammermann T, Bader BL, Monkley SJ, Worbs T, Wedlich-Soldner R, Hirsch K, et al. Rapid leukocyte migration by integrin-independent flowing and squeezing. Nature 2008;453(7191):51-5.
140. Banchereau J, Briere F, Caux C, Davoust J, Lebecque S, Liu YJ, et al. Immunobiology of dendritic cells. Annu Rev Immunol 2000;18:767-811.
141. Steinman RM, Banchereau J. Taking dendritic cells into medicine. Nature 2007;449(7161):419-26.
142. Nestle FO, Farkas A, Conrad C. Dendritic-cell-based therapeutic vaccination against cancer. Curr Opin Immunol 2005;17(2):163-9.
143. Timmerman JM, Levy R. Dendritic cell vaccines for cancer immunotherapy. Annu Rev Med 1999;50:507-29.
144. Gilboa E. DC-based cancer vaccines. J Clin Invest 2007;117(5):1195-203.
145. Lu W, Wu X, Lu Y, Guo W, Andrieu JM. Therapeutic dendritic-cell vaccine for simian AIDS. Nat Med 2003;9(1):27-32.
146. Lee KH, Wang E, Nielsen MB, Wunderlich J, Migueles S, Connors M, et al. Increased vaccine-specific T cell frequency after peptide-based vaccination correlates with increased susceptibility to in vitro stimulation but does not lead to tumor regression. J Immunol 1999;163(11):6292-300.

147. Rosenberg SA. Progress in the development of immunotherapy for the treatment of patients with cancer. J Intern Med 2001;250(6):462-75.
148. Palucka AK, Ueno H, Fay JW, Banchereau J. Taming cancer by inducing immunity via dendritic cells. Immunol Rev 2007;220:129-50.
149. Chappell DB, Restifo NP. T cell-tumor cell: a fatal interaction? Cancer Immunol Immunother 1998;47(2):65-71.
150. Staveley-O'Carroll K, Sotomayor E, Montgomery J, Borrello I, Hwang L, Fein S, et al. Induction of antigen-specific T cell anergy: An early event in the course of tumor progression. Proc Natl Acad Sci U S A 1998;95(3):1178-83.
151. Onrust SV, Hartl PM, Rosen SD, Hanahan D. Modulation of L-selectin ligand expression during an immune response accompanying tumorigenesis in transgenic mice. J Clin Invest 1996;97(1):54-64.
152. Ochsenbein AF, Klenerman P, Karrer U, Ludewig B, Pericin M, Hengartner H, et al. Immune surveillance against a solid tumor fails because of immunological ignorance. Proc Natl Acad Sci U S A 1999;96(5):2233-8.
153. Hermans IF, Daish A, Yang J, Ritchie DS, Ronchese F. Antigen expressed on tumor cells fails to elicit an immune response, even in the presence of increased numbers of tumor-specific cytotoxic T lymphocyte precursors. Cancer Res 1998;58(17):3909-17.
154. Candido KA, Shimizu K, McLaughlin JC, Kunkel R, Fuller JA, Redman BG, et al. Local administration of dendritic cells inhibits established breast tumor growth: implications for apoptosis-inducing agents. Cancer Res 2001;61(1):228-36.
155. Melero I, Duarte M, Ruiz J, Sangro B, Galofre J, Mazzolini G, et al. Intratumoral injection of bone-marrow derived dendritic cells engineered to produce interleukin-12 induces complete regression of established murine transplantable colon adenocarcinomas. Gene Ther 1999;6(10):1779-84.
156. Nishioka Y, Hirao M, Robbins PD, Lotze MT, Tahara H. Induction of systemic and therapeutic antitumor immunity using intratumoral injection of dendritic cells genetically modified to express interleukin 12. Cancer Res 1999;59(16):4035-41.
157. Schrama D, Pedersen LO, Keikavoussi P, Andersen MH, Straten Pt P, Brocker EB, et al. Aggregation of antigen-specific T cells at the inoculation site of mature dendritic cells. J Invest Dermatol 2002;119(6):1443-8.
158. Yu P, Lee Y, Liu W, Chin RK, Wang J, Wang Y, et al. Priming of naive T cells inside tumors leads to eradication of established tumors. Nat Immunol 2004;5(2):141-9.
159. Sato M, Chamoto K, Nishimura T. A novel tumor-vaccine cell therapy using bone marrow-derived dendritic cell type 1 and antigen-specific Th1 cells. Int Immunol 2003;15(7):837-43.
160. Guo Z, Zhang M, Tang H, Cao X. Fas signal links innate and adaptive immunity by promoting dendritic-cell secretion of CC and CXC chemokines. Blood 2005;106(6):2033-41.
161. Ngo VN, Tang HL, Cyster JG. Epstein-Barr virus-induced molecule 1 ligand chemokine is expressed by dendritic cells in lymphoid tissues and strongly attracts naive T cells and activated B cells. J Exp Med 1998;188(1):181-91.
162. Sallusto F, Palermo B, Lenig D, Miettinen M, Matikainen S, Julkunen I, et al. Distinct patterns and kinetics of chemokine production regulate dendritic cell function. Eur J Immunol 1999;29(5):1617-25.

163. Christopherson KW, 2nd, Campbell JJ, Travers JB, Hromas RA. Low-molecular-weight heparins inhibit CCL21-induced T cell adhesion and migration. J Pharmacol Exp Ther 2002;302(1):290-5.
164. Eggert AA, van der Voort R, Torensma R, Moulin V, Boerman OC, Oyen WJ, et al. Analysis of dendritic cell trafficking using EGFP-transgenic mice. Immunol Lett 2003;89(1):17-24.
165. Kabashima K, Banks TA, Ansel KM, Lu TT, Ware CF, Cyster JG. Intrinsic lymphotoxin-beta receptor requirement for homeostasis of lymphoid tissue dendritic cells. Immunity 2005;22(4):439-50.
166. Kamath AT, Henri S, Battye F, Tough DF, Shortman K. Developmental kinetics and lifespan of dendritic cells in mouse lymphoid organs. Blood 2002;100(5):1734-41.
167. Eggert AA, Schreurs MW, Boerman OC, Oyen WJ, de Boer AJ, Punt CJ, et al. Biodistribution and vaccine efficiency of murine dendritic cells are dependent on the route of administration. Cancer Res 1999;59(14):3340-5.
168. Lappin MB, Weiss JM, Delattre V, Mai B, Dittmar H, Maier C, et al. Analysis of mouse dendritic cell migration in vivo upon subcutaneous and intravenous injection. Immunology 1999;98(2):181-8.
169. Morse MA, Coleman RE, Akabani G, Niehaus N, Coleman D, Lyerly HK. Migration of human dendritic cells after injection in patients with metastatic malignancies. Cancer Res 1999;59(1):56-8.
170. Smith AL, Fazekas de St Groth B. Antigen-pulsed CD8alpha+ dendritic cells generate an immune response after subcutaneous injection without homing to the draining lymph node. J Exp Med 1999;189(3):593-8.
171. Andre F, Chaput N, Schartz NE, Flament C, Aubert N, Bernard J, et al. Exosomes as potent cell-free peptide-based vaccine. I. Dendritic cell-derived exosomes transfer functional MHC class I/peptide complexes to dendritic cells. J Immunol 2004;172(4):2126-36.
172. Kaiser A, Donnadieu E, Abastado JP, Trautmann A, Nardin A. CC chemokine ligand 19 secreted by mature dendritic cells increases naive T cell scanning behavior and their response to rare cognate antigen. J Immunol 2005;175(4):2349-56.
173. Lebre MC, Burwell T, Vieira PL, Lora J, Coyle AJ, Kapsenberg ML, et al. Differential expression of inflammatory chemokines by Th1- and Th2-cell promoting dendritic cells: a role for different mature dendritic cell populations in attracting appropriate effector cells to peripheral sites of inflammation. Immunol Cell Biol 2005;83(5):525-35.
174. Tang HL, Cyster JG. Chemokine Up-regulation and activated T cell attraction by maturing dendritic cells. Science 1999;284(5415):819-22.
175. Kranz DM, Tonegawa S, Eisen HN. Attachment of an anti-receptor antibody to non-target cells renders them susceptible to lysis by a clone of cytotoxic T lymphocytes. Proc Natl Acad Sci U S A 1984;81(24):7922-6.
176. Proudfoot AE, Handel TM, Johnson Z, Lau EK, LiWang P, Clark-Lewis I, et al. Glycosaminoglycan binding and oligomerization are essential for the in vivo activity of certain chemokines. Proc Natl Acad Sci U S A 2003;100(4):1885-90.
177. Proudfoot AE. The biological relevance of chemokine-proteoglycan interactions. Biochem Soc Trans 2006;34(Pt 3):422-6.
178. Friedman RS, Jacobelli J, Krummel MF. Surface-bound chemokines capture and prime T cells for synapse formation. Nat Immunol 2006;7(10):1101-8.
179. Smetana K, Jr. Cell biology of hydrogels. Biomaterials 1993;14(14):1046-50.

180. Friedl P, Brocker EB. The biology of cell locomotion within three-dimensional extracellular matrix. Cell Mol Life Sci 2000;57(1):41-64.
181. Friedl P, Entschladen F, Conrad C, Niggemann B, Zanker KS. CD4+ T lymphocytes migrating in three-dimensional collagen lattices lack focal adhesions and utilize beta1 integrin-independent strategies for polarization, interaction with collagen fibers and locomotion. Eur J Immunol 1998;28(8):2331-43.
182. Steinman RM, Dhodapkar M. Active immunization against cancer with dendritic cells: the near future. Int J Cancer 2001;94(4):459-73.
183. Gimbel MI, Delman KA, Zager JS. Therapy for unresectable recurrent and in-transit extremity melanoma. Cancer Control 2008;15(3):225-32.
184. Crittenden MR, Thanarajasingam U, Vile RG, Gough MJ. Intratumoral immunotherapy: using the tumour against itself. Immunology 2005;114(1):11-22.
185. Joosten J, Jager G, Oyen W, Wobbes T, Ruers T. Cryosurgery and radiofrequency ablation for unresectable colorectal liver metastases. Eur J Surg Oncol 2005;31(10):1152-9.
186. Herber DL, Nagaraj S, Djeu JY, Gabrilovich DI. Mechanism and therapeutic reversal of immune suppression in cancer. Cancer Res 2007;67(11):5067-9.
187. Zou W. Immunosuppressive networks in the tumour environment and their therapeutic relevance. Nat Rev Cancer 2005;5(4):263-74.
188. Li J, Song W, Czerwinski DK, Varghese B, Uematsu S, Akira S, et al. Lymphoma immunotherapy with CpG oligodeoxynucleotides requires TLR9 either in the host or in the tumor itself. J Immunol 2007;179(4):2493-500.
189. Nierkens S, den Brok MH, Sutmuller RP, Grauer OM, Bennink E, Morgan ME, et al. In vivo colocalization of antigen and CpG [corrected] within dendritic cells is associated with the efficacy of cancer immunotherapy. Cancer Res 2008;68(13):5390-6.
190. Broomfield SA, van der Most RG, Prosser AC, Mahendran S, Tovey MG, Smyth MJ, et al. Locally administered TLR7 agonists drive systemic antitumor immune responses that are enhanced by anti-CD40 immunotherapy. J Immunol 2009;182(9):5217-24.
191. Heikenwalder M, Polymenidou M, Junt T, Sigurdson C, Wagner H, Akira S, et al. Lymphoid follicle destruction and immunosuppression after repeated CpG oligodeoxynucleotide administration. Nat Med 2004;10(2):187-92.
192. Vonderheide RH, Flaherty KT, Khalil M, Stumacher MS, Bajor DL, Hutnick NA, et al. Clinical activity and immune modulation in cancer patients treated with CP-870,893, a novel CD40 agonist monoclonal antibody. J Clin Oncol 2007;25(7):876-83.
193. Egilmez NK, Jong YS, Sabel MS, Jacob JS, Mathiowitz E, Bankert RB. In situ tumor vaccination with interleukin-12-encapsulated biodegradable microspheres: induction of tumor regression and potent antitumor immunity. Cancer Res 2000;60(14):3832-7.
194. Soon-Shiong P, Heintz RE, Merideth N, Yao QX, Yao Z, Zheng T, et al. Insulin independence in a type 1 diabetic patient after encapsulated islet transplantation. Lancet 1994;343(8903):950-1.
195. Sellke FW, Laham RJ, Edelman ER, Pearlman JD, Simons M. Therapeutic angiogenesis with basic fibroblast growth factor: technique and early results. Ann Thorac Surg 1998;65(6):1540-4.
196. Hasse C, Klock G, Schlosser A, Zimmermann U, Rothmund M. Parathyroid allotransplantation without immunosuppression. Lancet 1997;350(9087):1296-7.

197. Irvine DJ, Stachowiak AN, Hori Y. Lymphoid tissue engineering: invoking lymphoid tissue neogenesis in immunotherapy and models of immunity. Semin Immunol 2008;20(2):137-46.
198. Hori Y, Winans AM, Irvine DJ. Modular injectable matrices based on alginate solution/microsphere mixtures that gel in situ and co-deliver immunomodulatory factors. Acta Biomater 2008.
199. Dubois S, Patel HJ, Zhang M, Waldmann TA, Muller JR. Preassociation of IL-15 with IL-15R alpha-IgG1-Fc enhances its activity on proliferation of NK and CD8+/CD44high T cells and its antitumor action. J Immunol 2008;180(4):2099-106.
200. Epardaud M, Elpek KG, Rubinstein MP, Yonekura AR, Bellemare-Pelletier A, Bronson R, et al. Interleukin-15/interleukin-15R alpha complexes promote destruction of established tumors by reviving tumor-resident CD8+ T cells. Cancer Res 2008;68(8):2972-83.
201. Teague RM, Sather BD, Sacks JA, Huang MZ, Dossett ML, Morimoto J, et al. Interleukin-15 rescues tolerant CD8+ T cells for use in adoptive immunotherapy of established tumors. Nat Med 2006;12(3):335-41.
202. Rubinstein MP, Kovar M, Purton JF, Cho JH, Boyman O, Surh CD, et al. Converting IL-15 to a superagonist by binding to soluble IL-15R{alpha}. Proc Natl Acad Sci U S A 2006;103(24):9166-71.
203. Stoklasek TA, Schluns KS, Lefrancois L. Combined IL-15/IL-15Ralpha immunotherapy maximizes IL-15 activity in vivo. J Immunol 2006;177(9):6072-80.
204. Krieg AM, Vollmer J. Toll-like receptors 7, 8, and 9: linking innate immunity to autoimmunity. Immunol Rev 2007;220:251-69.
205. Quezada SA, Peggs KS, Curran MA, Allison JP. CTLA4 blockade and GM-CSF combination immunotherapy alters the intratumor balance of effector and regulatory T cells. J Clin Invest 2006;116(7):1935-45.
206. Ryschich E, Schmidt J, Hammerling GJ, Klar E, Ganss R. Transformation of the microvascular system during multistage tumorigenesis. Int J Cancer 2002;97(6):719-25.
207. Talmadge JE. Pathways mediating the expansion and immunosuppressive activity of myeloid-derived suppressor cells and their relevance to cancer therapy. Clin Cancer Res 2007;13(18 Pt 1):5243-8.
208. Melief CJ. Cancer immunotherapy by dendritic cells. Immunity 2008;29(3):372-83.
209. Mohamadzadeh M, Berard F, Essert G, Chalouni C, Pulendran B, Davoust J, et al. Interleukin 15 skews monocyte differentiation into dendritic cells with features of Langerhans cells. J Exp Med 2001;194(7):1013-20.
210. Ohteki T, Suzue K, Maki C, Ota T, Koyasu S. Critical role of IL-15-IL-15R for antigen-presenting cell functions in the innate immune response. Nat Immunol 2001;2(12):1138-43.
211. Galon J, Costes A, Sanchez-Cabo F, Kirilovsky A, Mlecnik B, Lagorce-Pages C, et al. Type, density, and location of immune cells within human colorectal tumors predict clinical outcome. Science 2006;313(5795):1960-4.
212. Zhang L, Conejo-Garcia JR, Katsaros D, Gimotty PA, Massobrio M, Regnani G, et al. Intratumoral T cells, recurrence, and survival in epithelial ovarian cancer. N Engl J Med 2003;348(3):203-13.
213. Wendel M, Galani IE, Suri-Payer E, Cerwenka A. Natural killer cell accumulation in tumors is dependent on IFN-gamma and CXCR3 ligands. Cancer Res 2008;68(20):8437-45.

214. Mineo JF, Bordron A, Quintin-Roue I, Maurage CA, Buhe V, Loisel S, et al. Increasing of HER2 membranar density in human glioblastoma U251MG cell line established in a new nude mice model. J Neurooncol 2006;76(3):249-55.
215. Younes E, Haas GP, Dezso B, Ali E, Maughan RL, Kukuruga MA, et al. Local tumor irradiation augments the response to IL-2 therapy in a murine renal adenocarcinoma. Cell Immunol 1995;165(2):243-51.
216. Rousseau RF, Biagi E, Dutour A, Yvon ES, Brown MP, Lin T, et al. Immunotherapy of high-risk acute leukemia with a recipient (autologous) vaccine expressing transgenic human CD40L and IL-2 after chemotherapy and allogeneic stem cell transplantation. Blood 2006;107(4):1332-41.
217. Irvine DJ, Stachowiak AN, Hori Y. Lymphoid tissue engineering: Invoking lymphoid tissue neogenesis in immunotherapy and models of immunity. Semin Immunol 2007 (In Press).
218. Gennadios A, Hanna MA, Kurth LB. Application of Edible Coatings on Meats, Poultry and Seafoods: A Review. Lebensmittel-Wissenschaft und-Technologie 1997;30(4):337-350.
219. Waldmann TA. The biology of interleukin-2 and interleukin-15: implications for cancer therapy and vaccine design. Nat Rev Immunol 2006;6(8):595-601.
220. Champion JA, Walker A, Mitragotri S. Role of particle size in phagocytosis of polymeric microspheres. Pharm Res 2008;25(8):1815-21.
221. Bulanova E, Budagian V, Duitman E, Orinska Z, Krause H, Ruckert R, et al. Soluble Interleukin IL-15Ralpha is generated by alternative splicing or proteolytic cleavage and forms functional complexes with IL-15. J Biol Chem 2007;282(18):13167-79.
222. Mortier E, Woo T, Advincula R, Gozalo S, Ma A. IL-15Ralpha chaperones IL-15 to stable dendritic cell membrane complexes that activate NK cells via trans presentation. J Exp Med 2008;205(5):1213-25.

Appendix A
Preliminary Studies: Injectable Matrix Material Selection

In order to select an appropriate material for creating vaccination nodes, we first compared collagen, Matrigel, and alginate as injectable matrices that can deliver immunomodulatory/immunostimulatory factors to continuously recruit and support desired effector immune cells as well as counter suppressive effects from the tumor cells. The matrix should also act as a platform for the recruited cells to fight against the tumor cells. An ideal matrix must be biocompatible, non-immunogenic, non-cytotoxic, and mechanically stable with the option of being able to control its biodegradability. Chemokines, cytokines, and other macromolecules should be able to diffuse through the matrix at rates appropriate for regulating the immune responses.

In order to choose a matrix or matrices that satisfy these criteria, candidate materials including collagen, Matrigel, and alginate crosslinked with calcium ions were injected *in vivo* with or without factors (lymphoid stromal cells, dendritic cells, CCL21, CXCL13) to assess their performance. Their qualitative mechanical properties and integrity *in vivo*, the types of cellular infiltrates they attracted at baseline, reproducibility of results, and ease of injections, recovery, and processing for analyses were compared.

Collagen is a natural biopolymer widely used for cell culture, and it has successfully been implemented *in vitro* as a three-dimensional scaffold to study lymphocyte migration in our lab. It is liquid at 4°C but polymerizes and gels when placed at 37°C. Matrigel is also a natural biopolymer with composition of basement membranes which resembles the composition of the reticular fibers in the lymph node. Like collagen, it is fluid at 4°C but gels very quickly upon heating to body temperature. In addition to the three candidate materials, 50/50 mixtures of alginate and collagen as well as alginate and Matrigel were compared to examine the effect of having adhesion molecules in alginate and to let collagen and Matrigel hold the gel together instead of adding calcium ions.

Results of qualitative comparisons among the matrices are shown in Table S1; more '+' signs indicating better performance. Alginate crosslinked with calcium chloride had the best overall performance, demonstrating good mechanical integrity while *in vivo*, thus allowing good recoverability. Preparation for flow cytometry by digestion with enzymes and EDTA to obtain cell infiltrates was successful, although some cell loss was inevitable. In the preliminary studies, solution of $CaCl_2$ was used to gel the alginate: the alginate matrix precursor solution, mixed with factors to be delivered, was injected into the mice first and 1w/v% $CaCl_2$ solution in PBS was injected as a second step. The use of calcium chloride, however, seemed to increase the number of inflammatory cell infiltrates recruited to the alginate matrix, but not the distribution of the cell types recruited compared to when $CaCl_2$ was not added. Collagen induced very little inflammation but dissolved *in vivo* over time and therefore had poor mechanical properties and poor cell recoverability. Matrigel also exhibited good mechanical integrity *in vivo* but low

numbers of infiltrating inflammatory cells. Mixtures of alginate and collagen or Matrigel did not seem to improve any of the properties of the pure matrix alone.

When alginate and Matrigel were compared in their ability to recruit specific cell types, i.e. T cells, alginate produced the most consistent data. The presence of adhesion molecules in Matrigel may have therefore been less important for immune cell recruitment and cell retention at the site than the innate properties alginate possesses as a hydrogel material. More importantly, Matrigel is an attractive experimental model, but since it is derived of animal origin it cannot be used in human subjects. Alginate has been safely used in humans before(194-196)and exhibited many favorable properties for our applications, as described in Chapter 2 of this thesis work, and alginate was thus chosen as a starting base material for our vaccination node matrix.

Table S1: Qualitative comparison of injectable matrices *in vivo*. The number of '+' signs indicates how well each matrix did in each category of assessment.

	Mechanical integrity	Recoverability of the Matrices	Cell Recovery for Cytometry	Non-immunogenicity
Collagen	+	+	++	+++++
Matrigel	++++	++++	+++	+++++
Alginate (+$CaCl_2$)	+++++	+++++	++++	+++
Alginate+collagen	++	+++	++	+++++
Alginate+Matrigel	+++	+++	+++	+++++

Appendix B
Supplemental Data and Figures

Appendix B.1: T cell recruitment to alginate gels carrying live vs dead mDCs

In order to determine whether the attraction of T cells was a nonspecific inflammatory response to the presence of a large number of dead cells (i.e. DCs may die inside the gels after injection), we compared the recruitment of T cells to alginate carrying live DCs (mDCs= activated, mature DCs), apoptotic DCs, and necrotic DCs. Apoptosis was induced by irradiation of mature DCs with 254nm UV, using Model UVGL-55 Minerlight lamp, Multiband UV-254/365nm, 115V-60Hz for 45 seconds in 100 mm^2 culture dish. The kill curve for irradiation with UV is shown in Figure S1. The viability of the cells did not reach 0 % because the serum in culture media prevented apoptosis (as told by Patrick Stern from Hynes Lab). Since over-irradiating the cells seem to have adverse effects on the morphology (and perhaps functions) of the cells, irradiation time of 45 seconds was chosen for inducing apoptosis. To render the DCs necrotic, the live, activated, mature DCs were repeatedly freeze-thawed between liquid nitrogen bath and 37 °C bath for at least 5 times, with an overnight freezing at -80 °C. The cells were 0 % viable as confirmed by flow cytometry using propidium iodide (PI) live/dead staining.

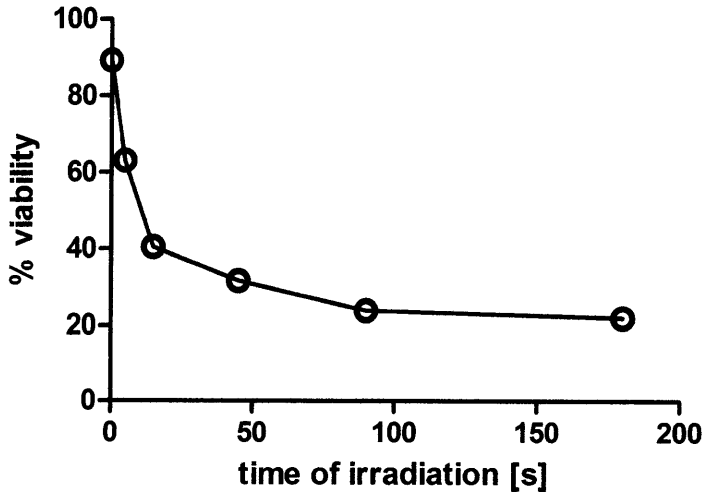

Figure S1: Induction of apoptosis by irradiation with UV. Activated, mature DCs were irradiated for different amounts of time in 100 mm^2 culture dishes to assess their viability after additional 24 hrs in culture at 37 °C. Irradiation time of 45 seconds was chosen for inducing apoptosis in further experiments.

The live, apoptotic, and necrotic DCs were then mixed with self-gelling alginate (2 x 10^6 cells per 150 µL of gel; 2 x 10^6 apoptotic or necrotic DCs had already been aliquoted into individual eppendorf tubes) and injected into the back flanks of mice as described in chapters 2, 3, and 4. The gels were explanted 7 days post-injection and were analyzed by flow cytometry. Figure S2 shows that live dendritic cells recruited the highest number of T cells to the injection site,

followed by apoptotic and necrotic DCs/control alginate. Since most of the 'apoptotic DCs' were still alive at the time of injection and died during the next 24 hrs, the number of T cells that infiltrated the gels seemed to be proportional to how many live DCs were the gels initially. These results confirmed that the T cell trafficking phenomenon to the alginate gels was a consequence of specific actions of live DCs, or any cascade of events that were initiated by live DCs, and not a result of a nonspecific inflammatory response against dead DCs.

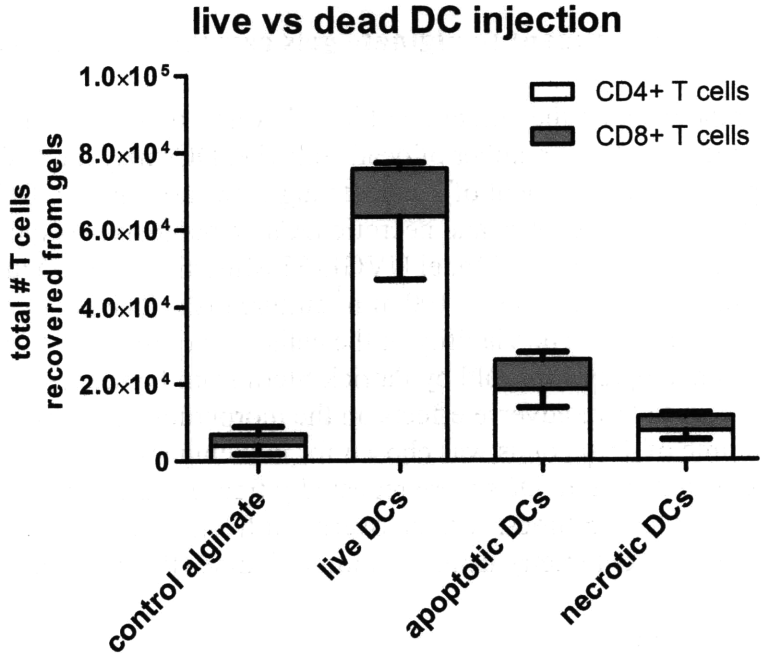

Figure S2: Recruitment of T cells to alginate gels delivering live vs. dead mDCs. Injection of alginate with dead mDCs, either apoptotic (induced by irradiation with 254nm UV, using Model UVGL-55 Minerlight lamp, Multiband UV-254/365nm, 115V-60Hz) or necrotic (induced by repeated freeze-thawing of the cells between -80 °C freezer and 37 °C water bath) cells resulted in inferior T cell attraction compared to alginate carrying live mDCs, confirming that the T cell attraction was a result of actions of live DCs delivered in the alginate matrices, and not a consequence of nonspecific inflammatory response against dead, injected DCs. Control, empty alginate recruited minimal T cells.

Appendix B.2: IL-15SA immobilization on protein-A coated polystyrene beads

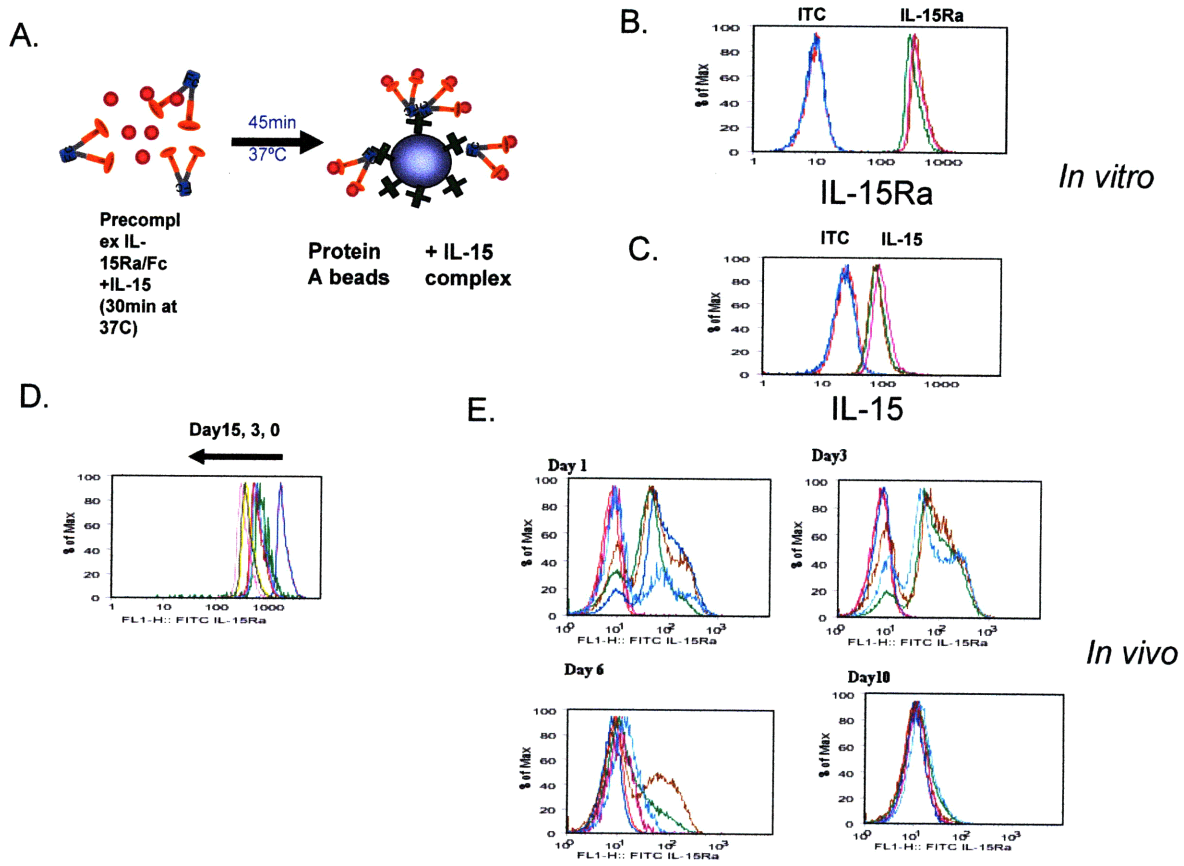

Figure S3: IL-15SA immobilization on the surface of commercially available protein-A beads. A) IL-15SA was formed by incubating IL-15Rα-Fc and IL-15 together for 30 minutes at 37 °C, followed by incubation with protein A-coated beads to capture the Fc fortions of the cytokine complex to immobilize the proteins on the bead surface. The IL-15Rα (B) and IL-15 (C) on the bead surfaces could be detected by flow cytometry using antibodies against the respective proteins. The lifetime of the IL-15SA immobilized on the beads *in vitro* was shown to be over two weeks (D), while that *in vivo* was about 6-10 days as detected by IL-15 Rα antibody (E).

from the monocyte or dendritic cell surfaces to the other two receptor chains (common IL-15/IL-2Rβ and γ chains) on T cell surfaces (219). In order to mimic the presentation of the cytokine from IL-15Rα chain on cell surfaces, we used Protein A-coated polystyrene beads (~10μm in diameter, well above the size range shown to be optimum for phagocytosis of microspheres (220)) to capture the Fc portions of Il-15Rα/Fc chimera proteins, as shown in Figure S3A (see Section 4.2.7 for Materials and Methods). When 1 x 10^6 Protein A beads were added to 36.7 μg IL-15SA (31.7 μg IL-15Rα + 5 μg IL-15), Protein A-coated beads bound about 8% of the IL-15 complex, leaving the rest of the complex in a soluble form in the self-gelling alginate. The number of Protein A-coated beads (1 million per gel) used was determined by keeping the endotoxin level to be below 0.1EU. This amount of Protein A beads themselves did not cause any activation of BMDCs *in vitro*, i.e. no upregulation of CD40 (a costimulatory molecule which is upregulated upon DC maturation) and MHC class II (upregulation of which is a sign of DC maturation) and no TNF-α (a proinflammatory cytokine) secretion.

The presence of IL-15 complex on the bead surfaces was confirmed by flow cytometry (Figures S3B and C), using mouse anti-IL-15Rα conjugated to FITC fluorophore (R&D Systems) and mouse anti-IL-15 (two-step staining usung biotin-IL-15 (R&D systems) and streptavidin-PE or streptavidin-APC (BD Biosciences)). Staining solutions consisted of ~1.2 μg/mL FITC-anti-IL-15Rα and ~0.6-1 μg/mL biotinylated anti-IL-15 for the first staining step and ~2-5 μg/mL of streptavidin-fluorophore for the second staining step (~20-30 minutes on ice at each step, followed by 3X washes with FACS buffer). The lifetime of the immobilized IL-15SA was over two weeks in culture media *in vitro* (Figure S3D) at 37 °C, and about ~6 days when injected with self-gelling alginate *in vivo* (Figure S3E). The beads injected *in vivo* were harvested back from the explanted gels the same way cell suspensions were obtained for flow cytometry, as described in Appendix D.3.

Appendix B.3: IL-15SA release *in vivo*, detected by two-site IL-15Rα/IL-15 ELISA

Ref: Figure 4-2

In order to quantify the amount of IL-15SA by ELISA, we used IL-15Rα ELISA kit from R&D Systems and two-site IL-15Rα/IL-15 ELISA (using IL-15Rα capture antibody and IL-15 detection antibody from respective ELISA kits). Detection of IL-15 bound to IL-15Rα by IL-15 ELISA kit did not generate signal, possibly because binding of IL-15 to the receptor alpha chain occludes its epitope for antibody binding (for at least the specific antibodies we used), or because of conformational changes associated with receptor binding. The technical difficulty in detecting IL-15SA by specific ELISA to IL-15 has also been reported in other studies (221, 222). The detection limit of IL-15SA using IL-15Rα ELISA was much lower (highest standard used = 8 ng/mL; lowest standard = 0.125 ng/mL) than that using two-site IL-15Rα/IL-15 ELISA (highest standard used = 50 ng/mL; lowest standard = 0.75 ng/mL). The absolute values of IL-15SA detected using the two-site ELISA were generally much lower than those (same samples) detected by IL-15Rα ELISA. It is possible that IL-15 either falls off the receptor chain or degrades faster than IL-15Rα (since IL-15Rα is conjugated to Fc portion of human IgG, its lifetime may be similar to that of IgG, which could be longer than native IL-15Rα itself). It is also possible that the two-site ELISA does not detect the whole complex efficiently, although we used the same IL-15 complex molecules for standards as the ones used for samples in experiments so this may not be very likely.

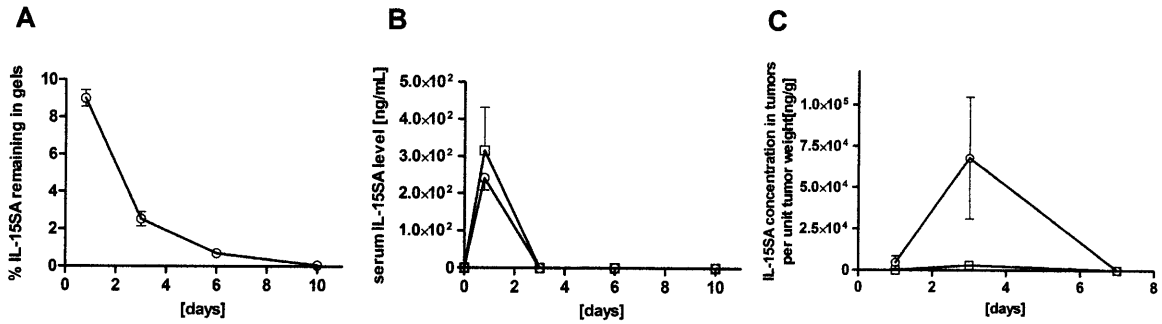

Figure S4: IL-15SA quantification by two-site IL-15Rα/IL-15 ELISA for *in vivo* samples presented in Figure 4-2. (A-C) 36.7 μg IL-15SA was mixed with 150 μL self-gelling alginate and injected peritumorally around 14-day-old B16-ova tumors (O). For comparison, the same quantity of IL-15SA was injected i.p. as a separate group (□). Cytokine present in the gels (A), serum (B), and tumor itself (C) was monitored by ELISA over 7-10 days (*n* = 3-4 samples per time-point).

Figure S4 shows the results of IL-15SA detection in the gels, in the sera, and in the tumors as detected by two-site IL-15Rα/IL-15 ELISA (as opposed to the results in Figure 4-2 which were detected by IL-15Rα. Although the absolute values detected were much lower in these cases, the results confirm that there were sustained release of IL-15SA from the gels *in vivo* and the tumor IL-15SA concentration was much more elevated using gels compared to bolus i.p. injections. The difference in the serum concentration of IL-15SA between gel vs i.p. deliveries were less pronounced.

Appendix C
Experimental Protocols For *In Vitro* Self-Gelling Alginate Formation And Characterization

Appendix C.1: Alginate particle synthesis
(as modified by A. Winans 09/09/08; edited by Y. Hori May 2009)

Ref: Chapter 2, 3, 4

1. Wash probe at homogenizing speed (8x1000/min) with H_2O, isooctane and acetone, in that order, at 3-5 min. per solvent.
2. Begin stirring 35 mL isooctane in 50 mL beaker at 300 rotations/min. Add 1.5 mL of Span80 (add 1 mL then 0.5 mL with 1000 µL pipettor), then 0.5 mL Tween80. Continue stirring until solution clears.
3. Stop stirring and remove stir bar with larger stir bar. Begin homogenizing at 8x1000/min. Make sure probe is at least 10 mm from bottom of flask (10-20 mm generally used) and is centered in the x,y plane. Homogenize for 3 min.
4. Add 400 µL of 1% SLG20 alginate in PBS (wt/vol) dropwise over approximately 20 sec. Homogenize for 3 more min.
5. Add 25 µL 5% $CaCl_2$ (aq) dropwise. Homogenize for 4 more min.
6. Remove alginate solution and pour into 50 mL polypropylene conical tube (purple top). Centrifuge down in large centrifuge (Allegra^{TM} 6KR centrifuge) at 3,200 rpm (~2060 x*g*) for 5 min. Pour off supernatant into organic waste disposal bin.
7. Resuspend pellet with 1 mL isooctane. Add another 30 mL of isooctane and vortex briefly at high speed.
8. Centrifuge down in Allegra^{TM} 6KR centrifuge again at 3200 rpm (~2060 *xg*) for 5 min. Pour off supernatant.
9. Resuspend pellet with 1 mL deionized, distilled (DD) H_2O. Will probably have to mash the pellet with pipet tip and vigorously pipet to fully dissolve pellet. Transfer to labeled 1.5 mL eppendorf tube.
10. Centrifuge down in benchtop mini centrifuge (VWR) at 11 krpm for 3 min.
11. Pour off supernatant and wash twice more with water (3 times total).
12. Store particles in 1 mL of DD H_2O.
13. Wash probe as described in #1.

Note: if making two batches in a row, wash the probe twice (go through solvent cycle twice) before synthesizing a second batch.

Appendix C.2: Measuring Ca^{2+} release from alginate particles into matrix alginate

(written by A. Winans, 9/26/08; edited by Y. Hori, May 2009)

Ref: Chapter 2

Note: alginate particle to alginate matrix ratios are same as the ones used for *in vivo* injections

Fluorescence plate reader

1. Put 100 μL of particles solution (around 1 million particles) into a 1.5 mL eppendorf tube. Make sure particle solution is well mixed before removing aliquot.
2. Centrifuge down at 7 krpm for 30 sec using benchtop mini centrifuge. Remove and discard supernatant carefully with pipet.
3. Gently vortex particle pellet then sonicate in bath sonicator for 2-3 minutes.
4. Add 160 μL matrix solution (pre-warm to 37 °C if desired) and pipet thoroughly to resuspend the particles in matrix.
5. Centrifuge down suspension at desired timepoint at 14 krpm using benchtop mini centrifuge for 10 min.
6. Carefully remove and collect supernatant (generally there is about 100 μL) and check under light microscope for particles—there should be none in the supernatant. It is more time efficient to put 5 μL of each sample on a glass slide and view them all at once, rather than using the hemacytometer.
7. Begin 96-well plate preparation: add 20 μL of 25 ug/mL mag-fura-2 in PBS to each well using multichannel pipet; add 20 μL of concentrated Ca^{2+} solutions to standards using PCR tubes and multichannel pipet; add pure SLM20 matrix (to standards) and the samples one well at a time. Add PBS with multichannel to desired final volume and mix thoroughly (either 100 μL of 150 μL generally).*
8. Let plate sit in the dark for several hours for the standards and the samples to equilibrate with the PBS and the dye.
9. Read on plate reader at 340ex/515em and 380ex/515em. Analyze data by taking the ratio of the 340/380 signals.

Epifluorescent microscope

1. Incubate mag-fura-2 dye in SLM20 matrix solution at a concentration of 25 μg/mL to ensure the dye is uniformly spread throughout the matrix (usually incubated for several hours or overnight).
2. Make Ca^{2+} standards (in duplicate) in 8-well Labtek. This is the most important part of the experiment, since if the standards are not thoroughly mixed, the calibration curve will not be reproducible. Add concentrated Ca^{2+} solution to Labtek middle wells followed by 200 μL of mag-fura-2 infused matrix. Mix thoroughly with single pipet or multichannel pipet. (I've found mixing two wells at once with the multichannel is better for reproducibility). Cover in foil and let sit for several hours.

---

3. Before Ca^{2+} release, take images of 200 μL of dye-infused SLM20. Focus epifluorescence microscope on Labtek edge then move microscope laterally away from edge toward the center of the Labtek. Take a Z stack to make sure fluorescence is uniform. Take images at 340 and 380 fura for 10 min.
4. Remove SLM20 in Labtek and mix thoroughly with roughly 1.25 million particles (normal preparation). Add slurry back to Labtek and continue images for 1-2 hours. Note: it is assumed the vertical placement of the Labtek and lense does not change between taking dye-matrix images and dye-matrix-particle images, even though intensity should be constant across a small z-range for both sets of images anyway. Once the Labtek is put back on the platform, particles should be visible immediately without focusing, if the microscope was focused properly for the matrix-dye measurement.
5. Analyze data by taking the average intensity of each collected image and dividing 340ex/380ex intensity measurements.

Appendix C.3: Determination of total Ca^{2+} loaded in alginate particles

(written by A. Winans, 9/26/08; edited by Y. Hori, May 2009)

Ref: Chapter 2

1. Take approximately 1 million particles (100 μL of particle solution), centrifuge down at 7 krpm (with benchtop mini centrifuge) for 30 sec and remove and discard supernatant.
2. Sonicate pellet for 1-2 min in bath sonicator.
3. Add 100 μL of 2.5 mM EDTA (0.25 μmoles) and mix thoroughly. Sonicate for 20 min.
4. Add 890 μL of PBS and mix thoroughly. Sonicate for 20 min.
5. Check for presence of particles with light microscope. If particles still present, add another 10 μL of 10 mM EDTA (0.1 μmoles), sonicate for another 10-20 minutes, and check again.
6. Prepare plate. Add 20 μL of 25 ug/mL mag-fura-2 dye in PBS to each well. Add dissolved particle solution to 96-well plate with as little dilution as possible. Prepare Ca^{2+} standards in PBS as well. Let plate sit for 1-2 hours to let dye and Ca^{2+} equilibrate. Run plate on reader at 340ex/515em and 380ex/515em.
7. Analyze data by taking the ratio of the 340/380 signals. Assume EDTA binds Ca^{2+} irreversibly and back-calculate amount of total Ca^{2+} from total EDTA added and the amount of free Ca^{2+} detected by the dye.

Note: the amount of EDTA added is calculated to chelate roughly half of the Ca^{2+} bound in particles. If no free Ca^{2+} is left after dissolving the articles, re-run experiment with less EDTA.

Appendix C.4: QTI Elemental Analysis Sample Preparation

Ref: Chapter 2

1. Alginate particle suspension was centrifuged down and the supernatent removed.

2. Pellet was resuspended with 300 μL of 100 mM EDTA solution (disodium EDTA dihydride).
3. Samples were packaged and sent off.
4. Once QTI received them, each sample was briefly vortexed then sonicated for 30 seconds.

5. 100 μL of sample was added to a nitric acid, then the quantity was diluted to the necessary sample to be run through the ICP-OES (inductively-coupled plasma – optical emission spectroscopy).

Appendix C.5: Alginate Labeling With Fluorescent Dye

Ref: Chapter 2
Source: Strand, B. L., Morch, Y. A., Espevik, T. & Skjak-Braek, G. (2003) *Biotechnol Bioeng* **82,** 386-94.

1. Prepare 2 w/v % alginate solution (i.e. add 12.5 mL PBS to 250 mg sterile Pronova SLM20 vial) and let it dissolve overnight at 4 °C.
2. Make 18 mM solution of EDC (1-Ethyl-3-[3-dimethylaminopropyl]carbodiimide hydrochloride) and 18 mM sulfo-NHS (*N*-hydroxysulfo succinimide) in PBS in separate eppendorf or conical tubes. The volume of the solutions should be such that the total of EDC and sulfo-NHS solutions will be equal to that of 2 % alginate solution to be labeled. (The final concentration of EDC and sufo-NHS will both be 9mM).
3. Add the EDC solution to the alginate solution. Vortex.
4. Add the sulfo-NHS solution to alginate solution containing EDC. Vortex.
   *Steps 3 and 4 can be done consecutively, i.e. without incubating with EDC for a while.
5. Shake for 2 hrs at room temperature.
6. Add the desired concentration of fluorescent dye to the alginate solution.
   *dissolve the dye in a small amount of PBS or H_2O first and then add to the alginate solution:
   i.e. 0.32 mM Hilyte Fluor 647 amine (Anaspec, Inc) in PBS
   4.5 mM 6-aminofluorescein (Sigma) in 70 % ethanol
   *6-aminofluorescein is insoluble in H_2O, so used 70 % ethanol. The dye does not dissolve fully, so it becomes a suspension of the dye powder in ethanol. Vortex well and add as much as you can to the alginate solution.
   *Other suggested solvents for 6-aminofluorescein by Sigma are:
   0.1 MTris buffer, pH 9.0
   0.1 M NaOH
   Methanol (0.1 % of dye recommended in ethanol or methanol)
7. Incubate and let the dye and alginate react at room temperature for 18 hrs while rotating/shaking.
8. Next day: Dialyze the alginate/dye solution with (using 7 kDa MWCO dialysis cassette from Pierce) against large volumes of PBS (> 1 L) at 4 °C for 3 days or until PBS becomes clear of freely floating dye.
   *Choose the size of cassette such that not much PBS can diffuse into it to dilute out the final alginate concentration.

9. Adjust the final volume of the alginate so the alginate concentration will be 0.01 g/mL (1 % alginate in PBS).
10. Sterile-filter the alginate solution with Sterile Acrodisc Syringe Filters (Pall Corporation) with 0.45 μL pore size.
11. Store at 4 °C in dark, covered with foil, till use.

*For *in vivo* use, keep the whole process sterile. Use sterile PBS for dissolving reagents and for dialysis. Perform as much of the procedure as possible in the TC hood.

Appendix C.6 Endotoxin Level Testing and BMDC Activation Assay (for Alginate Microspheres and Protein A-Coated Beads)

Ref: Chapters 2 and 4.

LAL Assay

*Follow the manufacturer's instructions (Limulus Amebocyte Lysate QCL-1000, Cambrex).
** Use sterile, flat-bottom 96-well plate (BD Falcon).
** Use "The Jitterbug" (Boekel Jitterbug Microplate Incubator Shaker, Model 130000) for steps that require the samples to be at 37 °C.

BMDC Activation Assay

1. Culture BMDCs as usual (i.e. isolate from bone marrow and culture in 10 ng/mL GM-CSF in RPMI + 10 % FCS; feed cells by replacing 800 μL of culture media with 800 μL of new media with GM-CSF every other day).
2. On day 5 of culture, add LPS standards (i.e. serial dilutions of LPS from 1 μg/mL down to 1-10 ng/mL) and add bead samples at different concentrations to each well (i.e. 1 x 10^5 – 1 x 10^6 beads per well). Have some wells untreated for negative control.
   *Prepare all samples and standards in triplicates.
   *It is easy to have the concentrated LPS standards and beads in culture media or PBS and add appropriate amount of standards/samples and add ~100 μL per well.
3. Incubate at 37 °C overnight (~18 hrs).
4. Harvest the cells by pipetting vigorously and collecting the cells in conical tubes. Add ~500 μL cold PBS per well and let stand for ~ 5 min to further detach cells from the bottom of the wells and collect the cell suspensions in the same conical tubes.
5. Centrifuge the cells down in conical tubes (~1,300 rpm / ~630 x*g* in Allegra™ 6KR big centrifuge) for 5 min.
6. Save the supernatants for ELISA (i.e. TNFα, IL-12p70 or IL-12p40, IL-6, etc).
7. Stain the cells for flow cytometry (i.e. CD11c, CD40, MHC II/I-A^b).

Appendix D
Experimental Protocols For *In Vivo* Gel Immunization And Analyses

Note: Most of the buffers and reagents were used as described in "Inverse opal hydrogel scaffolds as lymphoid microenvironments for the study of immune cell migration and immunotherapy" by Agnieszka Stachowiak (doctoral thesis, 2007), unless otherwise noted.

*Perform every step of the protocol in a TC hood to keep everything sterile for *in vivo* use.

Appendix D.1: Tumor Cell Preparation and Inoculation

Ref: Chapter 4

Tumor cell culture

Culture media: high-glucose DMEM (i.e. from Gibco) supplemented with L-glutamine and 10 v/v % FCS.

1. Take frozen vial of tumor cells (B16-ova) from liquid nitrogen cell bank and thaw it in the 37 °C water bath for 3-5 min or till the solution completely thaws.
2. Quickly transfer the cells into 20 mL of cold (or room temperature) culture media drop-wise using a 1 mL pipetteman.
3. Transfer the 20 mL media containing tumor cells into culture flasks (175 cm^2 culture area).
4. Let the cells settle and grow in the culture flask overnight.
5. Change culture media to one containing 2.5 μg/mL puromycin to select for GFP-OVA^+ cells.
6. Continue culturing the cells till they become ~60-70 % confluent.
7. Split cells as necessary until use.

Note: Do not culture the cells for more than one week. They are supposed to lose aggressiveness after a long culture.

Freezing tumor cells for future use

Freezing media: 90 v/v % FCS + 10 v/v % DMSO

1. Detach asd collect cells from culture flask using trypsin/EDTA (incubate for ~5 minutes at 37 °C).
2. Centrifuge the cells down at ~1200 rpm (~628 *xg*) with AllegraTM 6KR centrifuge for 3-5 minutes.

3. Resuspend the cells in freezing media at about 1.5-2 M cells/mL.
4. Put the cell suspensions in 1-2 mL cryovials and quickly bring them to the -80 °C freezer.
5. Freeze the cells at -80 °C overnight.
6. Transfer the cryovials to liquid nitrogen.

Tumor inoculation

1. Detach and collect the cells from culture flask using trypsin/EDTA (incubate at 37 °C for 3-5 min). It helps to tap the culture flask at the end of the incubation to help detach cells.
2. Centrifuge the cells down at ~1200 rpm (~628 xg) with AllegraTM 6KR centrifuge for 3-5 minutes.
3. Wash the cells with 10-15 mL of HBSS 2-3 X.
4. Resuspend at a concentration of 20,000-100,000 cells in 200 μL HBSS per sample.
5. Store the cell suspensions on ice till injections.
   *Minimize the time the cells stay in suspension.
6. (At the animal facility) anesthetize the mice with isoflurane.
7. Shave the back flanks of mice.
8. Draw the cell suspensions with 1 mL syringes without needles and then attach 26-30 gauge needles.
9. Subcutaneously inject the cells into the back flank of mice. Wait a few seconds before withdrawing the needle. Pinch the needle and the skin as you withdraw the needle.
   *Try to change needles as often as possible to avoid passing pathogens between mice.
10. Monitor tumor growth using digital caliper.

Appendix D.2: Gel Immunizations

Ref: Chapters 2, 3, 4

Alginate microsphere pellet preparation

1. Sythesize alginate microspheres (calcium reservoir microspheres) as described in Appendix C.1, within a week before injections.
2. Pool all the batches of microsphere suspensions together and mix well (alginate microspheres (1 batch of particles = 1 mL of as-sythesized particles in sterile, distilled, deionized H_2O).
3. Dispense 100 μL of the particle suspension in each eppendorf tube.
4. Centrifuge the particles down at ~0.3×10^3 x *g* for about 2.5 minutes in a table-top mini centrifuge.
5. Remove the supernatants carefully from each eppendorf tube.
6. Vortex and sonicate the particle pellets for 1-3 minutes.
7. Store at 4 °C till use.

Note: Keep all the procedures sterile.

Alginate matrix preparation

1. Prepare 1 w/v % Pronova SLM20 alginate solution in PBS (i.e. add 25 mL to the sterile alginate vial containing 25 mg alginate) and dissolve overnight at 4 °C.
2. Add 3-4 samples worth of matrix solution in each eppendorf tube (prepapre ~170 μL per sample to allow for loss from pipetting and syringes).
3. Add factors to be delivered into the matrix solutions in as little volume as possible (i.e. concentrated solution of the factors) to avoid dilution of alginate matrix and mix gently but very well.
   * Factors that need be equilibrated overnight, i.e. chemokines, should be mixed the day before injections.
4. If mixing dendritic cells, harvest and wash the dendritic cells 3X with cold PBS (~50 mL each time), immediately prior to injections.
5. Keep the alginate matrices containing cells and or other factors on ice till injections.

Note: Keep all the procedures very sterile.
Note 2: When mixing factors into the alginate solution, adjust the concentration so the desired amount of the factors will be in 150 μL of the matrix solution to be injected (i.e. 2.27 million DCs in 170 μL matrix).

Gel immunizations

Avertin stock solution: 25 g tribromoethanol (2,2,2 – Tribromoethanol, Sigma) + 15.5 mL tert-amyl-alcohol (Tert amyl alcohol, 99+%, Sigma). Store stock solution in dark, with no plastics (it can dissolve certain plastics) and wrapped in aluminum foil at room temperature or 4 °C for up to one year. The solution crystallizes upon exposure to light.
Avertin injection solution: 60 μL of stock solution in 5mL of sterile PBS or distilled H_2O (i.e. in 15 mL polystyrene conical tube). Cover the tube with foil and avoid exposure to sunlight. Recommended to make fresh solutions before each use, but can keep at 4 °C or on ice up to one week until use.

1. Anesthesize mice with Avertin (25 μL injection solution per unit gram weight of mouse, as recommended by the DCM: generally about 300-350 μL of working solution to an average sized female mouse.) *Do not overdose.
2. Immediately prior to injections, add ~165 μL of the matrix SLM20 solution with or without desired factors to the calcium microsphere pellet, and pipette gently but very well. Be careful not to produce any air bubbles.
   *Try to minimize volume loss from pipetting (and also from sticking to the sides of the eppendorf tubes).
3. Draw 150 μL of the mixed gel with 28 gauge insulin syringe.
4. Gently and slowly inject the gel subcutaneously, surrounding tumors.
   *May need to move and change injection directions to get the gels to go around tumors.

Appendix D.3: Gel and Tumor Isolation for Flow Cytometry Analyses and ELISA

Ref: Chapters 3 and 4.

Tumor and gel isolation from the mice

*Prepare 12-well culture plates with 500 μL PBS or RPMI (with or without 10 % FCS) in each well. Bring the plate on ice to the animal facility.

1. Euthanize ~2-4 mice at a time (to avoid keeping the mice dead for too long before isolation to keep cells as fresh as possible and also since the tissues harden up after death).
2. Spray the mice well with quatricide solutions and pin the mice down to the dissection board using 26 gauge syringe needles (one arm, two legs).
3. Cut the skin around the tumors and gels with dissection scissors. Leave as large margins as possible around the tumors and gels, but careful not to mess up the inguinal lymph nodes if isolating the lymph nodes as well.
4. Gently snip through the border of the tumors/gels and the tissues to separate them from the muscles first. The gels and the tumors are still attached to the skin.
5. Open the skin flap and pin them down so the skin is tightly spread over its tail.
6. Gently separate the gels and or tumors from the skin and from each other.
7. Place the explanted gels, tumors, and any other tissues into 500 μL PBS or RPMI (10% FCS) in each well of a 12-well tissue culture plate.
8. Keep the tissue culture plate on ice till all the samples have been isolated.

Tumor and gel digestion for flow cytometry

Digestion solution: 0.14-0.28Wü/mL Liberase Blendzyme 3 in PBS or RPMI (10 % FCS)
FACS buffer: HBSS (calcium and magnesium-free) + 0.1 w/v % sodium azide (NaN_3) + 1.0 w/v % bovine serum albumin (BSA, fraction V). Store up to 1 year at 4° C.

1. Add the digestion solutions to the explanted samples so that the total final solution volume will be 1 mL.
2. Chop the samples up in small pieces. Wash the fragmentns and solutions stuck to the scissors and forceps (still keeping the final solution volume to be 1 mL).
3. Add 100 μL of 10 mg/mL alginate lyase to gel samples.
4. Shake and incubate at 37 °C for 15-20 minutes.
5. Add 300 μL of 0.02% EDTA to gel samples.
6. Homogenize the samples using the backs of 1 mL syringe pistons in 40 μm cell strainer and pass the cells through the strainer mesh with 9 mL of PBS or RPMI (10 % FCS) into polystyrene 50 mL conical tubes. The total volume of cell suspension collected will be ~10 mL.
7. Centrifuge the cell suspensions down at 1,300 rpm (~630 *xg*) in the Allegra™ 6KR centrifuge.

8. Resuspend the cells in FACS buffer containing purified CD16/CD32 antibodies to block nonspecific binding sites and transfer the samples to V-bottom FACS staining 96-well plates. Wait 10 minutes.
9. Stain the cells with fluorophore-conjugated antibodies for 20-30 minutes on ice. (i.e. 1.2 μL of PE-antibody, 2.4 μL of FITC-antibody, and 1.5 μL of APC-antibody in 100 μL total staining solution, for antibodies from BD Biosciences).
10. Wash the cells with FACS buffer 3X (total volume in each well ~200 μL during washes).
11. Resuspend the cells in 70-100 μL FACS buffer and transfer them to FACS tubes.
12. Add PI (propidium iodide) to desired samples at 1.27 μg/mL final concentration to stain for dead cells.
13. Prepare calibration standards by adding known number of cells in the same amount of buffer used for samples. Do serial dilutions to have about 5 different concentrations of cells. *The actual number of cells and the count the FACS machine recorded can be used to calculate the'FACS reading error.'
14. Run the whole tubes on FACS machine (usually used FACSCalibur).

Note: When running flow cytometry on protein-A coated beads, with or without IL-15 complex conjugated to them, use FACS buffer supplemented with 0.05 v/v % Tween 20.

Tumor and gel digestion for ELISA

ELISA buffers:

Reagent diluent: 1 w/v % BSA in PBS, pH 7.4 (i.e. 10 g BSA in 1L PBS)
Block buffer: 1 w/v % BSA + 0.1 w/v % NaN_3 in PBS.
Stop solution: 1 M (2N) H_2SO_4 in H_2O

T-Per Tissue Protein Extraction Reagent (Pierce, Rockford, IL) supplemented by Halt Protease Inhibitor Cocktail (Pierce): 1.5 mL T-Per Reagent + 20 μL Halt Protease Inhibitor + 500 μL PBS (PBS is the original solution used for storing samples after isolation). *add 100 μL of 10 mg/mL alginate lyase for gel digestion.

1. Collect samples in eppendorf tubes containing 500 μL PBS on ice. Chop the samples up in small pieces as you harvest them from mice.
2. Add digestion solutions to the tubes.
   * can use either the collagenase/Blendzyme –based digestion solution as described in the "tumor and gel digestion for flow cytometry" section (add the digestion solution so that the final volume in the eppendorfs will be 1 mL), or use the T-Per reagent supplemented with Halt Protease Inhibitor (add 500 μL to each eppendorf tube).
3. Add 100 μL of 10 mg/mL alginate lyase to gel samples only (final lyase concentration = 1 mg/mL).
4. Vortex the samples quickly and immediately homogenize the samples using the backs of 1 mL syringe pistons in 40 μm cell strainer. Pass the cells through the strainer mesh with the rest of the digestion solution (1 mL) into polystyrene 50 mL conical tubes. The total volume of cell suspension collected will be ~2 mL.
   * adjust the final volume collected, depending on the concentration of the protein you are trying to detect using ELISA.

5. Centrifuge the collected supernatantns down at 2-3,000 rpm (~1,400-2000 *xg*) in the Allegra^{TM} 6KR centrifuge.
   * if doing flow cytometry on the cells with the same samples, centrifuge at 1,300 rpm instead.
6. Carefully collect the supernatants, not to pipet the cells or any other debris, and store in eppendorf tubes.
7. Perform ELISA according to the manufacturer's instructions (i.e. R&D Systems).
8. Read the plate with absorbance plate reader ($\lambda_1 - \lambda_2$; λ_1 = 450 nm; λ_2 = 540 nm).

Note: Always have 'digested' and 'non-digested' controls using soluble proteins (i.e. IL-15 complex) to calculate how much loss digestion incurs to the samples. Correct the values obtained with ELISA with loss factors to obtain actual values.
Note 2: Some cytokines (i.e. IFN-γ, IL-15) seem very sensitive to collagenase-based digestion. They seem to degrade quickly over time during storage (even at -20 °C), so use them right away if possible. If storing, have a digested and stored soluble control of the protein (treated exactly the same way as the samples are).

Appendix D.4: Intracellular Foxp3 Staining

Ref : Chapter 4

Live/Dead Fixable Dead Cell Stain Kit: from Invitrogen, catalogue # L23102
Anti-mouse/rat foxp3 staining kit: from eBioscience, catalogue # 72-5775-40

1. Digest and prepare single cell suspensions from explanted gels, tumors, and/or tissues as described in steps 1-7 of "Tumor and gel digestion for flow cytometry" in Appendix D.3.
2. Transfer the cell suspensions from conical tubes to V-bottom FACS staining 96-well plates.
3. Instead of resuspending the cell suspensions in FACS buffer for Fc-blocking with CD16/CD32, resuspend the cells with PBS.
3. Wash the cells 1-2X with PBS by centrifuging them down at 1,300 rpm (~630 x*g*) in the Allegra^{TM} 6KR big centrifuge.
4. Reconstitute live/dead fixable dye in DMSO (i.e. one vial in 50 µL DMSO), vortex well and leave on ice till use.
5. Add 10-25 µL of the dye stock in 10 mL PBS (suggested from manufacturer's protocol = 1 µL in 1 mL). *used ~25 µL for the data shown in this thesis work.
6. Use the solution from step 5 to resuspend the cells with the live/dead fixable dye (100 µL each well). Leave for 30 min on ice, in dark.
   *It is important not to have any amine-containing groups (i.e. BSA, FCS) in the cell suspensions for live/dead stains.
7. Wash 1-2X with PBS.
8. Fix cells with 100-200 µL of Fixation/Permeabilization Buffer (i.e. 6 mL Fix/Perm Diluent + 2 mL Fix/Perm Concentrate) and leave for 30 min- 18 hrs in dark. *did ~4 hrs for the data shown in this thesis work.
9. Centrifuge the cells down and resuspend and wash them 1-2X with Permeabilization Buffer (i.e. 1 mL Permeabilization Buffer + 9 mL distilled H_2O). *can probably proceed to

the next step immediately, but incubated in Permeabilization Buffer overnight (~18 hrs) at 4 °C for the data shown in this thesis work.
10. Next day: block the cells with purified anti-mouse CD16/32 for 10 min on ice or at room temperature.
11. Add fluorochromes (i.e. ~1 μg/mL PE-foxp3, ~10 μg/mL FITC-TCRβ, ~1.5 μg/mL in 100 μL final volume of staining solution) to the cells and incubate on ice for 30 min.
12. Wash 2X with Permeabilization Buffer (~185 μL each time).
13. Resuspend in FACS buffer and transfer to FACS tubes.
14. Run flow cytometry.

Appendix D.5: IL-15/IL-15Rα Complex Formation

Ref : Chapter 4

IL-15 used: R&D Systems Catalog # 447-ML (with or without carrier)
Most of the experiments used Lot # FCL1408071, endotoxin level = 0.7 EU/μg
The last experiment with 2X alg+IL-15SA immunization and foxp3 staining used Lot# FCL1408102, endotoxin level = 0.7 EU/μg
IL-15Rα used: R&D Systems Catalog # 551-MR (with or without carrier)
Lot# DKJ1208081, endotoxin level = 0.000364 EU/μg
Lot# DKJ1008041, endotoxin level = 0.0669 EU/μg

1. Reconstitute IL-15Rα/Fc (100 μg/vial) with 50 μL PBS (or 0.1 w/v %BSA in PBS for carrier-free IL-15Rα or IL-15) for the final concentration of 2 mg/mL.
2. Using the 2 mg/mL IL-15Rα/Fc solution from step 1, reconstitute IL-15 (i.e. 31.7 μL IL-15Rα/Fc solution to each vial of IL-15 containing 10 μg of the protein.
3. Soak the bottom of the vials in 37 °C water bath to warm up the vials.
4. Spray the vials and any container you will use to incubate the IL-15 complex with 70 % ethanol.
5. Incubate the IL-15 complex vials at 37 °C (tissue culture incubator) for 30 min.
6. Take out the vials from the incubator and combine all the IL-15 complex solutions from different vials into one. This is to make sure all the IL-15 complexes are homogenous and uniform, especially if using different lot numbers for the proteins (containing different endotoxin levels).
6'. Rotate or shake at 45 min at room temperature.
7. Store at 4 °C overnight (~16-18 hrs), covered in foil and rotating or shaking.
*Steps 6' and 7 were done to be consistent with IL-15 complex conjugated to protein A coated beads, which underwent 45 min incubation at room temperature followed by an overnight incubation at 4 °C (as described in Appendix D.6). The last two steps can be omitted and the IL-15SA solutions can be used right away if no additional steps are needed for conjugation, etc.

Appendix D.6: Protein A Bead Sterilization And Immobilization of IL-15SA on the Bead Surfaces

Ref: Chapter 4, Section 4.2.7

Bead sterilization

Sterile filtered 70 % ethanol: filter 70 % ethanol from tissue culture room using Sterile Acrodisc Syringe Filters (Pall Corporation) with 0.2 μm pore size.

0.05 v/v % Tween 20 in H_2O: sterile filter before use, store at 4 °C.

Sterile H_2O: sterile filter milliQ deionized, distilled H_2O before use

FACS buffer with 0.01-0.05 v/v % Tween 20: add appropriate amount of Tween 20 to FACS buffer

1. Aliquot the amount of Protein A-coated beads needed into an eppendorf tube.
2. Wash the beads 2X with sterile H_2O (milliQ) by centrifuge (2.5-4 min at 3-7,000 x*g*).
3. Add 500–1,000 μL of 70 % ethanol to the tube, vortex, and immediately centrifuge it down in the bench-top mini centrifuge for 2.5-3 min at 3-7,000 x*g*.
4. Discard the 70 % ethanol supernatant by flipping the tube.
5. Add 1 mL of 0.05 % Tween 20 in H_2O, vortex, and centrifuge it down.
6. Wash 1X or 2X with sterile H_2O.
   * the point here is to get rid of as much Tween 20 as possible to have just he minimum amout of it needed to keep the protein A beads from sticking to the sides of the eppendorfs. We want to avoid having too much Tween 20 because it could potentially affect the immune response (i.e. act as adjuvant) *in vivo*. Keep in mind that there will be another 'wash' or 'centrifuge' step before conjugating IL-15/IL-15Rα.
7. Keep suspended in H_2O and stored at 4 °C until use. It is recommended to use the beads as freshly sterilized as possible.

Note: Whenever the beads start sticking to the walls of the eppendorfs or do not pellet well, add 0.05 % Tween 20 in H_2O.

Conjugation to IL-15/IL-15Rα

1. Centrifuge and pellet the sterilized protein A-coated beads.
2. Add IL-15/IL-15Rα complex as prepared in Appendix D.5 to the eppendorfs containing bead pellets. Do not touch or pipet the beads up and down (because a lot of them can stick to the pipet tips).
3. Vortex the beads gently.
4. Rotate or shake at room temperature for 45 min.
5. Cover with foil and rotate or gently shake overnight (~16-18 hrs) at 4 °C.
6. Before use: centrifuge down the beads and gently vortex them so the beads disperse into a suspension (and not stay in pellet) but they do not splash up and stick to the sides of the eppendorfs.
   * If incorporating into self-gelling alginate, pipet the beads into the alginate precursor solution and then vortex the whole solution instead of pipetting (to avoid losing gels and beads from pipetting).